doi.org/10.26434/chemrxiv.12052410.v1

Discovery and Biocatalytic Application of a PLP-Dependent Amino Acid γ-Substitution Enzyme that Catalyzes C-C Bond Formation

Mengbin Chen, Chun-Ting Liu, Yi Tang

Submitted date: 31/03/2020 • Posted date: 01/04/2020

Citation information: Chen, Mengbin; Liu, Chun-Ting; Tang, Yi (2020): Discovery and Biocatalytic Application of a PLP-Dependent Amino Acid γ-Substitution Enzyme that Catalyzes C-C Bond Formation. ChemRxiv. Preprint. https://doi.org/10.26434/chemrxiv.12052410.v1

Pyridoxal phosphate (PLP)-dependent enzymes can catalyze various transformations of amino acids at alpha, beta, and gamma positions. These versatile enzymes are prominently involved in the biosynthesis of nonproteinogenic amino acids as building blocks of natural products, and are attractive biocatalysts. Here, we report the discovery of a two-step enzymatic synthesis of (2S, 6S)-6-methyl pipecolate 1, from the biosynthetic pathway of indole alkaloid citrinadin. The key enzyme CndF is PLP-dependent and catalyzes synthesis of (S)-2-amino-6-oxoheptanoate 3 that is in equilibrium with the cyclic Schiff base. The second enzyme CndE is a stereoselective imine reductase that gives 1. Biochemical characterization of CndF showed this enzyme performs gamma-elimination of O-acetyl L-homoserine to generate the vinylglycine ketimine, which is subjected to nucleophilic attack by acetoacetate to form the new C_{gamma}-C_{delta} bond in 3 and complete the gamma-substitution reaction. CndF displays substrate promiscuity towards different beta-keto carboxylate and esters. Using a recombinant Aspergillus strain expressing CndF and CndE, feeding various alkyl-beta-keto esters led to the biosynthesis of 6-substituted L-pipecolates. The discovery of CndF expands the repertoire of reactions that can be catalyzed by PLP-dependent enzymes.

File list (2)

Discovery and Biocatalytic Application of a PLP-Dependent Amino Acid γ-Substitution Enzyme that Catalyzes C-C Bond Formation

Mengbin Chen,[1] Chun-Ting Liu,[1,3] Yi Tang[1,2,*]

[1]Department of Chemical and Biomolecular Engineering, [2]Department of Chemistry and Biochemistry, University of California Los Angeles, Los Angeles, California 90095, USA. [3]Massachusetts Institute of Technology, Cambridge, Massachusetts 02139, USA.

Supporting Information Placeholder

ABSTRACT: Pyridoxal phosphate (PLP)-dependent enzymes can catalyze various transformations of L-amino acids at α, β and γ positions. These versatile enzymes are prominently involved in the biosynthesis of nonproteinogenic amino acids as building blocks of natural products, and are attractive biocatalysts. Here, we report the discovery of a two-step enzymatic synthesis of (2*S,* 6*S*)-6-methyl pipecolate **1**, from the biosynthetic pathway of indole alkaloid citrinadin. The key enzyme CndF is PLP-dependent and catalyzes synthesis of (*S*)-2-amino-6-oxoheptanoate **3** that is in equilibrium with the cyclic Schiff base. The second enzyme CndE is a stereoselective imine reductase that gives **1**. Biochemical characterization of CndF showed this enzyme performs γ-elimination of *O*-acetyl L-homoserine to generate the vinylglycine ketimine, which is subjected to nucleophilic attack by acetoacetate to form the new C_γ-C_δ bond in **3** and complete the γ-substitution reaction. CndF displays substrate promiscuity towards different β-keto carboxylate and esters. Using a recombinant *Aspergillus* strain expressing CndF and CndE, feeding various alkyl-β-keto esters led to the biosynthesis of 6-substituted L-pipecolates. The discovery of CndF expands the repertoire of reactions that can be catalyzed by PLP-dependent enzymes.

Nature is remarkable in building and using structurally diverse amino acids.[1-2] Nonproteinogeneic amino acids (NAAs), which constitute 96% of the naturally occurring amino acids,[1] are frequently incorporated into small molecules to broaden reactivity and to establish biologically relevant conformers.[3] Peptides that contain NAAs are less susceptible to proteolysis, thereby increasing the half-lives during circulation.[4-5] The usefulness of NAAs have also been extensively explored through incorporation into recombinant proteins in *Escherichia coli*, yeast, and mammalian cells.[6] Because of these features, new methods to efficiently synthesize NAAs have gained significant attention.[7-8]

Parallel to organic synthesis, biocatalysis has been applied in the enantioselective synthesis of NAAs.[9] For example, threonine aldolases can produce β-hydroxy-α-amino acids with complete stereoselectivity at C_α positions and moderate stereospecificity at C_β positions.[10] Aminomutases have been used to convert α-amino acids to value-added β-amino acids.[11] Enzymes discovered from natural product biosynthetic pathways that catalyze challenging C-H functionalization have been recently used as biocatalysts for NAA synthesis.[12-14] A notable example by Renata and coworkers showed that GriE, α-ketoglutarate (αKG)-dependent hydroxylase, can stereospecifically hydroxylate remote sp^3 carbons in a wide range of α-amino acids at a preparative scale.[13] Chang et al recently identified αKG-dependent radical halogenases can halogenate unactivated sp^3 carbons of free amino acids.[14] In these examples, the natural functions of the enzymes are to build NAAs for further modification or uptake by nonribosomal peptide synthetases (NRPS).[15-16] Therefore, mining and characterization of new enzymes from secondary metabolism can be fruitful for discovery of new biocatalysts for NAA synthesis.

Pipecolate and derivatives are privileged building blocks frequently used in medicinal chemistry. Pipecolate is present in several FDA approved therapeutics, such as levobupivacaine and nelfinavir (Figure 1).[4] Pipecolate is also found in natural products as highlighted by rapamycin, in which the L-pipecolate is involved in formation of the macrolactam and interactions with FKBPs through hydrogen bonding.[17] Altering the L-pipecolate moiety can change the potency of rapamycin derivatives.[18]

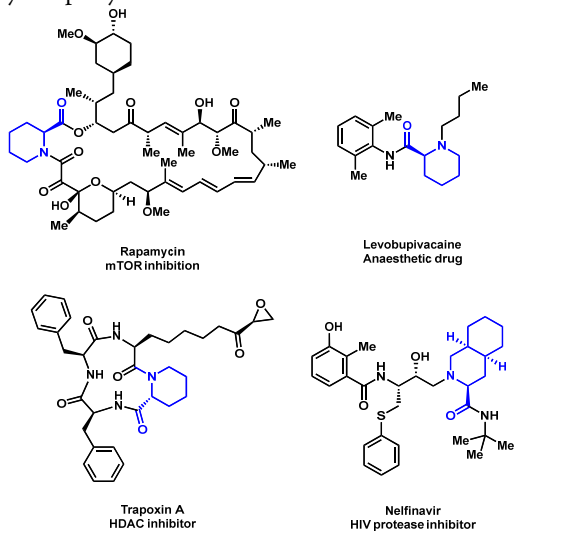

Figure 1. Pipecolates are important synthons in medicinal chemistry. Examples of FDA approved drugs containing *N*-heterocyclic amino acids.

Synthetically, pipecolates can be constructed via multiple approaches including aza Diels-Alder cycloaddition between an activated carbodiene and an imine,[19] full reduction of a substituted picolinate,[20] ring closing metathesis (RCM),[21] or cyclization/reduction of oxo α-amino acids generated from sulfinimine-mediated asymmetric Strecker synthesis.[22] The last approach resembles one way used by Nature to synthesize unsubstituted L-pipecolate: L-lysine is deaminated to give a cyclic imine, followed by reduction to pipecolate.[23] In rapamycin biosynthesis, a single cyclodeaminase LCD catalyzes both L-lysine deamination and imine reduction (Scheme 1A).[24] In plants, the α-amine of L-lysine is first converted to ketone followed by Schiff base formation between C_α and N_ζ.[25] Subsequent reduction takes place stereospecifically to give L-pipecolate (Scheme 1B). In fungi, flavin-dependent saccharopine oxidase can generate a C_ε-semialdehyde from saccharopine, which can form an imine between N_α and C_ε (Scheme 1C).[26] This mechanism is analogous to microbial biosynthesis of methylprolines, common building blocks in natural products. Oxygenases can first catalyze remote oxidation of aliphatic amino acids such as L-leucine or L-isoleucine, followed by imine reduction (Scheme 1D).[27-28]

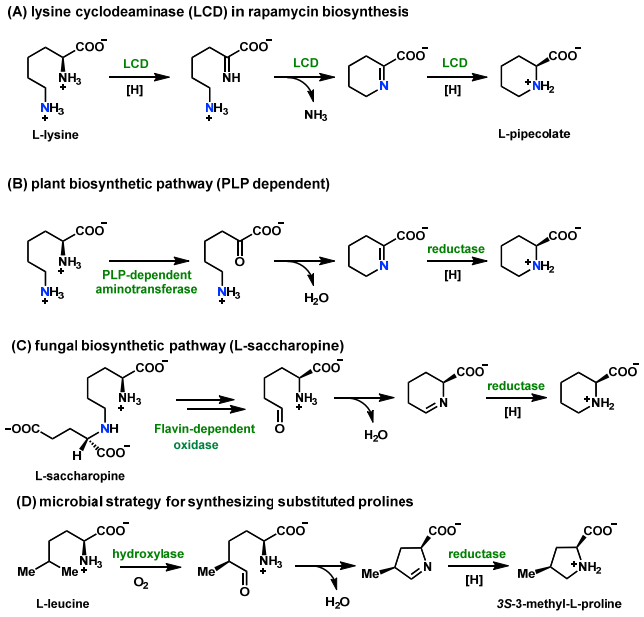

Scheme 1. Enzymatic routes to pipecolate and methylated prolines.

Despite their occurrences in drugs such as Nelfinavir, alkyl-substituted pipecolates are extremely rare in natural products. To our knowledge, our recent discovery of 5,5-dimethyl-L-pipecolate in flavunoidine is the only example.[29] Given the linear aliphatic chain in L-lysine and the limited side chain lengths of natural aliphatic amino acids, it is evident that formation of an alkyl-substituted pipecolate via mechanisms shown in Scheme 1 is not possible. Instead, biosynthesis of alkyl-substituted pipecolates will likely involve C-C bond formation between two building blocks to reach the required number of carbons. Uncovering the enzymes that can perform such function can therefore lead to development of biocatalysts for diverse pipecolate synthesis. Here, we reported the discovery of a two-enzyme pathway, including a PLP-dependent γ-substitution enzyme and an imine reductase, to produce (2*S*, 6*S*)-6-methyl pipecolate **1**. We explored the synthetic utility beyond the native substrate to produce a suite of 6-alkyl-pipecolates starting from β-keto esters.

RESULTS AND DISCUSSIONS

Citrinadin contains a substituted piperidine. Active against murine leukemia L1210 cells, citrinadin A and B were isolated from marine *Penicillium citrinum* (Scheme 2).[30-31] Citrinadin A is further modified from citrinadin B with an *N,N*-dimethylvaline ester.[31] Both Citrinadin A and B contain a pentacyclic core structure comprised of spirooxindole and quinolizidine. The complex structures have inspired numerous total synthesis of citrinadin A and B, and the structurally related PF1270A–C.[32-36] Biosynthetically, citrinadin A is a prenylated indole alkaloid, which can be morphed from a monoketopiperazine that is derived from two amino acid building blocks.[37-39] One of the two amino acid is L-tryptophan as evident by the oxoindole moiety, while the other becomes part of the quinolizidine, and is predicted to be (2*S*, 6*S*)-6-methyl pipecolate **1** (Scheme 2). Retrobiosynthetically, we propose **1** can be derived from the stereospecific reduction of the Schiff base **2**, analogous to the last step in proline and pipecolate biosynthesis (Scheme 1). **2** is expected to be in equilibrium with the ring opened amino acid (*S*)-2-amino-6-oxoheptanoate **3**, which should be bio-synthesized by dedicated enzymes in the citrinadin biosynthetic cluster from primary metabolites (Scheme 2B).

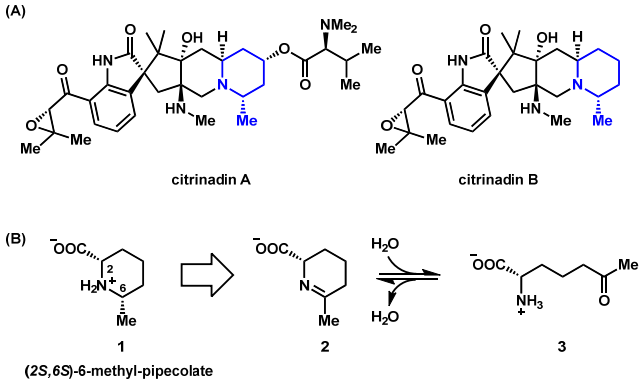

Scheme 2. Citrinadin A and B contains a methylpiperidine that is likely derived from 6-methyl-pipecolate**1.**

The biosynthesis of citrinadin A therefore requires a two-module NRPS that activates and condenses tryptophan and **1**, and at least one dimethylallyl diphosphate transferases (DMAT). The *N,N*-dimethylvaline ester group in citrinadin A is likely installed by an additional single-module NRPS.[29] Using the colocalizations of genes encoding a two-module NRPS and DMAT as requirement, we located a biosynthetic cluster (renamed *cnd*) in several sequenced *Penicillium citrinum* strains (Figure 2A). Among a handful of *P. citrinum* strains that we screened, *P. citrinum* DSM1997 was the only one that produce citrinadin A under laboratory conditions with a titer of 5 mg/L when grown on potato dextrose agar (Figure S2A). To confirm the detected compound is citrinadin A, we performed large-scale culturing of *P. citrinum* DSM1997, purified the compound and verified its structure by NMR analysis (Table S1-2, Figures S13-S14). Next, the *cndA* gene encoding the NRPS was deleted by homologous recombination from the genome to generate *P. citrinum* Δ*cndA* (Figure S2B). Metabolic analysis of *P. citrinum* Δ*cndA* showed that citrinadin A production was completely abolished (Figure S2), confirming the *cnd* cluster is responsible for citrinadin biosynthesis.

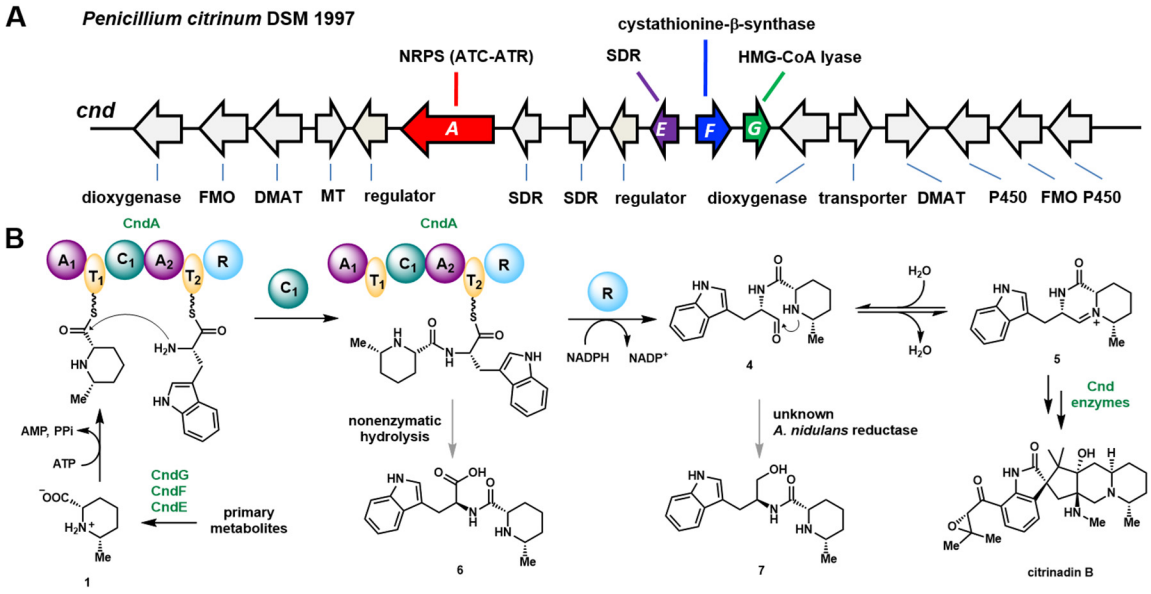

Figure 2. Biosynthesis of citrinadin by *Penicillium citrinum* DSM 1997. (**A**) The identified *cnd* gene cluster. The four enzymes that are studied here are colored. Abbreviations: FMO: flavin-dependent monooxygenase; DMAT: dimethylallyltransferases; MT: methyltransferase; SDR: short-chain dehydrogenase/reductase; NRPS: nonribosomal peptide synthetase (A: adenylation; C: condensation; T: thiolation; R: reductase); (**B**) Proposed early steps of citrinadin biosynthesis involves the NRPS CndA and (*2S,6S*)-6-methyl-pipecolate **1**.

Identification of *cnd* biosynthetic cluster. Since **1** is not a known metabolite, we reasoned enzymes responsible for its biosynthesis are encoded in *cnd* cluster. Through comparative analysis of *cnd* and known gene clusters of other related indole alkaloids that do not incorporate **1**, such as notoamide B and taichuanamide A (Figure S3),[37] a set of *cnd* genes (*cndE*-*cndG*) that are uniquely present in *cnd* cluster were identified and highlighted in Figure 2A. Basic local alignment search tool (BLAST) searches using CndE as a query revealed that it belongs to short-chain dehydrogenase/reductase (SDR) family. Considering that the final steps in L-proline and L-pipecolate biosynthesis both require reduction of cyclized imine by imine reductases (Scheme 1), we reason that CndE may play a similar role in biosynthesis of **1**.[23, 27-28] The remaining two unique enzymes encoded in the cluster are a pyridoxal phosphate (PLP)-dependent enzyme CndF, and a putative HMG-CoA lyase CndG.[40] The closest known homologue of CndF is PLP-dependent cystathionine-γ-synthase (CGS), with a sequence identity of 36%.[41-42] In fungi, CGS catalyzes the γ-elimination of *O*-acetyl homoserine **9** to give a vinylglycine ketimine.[43] The nucleophilic thiolate of cysteine can subsequently attacks C_γ atom to form a new C-S bond.[44] We reasoned that CndF may catalyze C-C bond formation between vinylglycine and a three-carbon precursor in a γ-substitution reaction to give (*S*)-2-amino-6-oxoheptanoate **3** (Scheme 2). If so, CndF would be the first example of a γ-substitution, PLP-dependent enzyme that catalyzes C-C bond formation.

To determine whether **1** is a building block of citrinadins, we heterologously expressed CndA in *Aspergillus nidulans* A1145 ΔEM.[45] Expressing *cndA* alone did not lead to new metabolites, indicating possible lack of a specific amino acid substrate. Feeding commercially available (±)-*cis*-6-methyl pipecolate, which contain both (*2S, 6S*) and (*2R, 6R*) enantiomers, to the *cndA* expression strain led to the production of two new compounds **6** and **7** (Figure 3, vii). NMR characterization revealed **6** and **7** are dipeptides derived from tryptophan and **1** (Tables S5 and S6, Figures S26-S35). Therefore, the exogenously supplied pipecolate is recognized by the NRPS and is incorporated into the dipeptide (Figure 2). Both compounds are proposed to be off-pathway shunt products that are related to the on-pathway intermediate monoketopiperazine **5**. Formation of the carboxylic acid **6** can be a result of nonenzymatic hydrolysis of dipeptidyl-*S*-PCP from the peptide carrier protein (T_2) domain of CndA, prior to reductive release as the aldehyde **4** by the R domain (Figure 2B). A sluggish R domain in the heterologous host *A. nidulans* can lead to nonenzymatic hydrolysis of the thioester bond to offload **6**. On the other hand, once released, **4** is in equilibrium with the monoketopiperazine **5**, in which the amide bond is in a less favorable *cis* configuration.[46] In the absence of downstream enzymes that can process **5** to more advanced intermediates, the aldehyde of **4** can be further reduced to the alcohol **7** by endogenous reductases as a detoxification mechanism (Figure 2B).[47]

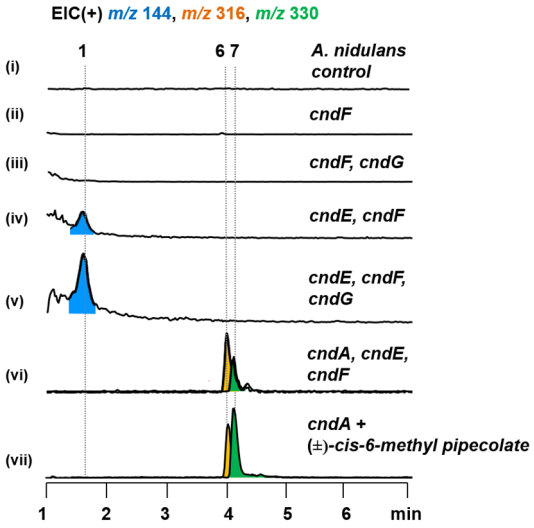

Figure 3. Heterologous expression in *A. nidulans* established that CndE and CndF are necessary and sufficient for the formation of **1**.

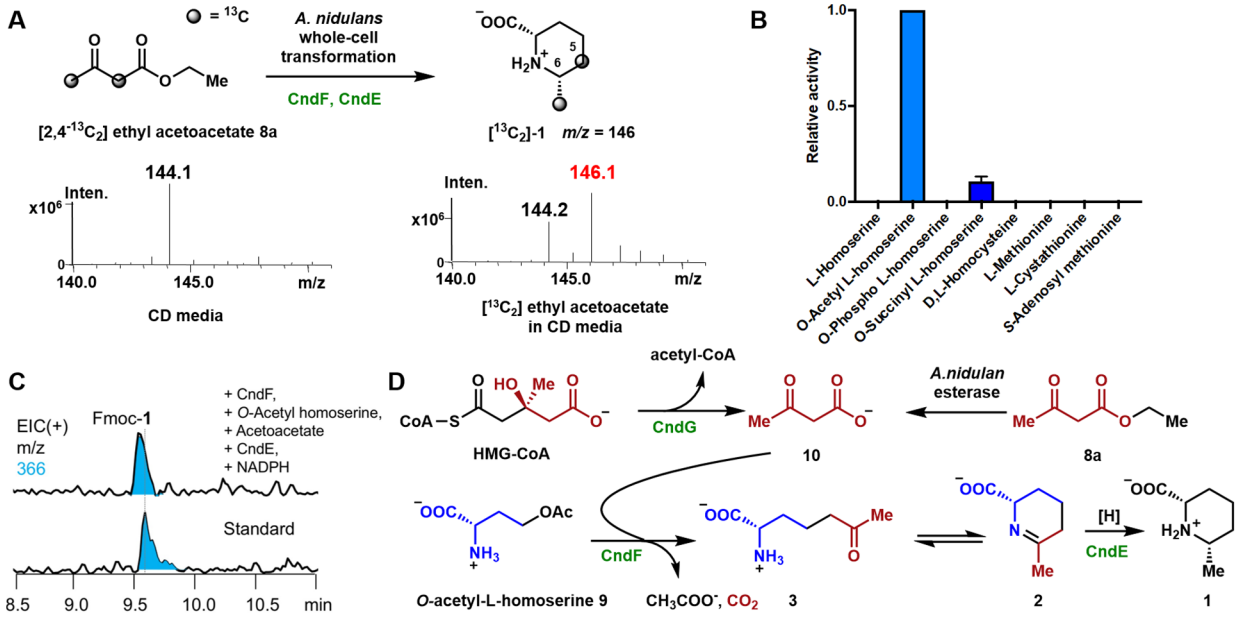

Figure 4. CndF and CndE catalyze tandem reactions to yield **1**. (**A**) Acetoacetate is the precursor to **1**. (**B**) *In vitro* characterization of CndF revealed that *O*-acetyl-L-homoserine is the preferred amino acid substrate. (**C**) In vitro reconstitution of activities of CndF and CndE to give **1.** (**D**) Proposed biosynthetic pathway to **1**.

Determination of the biosynthetic enzymes responsible for producing 1. To identify the enzymes required to biosynthesize **1** and test the hypothesis that the PLP-dependent CndF catalyzes a C-C bond forming reaction, we reconstituted the activities of CndE, CndF and CndG in *A. nidulans*. Expression of *cndF* alone or with *cndG* did not yield any new product compared to control (Figure 3, i-iii). Co-expression of *cndE* and *cndF* led to formation of a new product with a *m/z* =144 ($[M+H]^+$) (Figure 3, iv) that agrees with the molecular weight of **1**. We purified the compound with a titer of 5 mg/L and confirmed the structure to be that of **1** by NMR (Table S3, Figures S15-S20). NOESY analysis showed that 2-carboxylate and 6-methyl substituents in **1** are in a *cis* configuration. Purified **1** was derivatized with Marfey's reagent,[48] and the product profile was compared with that of derivatized (±)-*cis*-6-methyl pipecolate (Figure S4). Derivatized **1** elutes as a single peak, whereas the derivatized (±)-*cis*-6-methyl pipecolate elutes as two separate peaks (Figure S4). This demonstrates that **1** is a single enantiomer. Based on the total synthesis and stereochemical assignment of the quinolizidine methyl group in citrinadin to be in *S* configuration,[33-34] we suggest the C6-methyl group in **1** is also in *S* configuration. Hence the structure of **1** is assigned to be (2*S*, 6*S*)-6-methyl-pipecolate. This result shows that *cndE* and *cndF* are necessary and sufficient to produce **1**. Expression of *cndE* and *cndF* in the presence of *cndA* led to the production of **6** and **7** (Figure 3, vi), which is consistent with the feeding study with (±)-*cis*-6-methyl pipecolate.

When *cndG* encoding a predicted HMG-CoA lyase was coexpressed in the strain expressing CndE and CndF, the titer of **1** increased by approximately 3-fold (Figure 3, v) to ~15 mg/L, suggesting the activity of CndG increases the availability of precursors to **1.** CndG shows >60% sequence identity with fungal HMG-CoA lyases, which indicates CndG is likely to catalyze the same reaction: the cleavage of HMG-CoA into acetyl-CoA and acetoacetate **10** (Figure 4D).[40] The product **10** could therefore be the three-carbon building block that is used by CndF in constructing **1**. Although extensive efforts were made to obtain cDNA of *cndG* from the native producer, we found that *cndG* remained silent under the citrinadin producing conditions tested in the lab. Suppression *of* cndG expression may be due to sufficient cytosolic concentration of acetoacetate through primary metabolism to maintain the production of citrinadin.

To verify **1** is derived from acetoacetate **10**, we supplied [2,4-$^{13}C_2$] ethyl acetoacetate **8a** to *A. nidulans* expressing *cndE* and *cndF*. We reasoned the ethyl ester of **8a** may be hydrolyzed by an endogenous esterase to give **10.** As a result of feeding, an increase of 2 mu in MWT of **1** was detected by mass spectrometry (Figure 4A). This indicates both ^{13}C atoms of **8a** were incorporated into **1**. We purified this labeled compound and NMR analysis revealed that carbon atoms at C5 and the C6-methyl group are isotopically labeled (Figure 4A, Table S4, Figures S21-25). Based on differences in reactivities, we assigned C5 of **1** to correspond to the more nucleophilic C_α atom of **8a**, while C6-methyl to correspond to the terminal C_γ of **8a**. C-C bond formation thus occurs between C_γ (C4 in **1**) and C_δ (C5 in **1**) to forge **3**, the precursor of **1** (Figure 4D). This agrees with our hypothesis that PLP-dependent enzyme CndF catalyzes C-C bond formation between two smaller precursors.

CndF is a PLP-dependent γ-substitution enzyme that catalyzes C-C bond formation. Having established **10** is a building block of **1**, we next sought to elucidate the mechanism of CndF. Since CndF is proposed to catalyze a γ-substitution reaction via a PLP-dependent mechanism, the first substrate must be an amino acid with a good leaving group at C_γ position. To identify the amino acid substrate of CndF, we heterologously expressed and purified it from *Escherichia coli* with 40 μM PLP supplemented in all purification buffers. To confirm that CndF binds PLP, we used UV-vis spectrophotometer to examine to absorbance profile. A characteristic absorption was observed at 420 nm for the purified enzyme, indicating the formation of internal aldimine between PLP and a lysine residue in the active site (Figure S5).[49] Extensive dialysis of CndF in the presence of hydroxylamine eliminated the absorbance peak at 420 nm, indicating the enzyme has been converted to the *apo* form (Figure S5).

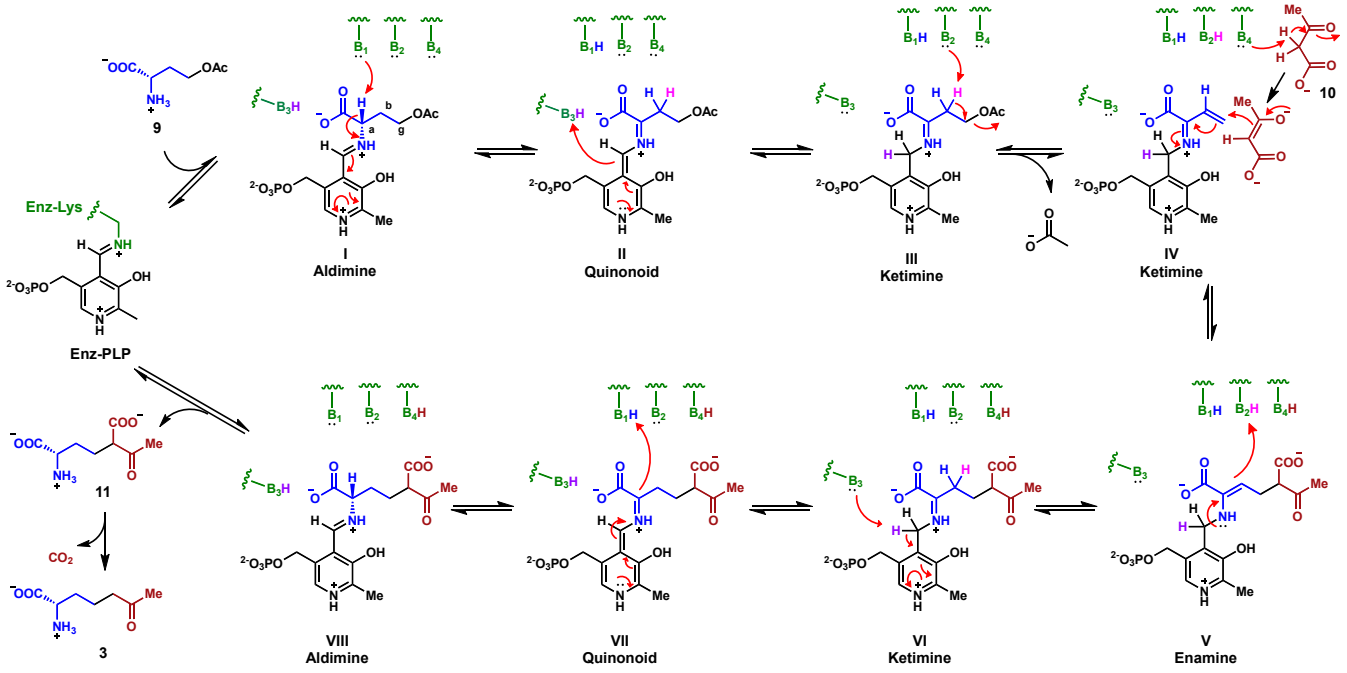

Scheme 3. Proposed mechanism of CndF in catalyzing the γ-substitution reactions to yield **3**.

Next, we tested a panel of amino acids, including L-homoserine, *O*-acetyl-L-homoserine **9**, *O*-phospho-L-homoserine, *O*-succinyl-L-homoserine, L-homocysteine, L-cystathionine, and *S*-adenosyl-L-methionine (SAM), as substrates of CndF in the γ-substitution reaction. *In vitro* reactions of *holo*-CndF were carried out in the presence of **10**. To facilitate product detection of **2** (in equilibrium with **3**) by LC-MS, we used *o*-aminobenzaldehyde (*o*-AB) to derivatize the cyclic imine **2** into the dihydroquinazolinium complex that has a distinct absorbance at 440 nm (Figure S6) and a *m/z* of 245. The assays showed that **9** displayed the highest activity among all substrates (Figure 4B), and is therefore the most likely natural substrate for CndF. The only other substrate that supported the formation of **2** was *O*-succinyl-L-homoserine.

The proposed mechanism of CndF is shown in Scheme 3. In the first step of the reaction following formation of the external aldimine (**I**) between PLP and **9**, PLP serves as an electron sink to delocalize the negative charge generated by the initial deprotonation event at Cα position of **9** to give quinonoid (**II**). Divalent metal ions are known to promote electron displacement as a way to stabilize the Cα carbanion and accelerate catalysis.[50] We carried out *in vitro* enzymatic reactions of CndF in the presence of different divalent metal ions, and found that Co^{2+} expedites the reaction most (Figure S7).[50] The remaining steps of γ-elimination and substitution by CndF are analogous to that of cystathionine γ-synthase.[44] Protonation of **II** gives the ketimine (**III**), which can undergo Cβ proton abstraction and expulsion of the acetyl group to yield the PLP-bound ketimine form of vinylglycine (**IV**). Next, the acidic proton at Cα position of acetoacetate is abstracted and the resulting enolate attacks the electrophilic **IV** to form an enamine adduct (**V**). Reprotonation of Cβ forms the ketimine (**VI**), followed by quinonoid (**VII**) formation and Cα protonation to arrive at the new external aldimine (**VIII**). Release of the adduct **11** as product regenerates the internal enzyme-PLP aldimine. The β-carboxylate of **11** can readily undergo decarboxylation to arrive at the desired ketone **3**.[51] While the C-C bond formation step (**IV** → **V**) may also be initiated through the decarboxylation of **10**, our data below with β-keto ethyl esters suggest the decarboxylation can take place after C-C bond formation. Although decarboxylation is depicted to occur after product release in Scheme 3, we cannot exclude that from taking place during the later catalytic steps of CndF (**V** → **VIII**).

CndF is a unique PLP-Dependent enzyme. PLP-dependent enzymes are essential in all kingdoms of life to catalyze many reactions in metabolism, and arguably represent the most versatile biocatalysts.[42] The PLP cofactor enables chemical transformations on amino acids that are otherwise difficult to perform, including transamination, decarboxylation, β/γ elimination and substitution, etc.[41] Recently, oxidase activities were also identified in PLP-dependent enzymes.[52] The mechanism of CndF reported here is distinct from known PLP-dependent, γ-substitution enzymes by catalyzing a C-C bond formation between the vinylglycine ketimine and the nucleophilic Cα in **10**. The closet examples to CndF are cystathionine-γ-synthase and LolC found in the loline biosynthetic pathway, which catalyze C-S and a proposed C-N bond formation using the vinylglycine ketimine as electrophile, respectively.[42, 44, 53] Other known C-C bond forming PLP-dependent enzymes, such as UstD in ustiloxin B biosynthesis, can perform β-substitutions using an enamine-PLP as a nucleophile.[42, 54] Threonine aldolases and δ-aminolevulinate synthase, which are PLP-dependent enzymes, catalyze C-C bond formation at α-position of glycine using the nucleophilic glycyl-quinonoid.[10] Our recent discovery of bi-functional FlvA is proposed to be mechanistically similar to CndF, although biochemical validation is still pending.[29]

Searches of the nonredundant protein database in the National Center for Biotechnology Information (NCBI) for CndF homologues revealed numerous candidates across filamentous fungi. None of these homologues have known functions, implicating the untapped functional diversity of these enzymes. Phylogenetic analysis showed that the closest homologues to CndF are co-clustered with other biosynthetic enzymes (Figure S8-9). One group of these

clusters are highly conserved across several *Aspergillus* spp. and all contain a NRPS-independent siderophore (NIS) synthetase, while other cluster contains a single-module NRPS (Figure S9). It is likely that these PLP-dependent enzymes also provide NAAs for downstream incorporation in a secondary metabolite.

CndE is an imine reductase. To probe the role of the SDR homolog CndE in reducing **2** to **1**, we carried out combined enzymatic reactions *in vitro*. Purified CndE and CndF (28 μM each final concentration) were incubated with **9** (1 mM), **10** (1 mM), NADPH (1 mM), and $Co(NO_3)_2$ (2.5 mM) in 50 mM phosphate buffer (pH 6.5) for 1 hour at room temperature. Subsequently, the reaction mix was derivatized with Fmoc-Cl and analyzed by LC-MS. The Fmoc-derivatized product eluted at the same time as Fmoc-**1**(Figure 4C). Formation of **1** is not detected in the absence of CndE or NADPH. Together with earlier chiral derivatization result showing that **1** is a single enantiomer, these data established **2** that can be stereoselectively reduced to **1** with *S*-configuration at C6 by CndE.

CndF can synthesize enamines with β-keto esters. Having verified the activity of CndF, we next probed the substrate scope of CndF by varying the structures of β-keto nucleophile (Figure 5). We chose the ethyl esters **8** as substrates because very few β-keto acids are commercially available due to spontaneous β-decarboxylation. Substrates with different sizes at R_1, as well as those containing cyclic β-ketones are tested in the assay. We used LCMS to monitor appearance of new products, as well as quantifying the consumption of substrates (Figure S8). If **8** can be recognized by CndF and can form a C-C bond with the vinylglycine ketimine **IV**, then adduct **12** and the cyclized Schiff base are expected to be products. If the α-position of **8** is not substituted (R_2=H), the Schiff base is expected to tautomerize and form the stable enamine **13** (Figure 5).

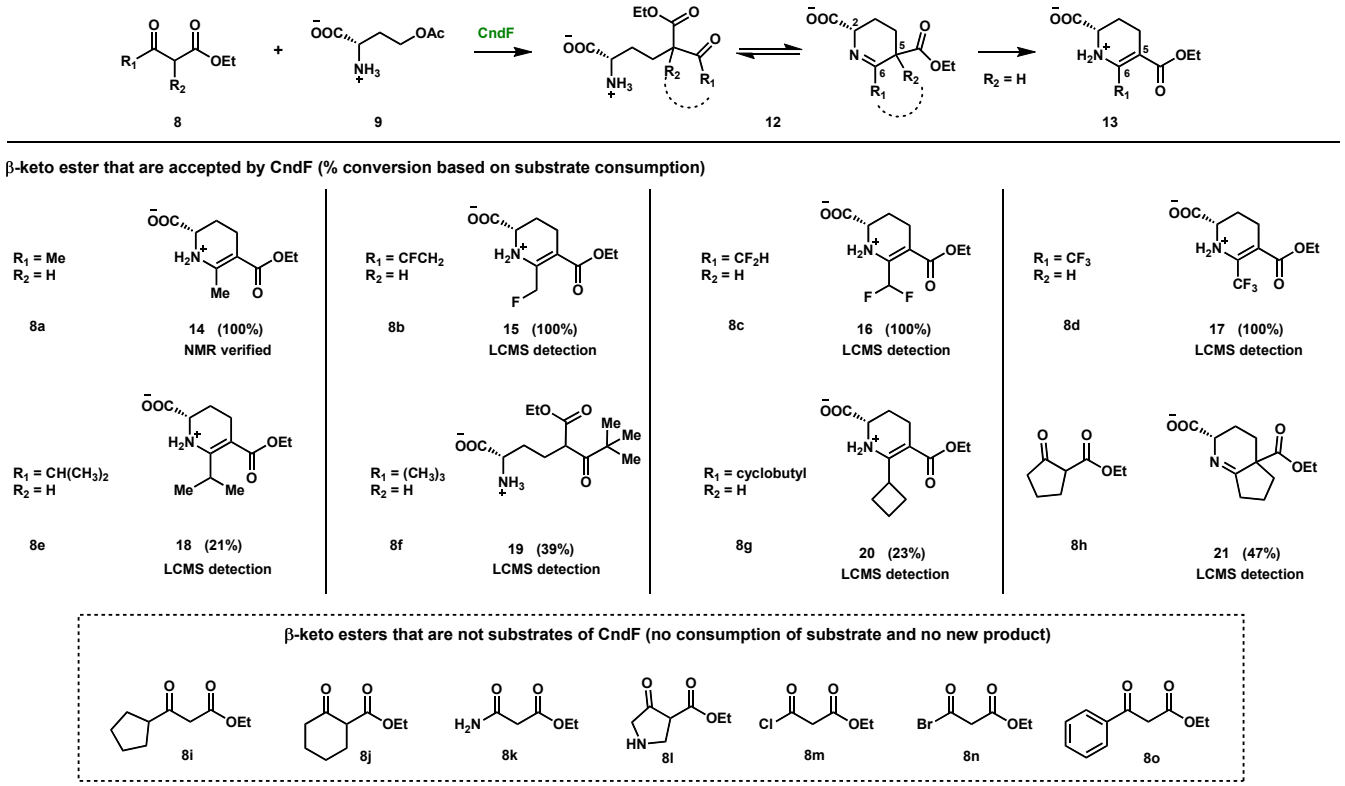

Figure 5. In vitro assay of β-keto esters with CndF.

We first tested **8a** in the in vitro assay to determine if ethyl esters can be accepted as nucleophiles without being hydrolyzed to the carboxylate. Surprisingly, **8a** can be efficiently converted to a new product **14**, with nearly complete consumption of **8a** (Figure S10A). To produce sufficient amount of **14** for structural determination, we transformed *E. coli* with a plasmid harboring homoserine *O*-acetyltransferase (HAT) and CndF. Overexpression of HAT increases the intracellular levels of **9** for the biotransformation. In addition, **8a** does not undergo hydrolysis readily in *E. coli* due to the absence of the esterase that is presumably present in *A. nidulans*. Feeding L-homoserine (10 mM final concentration) and ethyl acetoacetate **8a** (10 mM final concentration) to *E. coli* culture after IPTG-induced protein expression led to the production of **14** at 30 mg/L after 6 hours. The compound was purified and the structure was solved by NMR to be the enamine shown in Figure 5 (Table S8, Figures S36-S40). The λ_{max} of **14** at 286 nm is also consistent with reported enamine absorbance (Figure S10A).[55] Formation of enamine **14** confirms the cyclic Schiff base **12** to be the product of CndF. Coexpression of CndE in *E. coli* did not reduce **14**. This can be attributed to the more stringent substrate specificity of CndE against bulky, C5-substituted cyclic imines. The production of enamine ester **14** also provides mechanistic insight of CndF. In proposing a mechanism for CndF using **10** as the nucleophile, we did not know if decarboxylation is required for enolate formation. Conversion of **8a** to **14** indicates C-C bond formation by CndF does not require acetoacetate decarboxylation to drive enolate formation. Therefore, the presence of a general base (B_4 in Scheme 3) to abstract C_α proton is required to form the enolate.

4-Mono-, di-, tri-fluoro ethyl acetoacetate (**8b-d**) can all be converted into new products **15-17** based on LCMS analysis, with full consumption of substrates (Figure S10B-D). Increasing the sizes of

R_1 substituent in **8e-g** led to decrease in substrate conversions, although product (**18-20**) formation can still be clearly detected by LCMS (Figure S10E-G). When the *tert*-butyl substrate **8f** was used, only the mass of the uncyclized ketone **19** can be detected (Figure S10F). Formation of the cyclic Schiff base may be impeded by steric hindrances caused by two bulky substituents surrounding the ketone. Further increasing the sizes of R_1 substituent to **8i** and **8o** abolished conversion by CndF, indicating the cyclobutane β-keto ethyl ester **8g** is at the size limit of the CndF active site available for the nucleophile. Surprisingly, we observed ~50% consumption of the cyclopentanone-containing substrate **8h**, and the emergence of a product that matches the expected molecular weight of **21** (Figure S10H). NMR evidence for cyclopentanone incorporation into pipecolate is demonstrated in the next section (see **27**). This result indicates that CndF not only tolerates ethyl esters and R_1 substitutions, but also allows the R_2 position to be substituted. No product can be detected from ethyl 2-cyclohexanone-1-carboxylate **8j**, likely due to the increased size from **8h**. We also tested *N*-containing R_1 variants such as **8k** and **8l**, neither of which was consumed by the enzyme. The substitution of -NH_2 at R_1 position in **8k** increases pKa of C_α proton by 5 units and significantly reduces the nucleophilicity of the enolate. The amine in **8i** is protonated under assay conditions and may prevent binding in a presumably hydrophobic pocket in CndF that binds R_1, which may also explain the lack of reactivity of **8k.** Halogenated substituents **8m** and **8n** are also not recognized and may covalently inactivate CndF.[56]

A microbial platform to produce (2S, 6S)-6-alkyl pipecolate. The above data showed that CndF has considerable substrate promiscuity to form adducts between vinylglycine and different nucleophiles. However, the use of β-keto ethyl esters in vitro or in *E. coli* limits the utility of the enzyme to make alkyl-pipecolate derivatives, due to the inability of CndE to reduce the ester product **12**. The incorporation of [2,4-$^{13}C_2$]-**8a** to **1** using *A. nidulans* as a host showed that the ethyl esters can be converted to the corresponding β-keto carboxylates *in cellulo* by endogenous esterase and lipases (Figure 4A).[57] Encouraged by this finding, we explored the use of *A. nidulans* expressing CndF and CndE as a biotransformation host to convert various β-keto ethyl esters **8** into 6-alkyl-pipecolates (Figure 6). The esters were added to the *A. nidulans* culture and after growth for 4-5 days, formation of 6-alkyl-pipecolates was monitored by LCMS. New pipecolate compounds were extracted and purified from culture (Figure S11), and were structurally characterized by NMR (Figure 6).

We were able to obtain several 6-alkyl pipecolates by fermentation, with yields ranging from 1-5 mg/L. While the titers of molecules shown in Figure 6 are modest, we suspect the limiting substrate in *A. nidulans* is *O*-acetyl-L-homoserine **9**. Production of **9** completely relies on a single copy of HAT gene encoded in the genome. Increasing the pool of **9** by overexpressing additional copies of HAT gene may significantly improve the titer of the products.

The abilities of the different esters to be transformed into pipecolate generally match to what was observed *in vitro* (Figure 5), with several notable exceptions attributed to the removal of the ethyl ester *in cellulo*. For β-keto esters (**8e-g**) that can be consumed by CndF *in vitro* to give enamine esters, 6-substituted pipecolates **22**, **23**, and **24** were synthesized, respectively (Tables S9-S11, Figures S41-S58). Interestingly, the biosynthesis of **23** in the presence of the *tert*-butyl containing **8f** suggests that once the ethyl ester is hydrolyzed, the corresponding adduct can cyclize into the Schiff base. While **8i** was not transformed by CndF *in vitro*, we can detect and purify the corresponding 6-cyclopentane-pipecolate **25** from *A. nidulans* (Table S12, Figures S59-S64). This suggests that once the ethyl ester is hydrolyzed to the carboxylate, the active site of CndF can accommodate the bulky R_1 substituent. However, larger R_1 groups such as the phenyl group (**8o**) still cannot be recognized by CndF to make 6-phenyl-pipecolate. The formation of **22-25** also shows the SDR CndE can tolerate substantially larger substituents at C6 in performing imine reduction. The stereochemical configurations of these compounds have all been confirmed by NOESY analysis. There are no endogenous reductases in *A. nidulans* that can intercept the imine intermediates generated by CndF to produce diastereoisomers. Therefore, coupling CndF with a promiscuous *R*-specific imine reductase can potentially lead to the production of (2*S*, 6*R*)-6-alkyl pipecolate.[58]

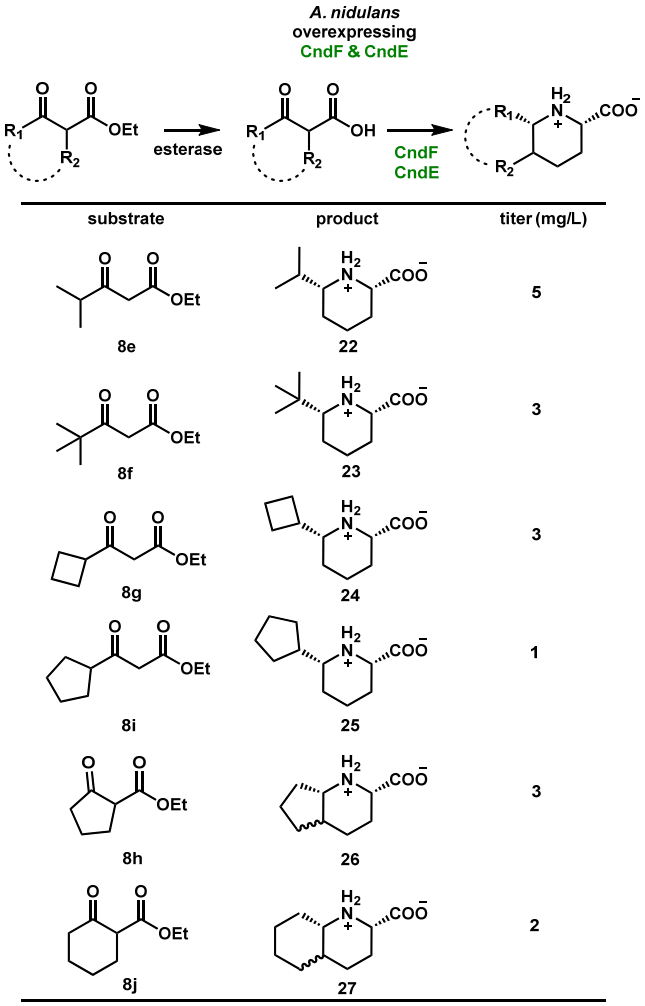

Figure 6. In vivo biosynthesis of substituted pipecolates.

In addition to **1**, we observed production of enamine **14** in large amounts from *A. nidulans* when **8a** is supplied (Figure S12A). When R_1 substituent is bulkier as in **8b** or **8c**, enamine formation becomes barely detectable (Figure S12A). We reasoned that the ethyl esters **8** is subjected to competing hydrolysis by esterases and C-C bond formation by CndF in *A. nidulans*. When R_1 substituent is small as in **8a**, the rates of hydrolysis and γ-substitution are comparable, which results in the formation of both enamine ester **14** and pipecolate **1**. When R_1 substituent becomes bulkier, the C-C bond formation rate

of ethyl ester is slower than that of ester hydrolysis, leading to the formation of nearly all 6-alkyl pipecolate products (Figure S12B).

Lastly, bicyclic **26** and **27** can be produced from ethyl 2-oxocyclopentanecarboxylate **8h** and ethyl 2-oxocyclohexanecarboxylate **8j**, respectively (Tables S13-15 and Figures S65-S82). Similar to **8i**, we did not observe enamine formation for **8j** in vitro, but **27** was detected and isolated *in vivo* as a result of ethyl ester hydrolysis. Both **8h** and **8j** were supplied as racemic mixtures due to facile racemization at the C_α position. From biotransformation, we observed a pair of diastereomers for both **26** and **27** at nearly 1:1 ratios (Figure S11). **8h** was converted to octahydro-1*H*-cyclopenta[b]pyridine-2-carboxylic acid $\mathbf{26}_{cis}$ and $\mathbf{26}_{trans}$ at 1:1 ratio, although we were only able to structurally characterize $\mathbf{26}_{cis}$ by NMR due to separation difficulties associated with $\mathbf{26}_{trans}$. Octahydro-1*H*-cyclopenta[b]pyridine-6-carboxylic acid, an analogue of **26**, is a conformationally restricted γ-aminobutyric acid (GABA) analogue.[59] Considering the noted neuroactivity of pipecolates,[60] we speculate that $\mathbf{26}_{cis}$ and $\mathbf{26}_{trans}$ could be useful as conformationally restricted analogues of L-pipecolates.[60-61] Similar to **8h**, **8j** is presumably hydrolyzed by *A. nidulans* esterase to yield racemic β-keto acids, which were converted to a pair of cyclic imines at 1:1 ratio by CndF. CndE can reduce the imines to either the *cis*-azadecalin $\mathbf{27}_{cis}$ or *trans*-azadecalin $\mathbf{27}_{trans}$, as confirmed by NMR analysis. Previous studies showed that racemic **27** produced by hydrogenation of quinoline-2-carboxylic acid is a potent inhibitor of Angiotensin I converting enzyme.[62] Coupling of CndF and CndE offers a biocatalytic route to produce decahydroquinoline-2-carboxylic acids. We reason that scrambling of the C5 stereocenter in **26** and **27** may occur as a result of β-decarboxylation after the C-C bond formation step, during which formation of an enol intermediate effectively scrambles the previously established C5 stereocenter.

SUMMARY

Abundant genome sequences have provided unprecedented opportunities to uncover new enzyme reactivities from natural product biosynthetic pathways. In this work, we identified a succinct, two-step pathway to synthesize the noncanonical amino acid (2*S*, 6*S*)-6-methyl pipecolate **1**. The first step is a C_γ-C_δ bond substitution reaction between *O*-acetyl L-homoserine and acetoacetate, catalyzed by a PLP-dependent enzyme. The second step is stereoselective Schiff base reduction catalyzed by an imine reductase. The substrate tolerances exhibited by the two enzymes enabled biocatalytic synthesis of a panel of 6-alkyl pipecolate derivatives. In addition, CndF can accept β-keto ethyl esters to generate enamine containing pipecolate molecules. CndF displays new catalytic mechanism in catalyzing γ-substitution and C-C bond formation using the PLP cofactor. CndF therefore represents an attractive starting point for biocatalyst engineering, as well interfacing with other enzymes or synthetic methodology to further elaborate the product structures.

ASSOCIATED CONTENT

AUTHOR INFORMATION

Corresponding Author

*Yi Tang yitang@ucla.edu

Notes

The authors declare no conflict of interest.

ACKNOWLEDGMENT

This work was supported by the NIH 1R35GM118056 to YT. Structural characterization by NMR is based upon work supported by the National Science Foundation under equipment grant no. CHE-1048804.We thank Drs. Y. Hai and W. Cheng for helpful discussions.

REFERENCES

1. Walsh, C. T.; O'Brien, R. V.; Khosla, C., Nonproteinogenic Amino Acid Building Blocks for Nonribosomal Peptide and Hybrid Polyketide Scaffolds. *Angew. Chem. Int. Ed.* **2013,** *52*, 7098-7124.
2. Hedges, J. B.; Ryan, K. S., Biosynthetic Pathways to Nonproteinogenic α-Amino Acids. *Chem. Rev.* **2019**.
3. Blaskovich, M. A. T., Unusual Amino Acids in Medicinal Chemistry. *J. Med. Chem.* **2016,** *59*, 10807-10836.
4. Baumann, M.; Baxendale, I. R., An overview of the synthetic routes to the best selling drugs containing 6-membered heterocycles. *Beilstein J. Org. Chem.* **2013,** *9*, 2265-2319.
5. White, C. J.; Yudin, A. K., Contemporary strategies for peptide macrocyclization. *Nat. Chem.* **2011,** *3*, 509-524.
6. Liu, C. C.; Schultz, P. G., Adding New Chemistries to the Genetic Code. *Annual Review of Biochemistry* **2010,** *79*, 413-444.
7. Lerchen, A.; Knecht, T.; Daniliuc, C. G.; Glorius, F., Unnatural Amino Acid Synthesis Enabled by the Regioselective Cobalt(III)-Catalyzed Intermolecular Carboamination of Alkenes. *Angew. Chem. Int. Ed.* **2016,** *55*, 15166-15170.
8. Kiss, L.; Fülöp, F., Synthesis of Carbocyclic and Heterocyclic β-Aminocarboxylic Acids. *Chem. Rev.* **2014,** *114*, 1116-1169.
9. Turner, N. J., Ammonia lyases and aminomutases as biocatalysts for the synthesis of α-amino and β-amino acids. *Curr. Opin. Chem. Biol.* **2011,** *15*, 234-240.
10. Steinreiber, J.; Fesko, K.; Reisinger, C.; Schürmann, M.; van Assema, F.; Wolberg, M.; Mink, D.; Griengl, H., Threonine aldolases—an emerging tool for organic synthesis. *Tetrahedron* **2007,** *63*, 918-926.
11. Wu, B.; Szymański, W.; Heberling, M. M.; Feringa, B. L.; Janssen, D. B., Aminomutases: mechanistic diversity, biotechnological applications and future perspectives. *Trends Biotechnol.* **2011,** *29*, 352-362.
12. Bornscheuer, U. T.; Huisman, G. W.; Kazlauskas, R. J.; Lutz, S.; Moore, J. C.; Robins, K., Engineering the third wave of biocatalysis. *Nature* **2012,** *485*, 185-194.
13. Zwick, C. R.; Renata, H., Remote C–H Hydroxylation by an α-Ketoglutarate-Dependent Dioxygenase Enables Efficient Chemoenzymatic Synthesis of Manzacidin C and Proline Analogs. *J. Am. Chem. Soc.* **2018,** *140*, 1165-1169.
14. Neugebauer, M. E.; Sumida, K. H.; Pelton, J. G.; McMurry, J. L.; Marchand, J. A.; Chang, M. C. Y., A family of radical halogenases for the engineering of amino-acid-based products. *Nat. Chem. Biol.* **2019,** *15*, 1009-1016.
15. Marchand, J. A.; Neugebauer, M. E.; Ing, M. C.; Lin, C. I.; Pelton, J. G.; Chang, M. C. Y., Discovery of a pathway for terminal-alkyne amino acid biosynthesis. *Nature* **2019,** *567*, 420-424.
16. Lukat, P.; Katsuyama, Y.; Wenzel, S.; Binz, T.; König, C.; Blankenfeldt, W.; Brönstrup, M.; Müller, R., Biosynthesis of methyl-proline containing griselimycins, natural products with anti-tuberculosis activity. *Chem. Sci.* **2017,** *8*, 7521-7527.
17. Wilson, K. P.; Yamashita, M. M.; Sintchak, M. D.; Rotstein, S. H.; Murcko, M. A.; Boger, J.; Thomson, J. A.; Fitzgibbon, M. J.; Black, J. R.; Navia, M. A., Comparative X-ray structures of the major binding protein for the immunosuppressant FK506 (tacrolimus) in unliganded form and in complex with FK506 and rapamycin. *Acta Crystallogr. D* **1995,** *51*, 511-521.
18. Graziani, E. I., Recent advances in the chemistry, biosynthesis and pharmacology of rapamycin analogs. *Nat. Prod. Rep.* **2009,** *26*, 602-609.
19. Barluenga, J.; Fernández, M. A.; Aznar, F.; Valdés, C., Catalytic imino-Diels–Alder reactions of 2-aminodienes: a simple entry into structurally diverse pipecolic acid derivatives. *Tetrahedron Lett.* **2002,** *43*, 8159-8163.
20. Kano, T.; Kumano, T.; Sakamoto, R.; Maruoka, K., Catalytic asymmetric synthesis of cyclic amino acids and alkaloid derivatives:

application to (+)-dihydropinidine and Selfotel synthesis. *Chem. Sci.* **2010,** *1*, 499-501.
21. Rutjes, F. P. J. T.; Schoemaker, H. E., Ruthenium-catalyzed ring closing olefin metathesis of non-natural α-amino acids. *Tetrahedron Lett.* **1997,** *38*, 677-680.
22. Davis, F. A.; Zhang, H.; Lee, S. H., Masked Oxo Sulfinimines (N-Sulfinyl Imines) in the Asymmetric Synthesis of Proline and Pipecolic Acid Derivatives. *Org. Lett.* **2001,** *3*, 759-762.
23. Pérez-García, F.; Max Risse, J.; Friehs, K.; Wendisch, V. F., Fermentative production of L-pipecolic acid from glucose and alternative carbon sources. *Biotechnol. J.* **2017,** *12*, 1600646.
24. Gatto, G. J.; Boyne, M. T.; Kelleher, N. L.; Walsh, C. T., Biosynthesis of Pipecolic Acid by RapL, a Lysine Cyclodeaminase Encoded in the Rapamycin Gene Cluster. *J. Am. Chem. Soc.* **2006,** *128*, 3838-3847.
25. Hartmann, M.; Kim, D.; Bernsdorff, F.; Ajami-Rashidi, Z.; Scholten, N.; Schreiber, S.; Zeier, T.; Schuck, S.; Reichel-Deland, V.; Zeier, J., Biochemical Principles and Functional Aspects of Pipecolic Acid Biosynthesis in Plant Immunity. *Plant Physiol.* **2017,** *174*, 124.
26. Wickwire, B. M.; Harris, C. M.; Harris, T. M.; Broquist, H. P., Pipecolic acid biosynthesis in Rhizoctonia leguminicola. I. The lysine saccharopine, delta 1-piperideine-6-carboxylic acid pathway. *J. Biol. Chem.* **1990,** *265*, 14742-7.
27. Li, L.; Tang, M.-C.; Tang, S.; Gao, S.; Soliman, S.; Hang, L.; Xu, W.; Ye, T.; Watanabe, K.; Tang, Y., Genome Mining and Assembly-Line Biosynthesis of the UCS1025A Pyrrolizidinone Family of Fungal Alkaloids. *J. Am. Chem. Soc.* **2018,** *140*, 2067-2071.
28. Luesch, H.; Hoffmann, D.; Hevel, J. M.; Becker, J. E.; Golakoti, T.; Moore, R. E., Biosynthesis of 4-Methylproline in Cyanobacteria: Cloning of nosE and nosF Genes and Biochemical Characterization of the Encoded Dehydrogenase and Reductase Activities. *J. Org. Chem.* **2003,** *68*, 83-91.
29. Yee, D. A.; Kakule, T. B.; Cheng, W.; Chen, M.; Chong, C. T. Y.; Hai, Y.; Hang, L. F.; Hung, Y.-S.; Liu, N.; Ohashi, M.; Okorafor, I. C.; Song, Y.; Tang, M.; Zhang, Z.; Tang, Y., Genome Mining of Alkaloidal Terpenoids from a Hybrid Terpene and Nonribosomal Peptide Biosynthetic Pathway. *J. Am. Chem. Soc.* **2020,** *142*, 710-714.
30. Tsuda, M.; Kasai, Y.; Komatsu, K.; Sone, T.; Tanaka, M.; Mikami, Y.; Kobayashi, J. i., Citrinadin A, a Novel Pentacyclic Alkaloid from Marine-Derived Fungus Penicillium citrinum. *Org. Lett.* **2004,** *6*, 3087-3089.
31. Mugishima, T.; Tsuda, M.; Kasai, Y.; Ishiyama, H.; Fukushi, E.; Kawabata, J.; Watanabe, M.; Akao, K.; Kobayashi, J. i., Absolute Stereochemistry of Citrinadins A and B from Marine-Derived Fungus. *J. Org. Chem.* **2005,** *70*, 9430-9435.
32. Kushida, N.; Watanabe, N.; Okuda, T.; Yokoyama, F.; Gyobu, Y.; Yaguchi, T., PF1270A, B and C, Novel Histamine H3 Receptor Ligands Produced by Penicillium waksmanii PF1270. *J. Antibiot.* **2007,** *60*, 667-673.
33. Bian, Z.; Marvin, C. C.; Martin, S. F., Enantioselective Total Synthesis of (−)-Citrinadin A and Revision of Its Stereochemical Structure. *J. Am. Chem. Soc.* **2013,** *135*, 10886-10889.
34. Kong, K.; Enquist, J. A.; McCallum, M. E.; Smith, G. M.; Matsumaru, T.; Menhaji-Klotz, E.; Wood, J. L., An Enantioselective Total Synthesis and Stereochemical Revision of (+)-Citrinadin B. *J. Am. Chem. Soc.* **2013,** *135*, 10890-10893.
35. Guerrero, C. A.; Sorensen, E. J., Concise, Stereocontrolled Synthesis of the Citrinadin B Core Architecture. *Org. Lett.* **2011,** *13*, 5164-5167.
36. Mercado-Marin, E. V.; Garcia-Reynaga, P.; Romminger, S.; Pimenta, E. F.; Romney, D. K.; Lodewyk, M. W.; Williams, D. E.; Andersen, R. J.; Miller, S. J.; Tantillo, D. J.; Berlinck, R. G. S.; Sarpong, R., Total synthesis and isolation of citrinalin and cyclopiamine congeners. *Nature* **2014,** *509*, 318-324.
37. Klas, K. R.; Kato, H.; Frisvad, J. C.; Yu, F.; Newmister, S. A.; Fraley, A. E.; Sherman, D. H.; Tsukamoto, S.; Williams, Robert M., Structural and stereochemical diversity in prenylated indole alkaloids containing the bicyclo[2.2.2]diazaoctane ring system from marine and terrestrial fungi. *Nat. Prod. Rep.* **2018,** *35*, 532-558.
38. Dan, Q.; Newmister, S. A.; Klas, K. R.; Fraley, A. E.; McAfoos, T. J.; Somoza, A. D.; Sunderhaus, J. D.; Ye, Y.; Shende, V. V.; Yu, F.; Sanders, J. N.; Brown, W. C.; Zhao, L.; Paton, R. S.; Houk, K. N.; Smith, J. L.; Sherman, D. H.; Williams, R. M., Fungal indole alkaloid biogenesis through evolution of a bifunctional reductase/Diels–Alderase. *Nat. Chem.* **2019,** *11*, 972-980.
39. Fraley, A. E.; Caddell Haatveit, K.; Ye, Y.; Kelly, S. P.; Newmister, S. A.; Yu, F.; Williams, R. M.; Smith, J. L.; Houk, K. N.; Sherman, D. H., Molecular Basis for Spirocycle Formation in the Paraherquamide Biosynthetic Pathway. *J. Am. Chem. Soc.* **2020,** *142*, 2244-2252.
40. Stegink, L. D.; Coon, M. J., Stereospecificity and Other Properties of Highly Purified β-Hydroxy-β-methylglutaryl Coenzyme A Cleavage Enzyme from Bovine Liver. *J. Biol. Chem.* **1968,** *243*, 5272-5279.
41. Eliot, A. C.; Kirsch, J. F., Pyridoxal Phosphate Enzymes: Mechanistic, Structural, and Evolutionary Considerations. *Annual Review of Biochemistry* **2004,** *73*, 383-415.
42. Du, Y.-L.; Ryan, K. S., Pyridoxal phosphate-dependent reactions in the biosynthesis of natural products. *Nat. Prod. Rep.* **2019,** *36*, 430-457.
43. Wiebers, J. L.; Garner, H. R., Acyl Derivatives of Homoserine as Substrates for Homocysteine Synthesis in Neurospora crassa, Yeast, and Escherichia coli. *J. Biol. Chem.* **1967,** *242*, 5644-5649.
44. Brzovic, P.; Holbrook, E. L.; Greene, R. C.; Dunn, M. F., Reaction mechanism of Escherichia coli cystathionine .gamma.-synthase: direct evidence for a pyridoxamine derivative of vinylglyoxylate as a key intermediate in pyridoxal phosphate dependent .gamma.-elimination and .gamma.-replacement reactions. *Biochemistry* **1990,** *29*, 442-451.
45. Zhang, Z.; Jamieson, C. S.; Zhao, Y.-L.; Li, D.; Ohashi, M.; Houk, K. N.; Tang, Y., Enzyme-Catalyzed Inverse-Electron Demand Diels–Alder Reaction in the Biosynthesis of Antifungal Ilicicolin H. *J. Am. Chem. Soc.* **2019,** *141*, 5659-5663.
46. Borthwick, A. D., 2,5-Diketopiperazines: Synthesis, Reactions, Medicinal Chemistry, and Bioactive Natural Products. *Chem. Rev.* **2012,** *112*, 3641-3716.
47. Singh, S.; Brocker, C.; Koppaka, V.; Chen, Y.; Jackson, B. C.; Matsumoto, A.; Thompson, D. C.; Vasiliou, V., Aldehyde dehydrogenases in cellular responses to oxidative/electrophilicstress. *Free Radical Biol. Med.* **2013,** *56*, 89-101.
48. Bhushan, R.; Brückner, H., Marfey's reagent for chiral amino acid analysis: A review. *Amino Acids* **2004,** *27*, 231-247.
49. Griswold, W. R.; Toney, M. D., Role of the Pyridine Nitrogen in Pyridoxal 5′-Phosphate Catalysis: Activity of Three Classes of PLP Enzymes Reconstituted with Deazapyridoxal 5′-Phosphate. *J. Am. Chem. Soc.* **2011,** *133*, 14823-14830.
50. Metzler, D. E.; Ikawa, M.; Snell, E. E., A General Mechanism for Vitamin B6-catalyzed Reactions1. *J. Am. Chem. Soc.* **1954,** *76*, 648-652.
51. Walsh, C. T., Biologically generated carbon dioxide: nature's versatile chemical strategies for carboxy lyases. *Nat. Prod. Rep.* **2020,** *37*, 100-135.
52. Han, L.; Vuksanovic, N.; Oehm, S. A.; Fenske, T. G.; Schwabacher, A. W.; Silvaggi, N. R., Streptomyces wadayamensis MppP is a PLP-Dependent Oxidase, Not an Oxygenase. *Biochemistry* **2018,** *57*, 3252-3264.
53. Faulkner, J. R.; Hussaini, S. R.; Blankenship, J. D.; Pal, S.; Branan, B. M.; Grossman, R. B.; Schardl, C. L., On the Sequence of Bond Formation in Loline Alkaloid Biosynthesis. *ChemBioChem* **2006,** *7*, 1078-1088.
54. Ye, Y.; Minami, A.; Igarashi, Y.; Izumikawa, M.; Umemura, M.; Nagano, N.; Machida, M.; Kawahara, T.; Shin-ya, K.; Gomi, K.; Oikawa, H., Unveiling the Biosynthetic Pathway of the Ribosomally Synthesized and Post-translationally Modified Peptide Ustiloxin B in Filamentous Fungi. *Angew. Chem. Int. Ed.* **2016,** *55*, 8072-8075.
55. Hofmann, D.; Kosower, E. M.; Wallenfels, K., The Effect of Solvent on Spectra. VII. The "Methyl Effect" in the Spectra of Dihydropyridines. *J. Am. Chem. Soc.* **1961,** *83*, 3314-3319.
56. Wang, E.; Walsh, C., Suicide substrates for the alanine racemase of Escherichia coli B. *Biochemistry* **1978,** *17*, 1313-1321.
57. Mayordomo, I.; Randez-Gil, F.; Prieto, J. A., Isolation, Purification, and Characterization of a Cold-Active Lipase from Aspergillus nidulans. *J. Agric. Food. Chem.* **2000,** *48*, 105-109.

58. Hussain, S.; Leipold, F.; Man, H.; Wells, E.; France, S. P.; Mulholland, K. R.; Grogan, G.; Turner, N. J., An (R)-Imine Reductase Biocatalyst for the Asymmetric Reduction of Cyclic Imines. *ChemCatChem* **2015,** *7*, 579-583.
59. Melnykov, K. P.; Volochnyuk, D. M.; Ryabukhin, S. V.; Rusanov, E. B.; Grygorenko, O. O., A conformationally restricted GABA analogue based on octahydro-1H-cyclopenta[b]pyridine scaffold. *Amino Acids* **2019,** *51*, 255-261.
60. Hallen, A.; Jamie, J. F.; Cooper, A. J. L., Lysine metabolism in mammalian brain: an update on the importance of recent discoveries. *Amino Acids* **2013,** *45*, 1249-1272.
61. Anna, J.; Rafal, K., Conformationally Restricted Peptides as Tools in Opioid Receptor Studies. *Curr. Med. Chem.* **2005,** *12*, 471-481.
62. Wright, G. C.; White, R. E. Decahydroquinoline-2-carboxylic acid compounds. U.S. Patent US4291163A, **1981**.

TOC Figure

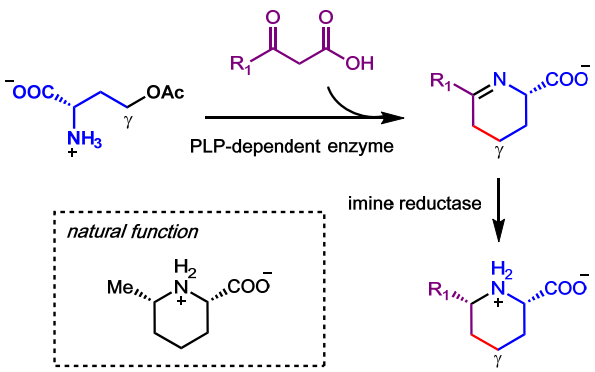
O
O
R1
OH
OOC
OAc
γ
NH3
PLP-dependent enzyme
R1
N
COO
γ
imine reductase
natural function
H2
N
Me
COO
H2
N
R1
COO
γ

Supporting Information

Discovery and Biocatalytic Application of a PLP-Dependent Amino Acid γ-Substitution Enzyme that Catalyzes C-C Bond Formation

Mengbin Chen,[1] Chun-Ting Liu,[1,3] Yi Tang[1,2]

[1]Department of Chemical and Biomolecular Engineering, University of California Los Angeles, Los Angeles, California 90095, United States
[2]Department of Chemistry and Biochemistry, University of California Los Angeles, Los Angeles, California 90095, United States
[3]Massachusetts Institute of Technology, Cambridge, Massachusetts 02139, United States

Email: yitang@ucla.edu

Table of Contents

1. Materials and Methods

1.1 Fungal genetics and culturing

Penicillium citrinum DSM1997 was cultivated on potato dextrose agar (BD) at 28 °C for 4-5 days. Genomic DNA extraction was carried out following the instructions of Zymo Quick-DNA Fungal/Bacterial Miniprep Kit. RNA extraction was carried out with Invitrogen RiboPure RNA purification Kit. RNA sample was then treated with DNase, followed by cDNA reverse transcription with Invitrogen SuperScript IV. Genes in the cluster of interest were amplified from cDNA by PCR using the primers in section 2.

Spores were collected from a potato dextrose agar (PDA) plate grown at 28 °C for 4-5 days. For gene disruption of *cndA*, Czapek Dox agar (Sigma-Aldrich) supplemented with 1.2 M sorbitol and 200 mg/mL hygromycin was used for protoplast regeneration and transformant selection.[1] After hygromycin-resistant transformants were obtained, first-round selection of transformants by metabolism profiling led to the identification of a transformant without citrinadin production. Gene disruption of this transformant, namely *P. citrinum ΔcndA*, was verified by PCR amplification of the target locus and neighboring loci using the corresponding primer deck.

1.2 Heterologous expression in *Aspergillus nidulans*

Plasmids used for heterologous expression in *Aspergillus nidulans* were constructed by yeast homologous recombination. Corresponding gene fragments were amplified from genomic DNA of *P. citrinum* DSM 1997, and were ligated to double-digested pYTU and pYTR-based vectors. After confirming the DNA sequences of the plasmids as shown below, heterologous expression in *Aspergillus nidulans* was carried out as described in previous studies.[2] Briefly, protoplast was transformed with different combinations of plasmids and grown on CD-sorbitol agar at 37 °C for 2-3 days. Depending on the nature of the following experiments, transformants were then transferred to CD agar or CDST agar and grown at 28 °C for 3-4 days.

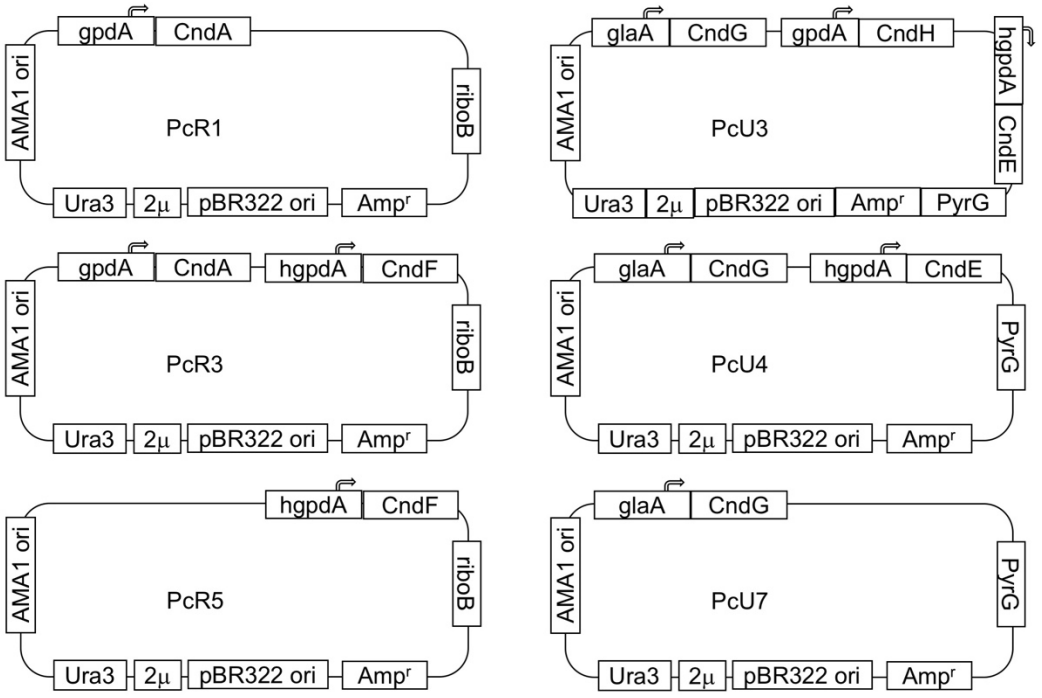

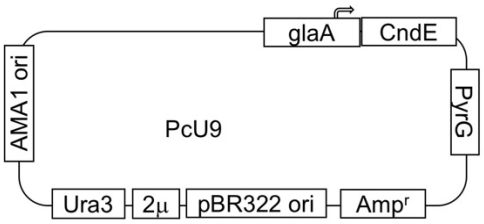

1.3 Compound identification, isolation, and characterization

To detect compound production from heterologous expression in *A. nidulans*, a single transformant was grown on CDST agar (2% starch, 2% casein, 50 mL/L nitrate salts, 2 mL/L trace elements, 1.5% Bacto agar) at 28 °C for 3-4 days. A chunk of agar with dense fungal mycelia was scraped and vortexed with 300 μL of acetone for 2 minutes. Crude extract was obtained by centrifugation to spin down the insoluble portion, and was dried *in vacuo*. The residual was subsequently dissolved in methanol and was subject to LC-MS analysis. All LC-MS analyses were performed on a Shimadzu 2020 EVLC-MS system (Phenomenex Kinetex, 1.7 μm, 2.0 x 100 mm, C18 column) using positive and negative mode electrospray ionization at a flow rate of 0.3 mL/min using the following gradient of solvents A (0.1% formic acid in water) and B (0.1% formic acid in acetonitrile): holding 5% B for 0.25 min, followed by a 13-min linear gradient of 5-95%, and finished with holding at 95% for 4.75 min.

For isotope labeling experiment, *A. nidulans* transformant was grown on CD agar (1% glucose, 50 mL/L nitrate salts, 2 mL/L trace elements, 1.5% Bacto-agar) supplemented with 1 mg/mL ethyl acetoacetate (2,4-$^{13}C_2$, 99%, Cambridge Isotope Laboratories) at 28 °C for 3 days. Metabolic analysis was carried out in a similar fashion as aforementioned.

To access unnatural alkyl pipecolate, 0.5-5 mM β-keto acid ester was supplemented to CD agar where *A. nidulans* transformants grew. Metabolic analysis was carried out after 3-day growth at 28 °C. For compound isolation, spores of *A. nidulans* transformant harboring CndE and CndF were spread on 1-liter CD agar supplemented with corresponding β-keto acid ester that was evenly poured in 15x150 mm petri dishes. After 4-day growth at 28 °C, solid culture was cut into small pieces and was extracted extensively with acetone. Crude extract was evaporated in vacuo, and the remaining aqueous phase was acidified by 1M hydrochloric acid until pH reaches 1. Clarified supernatant was obtained by centrifugation at 5,000 g for 15 min, and was subsequently applied to a 10x2.5 cm column packed with cation-exchange Dowex 50WX8 resin (hydrogen form 200-400 mesh). The resin was pre-treated with extensive washes by 0.1M sodium hydroxide, water, methanol, and pre-equilibrated in 0.1M hydrochloric acid. After loading the supernatant, the column was washed with 0.1M hydrochloric acid (300 mL), and followed by 0.1M hydrochloric acid in methanol (300 mL). The majority of the alkyl pipecolic acid was eluted during the methanol wash. The remaining was eluted by 2M ammonium hydroxide. Fractions with most abundant target compound were combined and concentrated, and were subjected to reverse-phase HPLC chromatography with a COSMOSIL column (Nacalai Tesque Inc., C18 AR-II, flowrate 4 mL/min). A linear gradient wash of water/methanol (5-20% over 15 minutes) supplemented with 0.1% formic acid was applied. Gradients for purifying different alkyl pipecolates were slightly adjusted. Purified alkyl pipecolates were then characterized by NMR and HRMS.

As for dipeptide large-scale production and purification, *A. nidulans* transformant was grown on 1-liter CD agar or CDST agar at 28 °C for 4-5 days. After extensive extraction by acetone, crude extract was evaporated in vacuo, and the remaining aqueous phase was extracted with ethyl acetate. The organic layer contained dipeptide alcohol and was dried in vacuo. The residual was loaded on a Teledyne Redisep Rf Gold Reversed-phase C18 column and was subject to flash chromatography with a gradient of water/acetonitrile supplemented with 0.1% formic acid.

Fractions containing **7** were combined and concentrated, and was further purified by reverse-phase HPLC chromatography with a COSMOSIL column (Nacalai Tesque Inc., C18 MS-II, flowrate 4 mL/min). A linear gradient wash of water/acetonitrile (5-50% over 20 minutes) supplemented with 0.1% formic acid was applied. On the other hand, **6** remained in the aqueous phase after ethyl acetate extraction. Crude sample containing **6** was loaded onto a column packed with Amberlite XAD-16N resin (Sigma-Aldrich). **6** was eluted with 30-50% methanol in water. Fractions were combined and concentrated, and **6** was purified via similar steps (flash chromatography followed by reverse-phase HPLC chromatography).

To access compound **14**, 1 liter LB media inoculated with *E.coli* BL21(DE3) harboring plasmid pCDFDuet-1 expressing homoserine O-acetyltransferase (HAT) and CndF was grown until OD_{600} reached 1.0. 0.1 mM IPTG was added after the culture was cooled down to 25 °C to induce protein expression. The production of **14** was monitored after 3, 6, and 12 hrs, and we found that it peaked after 6 hrs. Cells were collected by centrifugation, and were subsequently disrupted by acetone to extract **14**. Crude extract was dried *in vacuo*, and resulting residue was combined with media to incubate with XAD-16N resin overnight. The resin was then packed onto a column, and washed with water, 10% methanol in water, 20% methanol in water, 30% methanol in water, and methanol. **14** was most abundant in 10% and 20% methanol elution. These two fractions were combined and dried, and further purified by HPLC with a COSMOSIL column (Nacalai Tesque Inc., C18 AR-II, flowrate 4 mL/min).

NMR spectra were acquired on a Bruker AV500 spectrometer with a 5 mm dual cryoprobe (^{1}H 500 MHz, ^{13}C 125 MHz). HRMS measurements were carried out on a Thermo Exactive Plus Orbitrap with IonSense ID-CUBE DART source.

1.4 Protein expression and purification

E.coli BL21(DE3) was transformed with N-terminal hexa-histidine tagged CndF via heat shock. A single colony selected by growing on kanamycin-supplemented (50 mg/mL) LB agar plates was inoculated to 5x5-mL LB starting culture with kanamycin and grew overnight with aeration at 37 °C. The overnight culture was then inoculated to 5x1-liter LB medium supplemented with kanamycin. After OD_{600} reached 0.8-1.0, the culture was cooled down to 16 °C, and protein expression was induced with 0.1 mM IPTG. The culture was continued to grow at 16 °C with aeration for 20 hrs, and cells were collected by centrifugation and stored at -80 °C. Cell pellets were resuspended in buffer A (50 mM K_2HPO_4, 200 mM NaCl, 5% glycerol, pH 7.8) supplemented with 40 μM PLP. Sonication (QSonica, 1 s pulse on, 2 s pulse off, 50% amplitude, 10-min total sonication time) was used to lyse the cells on ice. Cell debris was clarified by centrifugation, and supernatant was incubated with Ni-NTA resin for 1 hr at 4 °C. CndF was purified by washing the resin with increasing imidazole concentration in buffer A supplemented with 40 μM PLP. Fractions of CndF were analyzed by SDS-PAGE gel, and most concentrated ones were combined and concentrated by Amicon Ultra centrifugal filters (Millipore, EMD). Concentrated CndF was flash frozen by liquid nitrogen and stored at -80 °C. Protein concentrations were determined by Bradford assays.

Expression and purification procedure of CndE were similar as aforementioned, except that CndE was constructed with a C-terminal hexa-histidine affinity tag, and the selection antibiotic is ampicillin at 100 mg/mL.

1.5 Derivatization methods used in this study

1.5.1 Marfey's reagent derivatization

N^{α}-(2,4-Dinitro-5-fluorophenyl)-L-alaninamide (Marfey's reagent) was purchased from TCI, and derivatization was carried out as described in previous reports.[3] Marfey's reagent was dissolved in acetone to make a solution of 1.5%. Purified **1** was dissolved in water to a final concentration of 50 mM. *Rac-cis*-6-methyl pipecolate (Item #: D753872) was purchased from

Discovery Molecules. 100 μL of 1.5% Marfey's reagent acetone solution was added to 50 μL of **1**, followed by the addition of 20 μL of 1M $NaHCO_3$. The reaction mixture was incubated at 40 °C for 1 hr, and quenched with 10 μL of 2M HCl. The quenched reaction was diluted 10 fold with methanol, and subject to analysis by Agilent Q-TOF 6545 with a 3.0x50mm Agilent InfinityLab Poroshell 120 EC-C18 column. The gradient applied was 30-70% of water/acetonitrile supplemented with 0.1% trifluoroacetic acid over 11 minutes.

1.5.2 Fmoc-Cl derivatization

Fmoc-Cl derivatization was used to determine that CndF and CndE catalyze tandem reactions to give **1**. Purified equimolar CndE and CndF (28 μM final concentration) were incubated with **9** (1 mM), **10** (1 mM), NADPH (1 mM), and $Co(NO_3)_2$ (2.5 mM) in 50 mM phosphate buffer (pH 6.5) for 1 hour at room temperature. The reaction was then dried in *vacuo*, and was resuspended in 120 μL of 83% acetonitrile in water. Any precipitate would be cleared by centrifugation at this step. 10 μL 0.2 M sodium borate (pH 10.5) and 10 μL 100 mM Fmoc-Cl was added to the resuspended solution. The mixture was incubated at 50 °C for 30 min, and was subject to LC-MS analysis.

1.5.3 *O*-aminobenzaldehyde (*o*AB) derivatization

After reaction of interest was quenched with 3 volumes of acetonitrile, ~ 2 mg oAB solid was directly added to the quenched reaction and incubated at room temperature for 5 minutes. The mixture was then applied to LC-MS for analysis.

1.6 In vitro conversion of β-keto esters by CndF

In a 50 μL reaction, O-acetyl L-homoserine (final concentration: 8 mM) and β-keto esters (final concentration: 2 mM) was added into 50 mM phosphate buffer (pH 6.5) supplemented with 2.5 mM $Co(NO_3)_2$. 35 μM CndF was added last to initiate the reaction. Reactions were incubated at room temperature for 12 hrs, and were quenched with 3 volumes of acetonitrile. Protein precipitate was clarified by centrifugation. The supernatant was subject to Shimadzu LC-MS analysis as described in 1.3. Standard curves were constructed with β-keto esters of known concentrations. Conversions by CndF were calculated by quantifying the remaining amounts of β-keto esters after reactions were quenched.

2. Oligomers used in this study.

Primers	Sequences
NTHLIC_CndF_1	CCATGAAAACCTGTACTTCCAATCCAATATGCGCGATCCCAATTTCCAAAATATTGAC
NTHLIC_CndF_2	CGAATTCGGATCCGTTATCCACTTCCAATTTAGCGCTCGCTTTTGCAAAATGTTG
CTHLIC_CndE_fw	GTTTAACTTTAAGAAGGAGATATAGTTATGAAATATAGCCACCAGGATATGACG
CTHLIC_CndE_rv	TGAGAGCCGGATTGGAAGTAGAGGTTAGCGTAGTTCTGGTGCCAAACATG
PcR1_ATCATR_fwb	ATTACCCCGCCACATAGACACATCTAAACAATGCATTCAACAGCAATCGCATCCGAAGCA
ATCATR_M1	GGATGGTTTGGTTAGCCCAACAGTGCG
ATCATR_M2	CGCGAAATCTGACATACAAAATGCGACAG
PcR3_0	CTCTCTGCGTCCGTCCGTCTCTCCGCATGGTTTGGGTGTTGTTTACCCTCATCCTTCT
PcR3_1b	GGTAAACAACACCCAAACCATGCGGAGAGACGGACGGACGCAGAGAGA
PcR3_2	GTCAATATTTTGGAAATTGGGATCGCGCATGGGAAAAGAAAGAGAAAAGAAAAGAGCAGC
PcR3_3	GCTGCTCTTTTCTTTTCTCTTTCTTTTCCCATGCGCGATCCCAATTTCCAAAATATTGAC
PcR3_4b	TAAAGGGTATCATCGAAAGGGAGTCATCCAGTAAACAAACCCTAATTTACTCGTGGCATA
PcR1_ATCATR_rv	GATATCGAATTCCTGCAGCCCGGGGGATCCGTTTGGGTGTTGTTTACCCTCATCCTTCTG
PcR5_1	ATTACCCCGCCACATAGACACATCTAAACAATGCGCGATCCCAATTTCCAAAATATTGAC
PcR5_2	CTAAAGGGTATCATCGAAAGGGAGTCATCCGTAAACAAACCCTAATTTACTCGTGGCATA
PcU3_1	CAGCATCATTACACCTCAGCATTAATTAAATGACGATCACAGAATCACCATTTGTGCG
PcU3_2	CCCGTCACCCAAATCAATTCACCGGAGTCCTACTACATAGCTAGTTTCCTGTAAAA
PcU3_3	TTTTACAGGAAACTAGCTATGTAGTAGGACTCCGGTGAATTGATTTGGGTGACGGG
PcU3_4	CTGGAAGTTGATGCTGGGCTTTCAACATTGTTTAGATGTGTCTATGTGGCGGGGTA

PcU3_5	TACCCCGCCACATAGACACATCTAAACAATGTTGAAAGCCCAGCATCAACTTCCAG
PcU3_6	TCTCTCTGCGTCCGTCCGTCTCTCCGCATGGGAATCTTGCACAGTTAAAATGCGTTGATC
PcU3_7	GATCAACGCATTTTAACTGTGCAAGATTCCCATGCGGAGAGACGGACGGACGCAGAGAGA
PcU3_8	CAACGTCATATCCTGGTGGCTATATTTCATGGGAAAAGAAAGAGAAAAGAAAAGAGCAGC
PcU3_9	GCTGCTCTTTTCTTTTCTCTTTCTTTTCCCATGAAATATAGCCACCAGGATATGACGTTG
PcU3_10	GGGATCCACTAGTTCTAGAGCGGCCGCCGTTTGGGAGTATTGATGGGTATTGAAAG
PcU4_2	TCTCTCTGCGTCCGTCCGTCTCTCCGCATGCCTACTACATAGCTAGTTTCCTGTAAAAAG
PcU4_3	CTTTTTACAGGAAACTAGCTATGTAGTAGGCATGCGGAGAGACGGACGGACGCAGAGAGA
PcU7_0	GGGGGATCCACTAGTTCTAGAGCGGCCGCCCCTACTACATAGCTAGTTTCCTGTAAAAAG
PcU9_1	CTTCATCCCCAGCATCATTACACCTCAGCAATGAAATATAGCCACCAGGATATGACGTTG
pcdfduet_HAT_5'__F	TTTAACTTTAATAAGGAGATATACCATGGTCGAAACCAGTGGTGCTCCTG
pcdfduet_HAT_5'_R	ACCATGGTATATCTCCTTATTAAAGTTAAACAAAATTATTTCTACAGGGG
pcdfduet_HAT_3'_F	AGTCGAGGATATTACCGCGTGGTAAAGCTTGCGGCCGCATAATGCTTAAG
pcdfduet_HAT_3'_R	CTTAAGCATTATGCGGCCGCAAGCTTTACCACGCGGTAATATCCTCGACT
pcdfduet_CndF_5'_F	GTTAAGTATAAGAAGGAGATATACAATGCGCGATCCCAATTTCCAAAATA
Pcdfduet_CndF_5'_R	GGGATCGCGCATTGTATATCTCCTTCTTATACTTAAC
pcdfduet_CndF_3'_F	ACAACATTTTGCAAAAGCGAGCGCTAATAACCTAGGCTGCTGCCACC
pcdfduet_CndF_3'_R	TCAGCGGTGGCAGCAGCCTAGGTTATTAGCGCTCGCTTTTGCAAAATGTT

3. Supplementary Tables

Table S1. ^{1}H spectrum data of citrinadin A ($CDCl_3$, 500 MHz) in comparison with published data.[4-5]

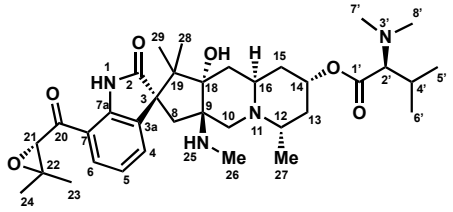

citrinadin A

Position	δ_H (mult.) (salt)	Citrinadin A (bis-salt)[I]	Citrinadin A (free base)[II]
1	9.70 (s)	9.61	9.51
2			
3			
3a			
4	7.62 (d, 7.6)	7.66	7.67
5	7.18 (m)	7.19	7.13
6	7.79 (d, 8.0)	7.78	7.74
7			
7a			
8	2.17 (m)	2.2	2.09, 2.05
9			
10	3.33 (d, 11.6 Hz)	3.26	3.16
	3.89 (m)	3.81	2.56
11		11.27	
12	3.60 (m)	3.69	3.03
13	1.70 (m)	1.88	1.77
	3.42 (m)	3.47	2.03
14	5.35 (m, overlap)	5.43	5.2
15	2.04 (m)	2	1.49
	1.92 (m)	3.13	1.8
16	4.10 (m)	4.07	3.18
17	1.90 (m)	1.8	1.35
	2.12 (m)	2.17	1.53
18			
18-OH	5.31 (s)	5.38	4.55
19			
20			
21	4.04 (s)	4.05	4.02
22			
23	1.59 (s)	1.6	1.58
24	1.27 (s)	1.37	1.27
25			
26	2.35 (s)	2.5	2.28
27	1.56 (d, 7.2 Hz)	1.59	1.2
28	1.01 (s)	1.02	0.98
29	1.37 (s)	1.37	1.35
1'			
2'	3.76 (d, 12.2)	3.77	2.68
3'			
4'	2.30 (m)	2.4	2.01
5'	1.10 (d, 6.9 Hz)	1.07	0.88
6'	0.96 (d, 6.6 Hz)	1.35	0.96
7'	2.62 (s)	2.99	2.29
8'	2.62 (s)	2.94	2.29

[I] Tsuda et al., Org. Lett., 2004, 6, 3087-3089.
[II] Bian et al., J. Am. Chem. Soc., 2013, 135, 10886-10889.

Table S2. ^{13}C spectrum data of citrinadin A ($CDCl_3$, 125 MHz) in comparison with published data.[4-5]

Position	δ_C (bis-salt)	Citrinadin A (bis-salt)[I]	Citrinadin A (bis-HCl salt)[II]
1			
2	185.58	184.89	184.99
3	60.70	60.42	60.47
3a	134.74	134.52	134.51
4	133.39	133.3	133.28
5	122.79	122.49	122.52
6	127.88	127.64	127.68
7	117.81	117.52	117.59
7a	142.79	142.67	142.71
8	41.69	41.52	41.62
9	67.90	67.9	67.97
10	51.37	51.31	51.34
11			
12	56.24	56.12	56.22
13	missing	32.7	32.75
14	missing	68.92	a
15	33.24	33.34	33.43
16	47.41	47.48	47.52
17	31.20	31.35	31.44
18	82.45	82.13	82.21
19	50.76	51	51.03
20	missing	194.84	194.84
21	64.25	64.06	64.06
22	61.99	61.72	61.72
23	24.5	24.31	24.33
24	18.81	18.62	18.65
25			
26	29.70	30.57	30.6
27	15.89	15.21	15.29
28	22.01	21.93	21.92
29	27.96	27.96	28
1'	165.65	166.72	missing
2'	72.43	71.38	missing
3'			
4'	28.16	28.35	28.25
5'	19.86	19.47	19.55
6'	21.27	21.37	b
7'	38.78	38.34	missing
8'	missing	43.14	missing

[I] Tsuda et al., Org. Lett., 2004, 6, 3087-3089.

[II] Bian et al., J. Am. Chem. Soc., 2013, 135, 10886-10889. [a] Bian et al. observed δ_c 68.5 ppm through HSQC; [b]Bian et al. observed δ_c 21.3 ppm through HSQC.

Table S3. Spectroscopic data of **1** in CD_3OD.

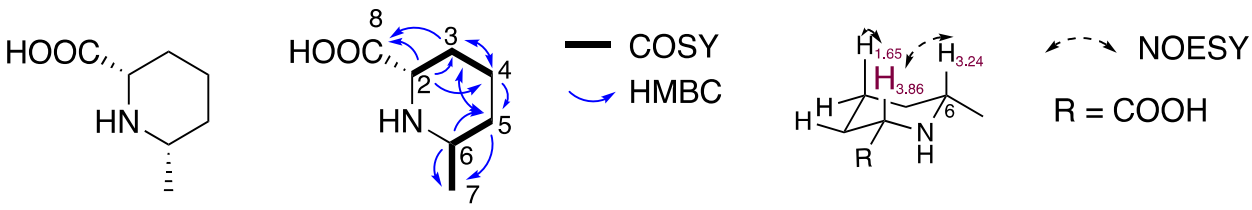

Position	δ_C	δ_H (mult.)
2	59.5	3.86 (dd, 1H, *J* = 12.35 Hz, 2.90 Hz)
3	27.4	1.61 (m, 1H), 2.32 (m, 1H)
4	23.9	1.65 (m, 1H), 1.95 (m, 1H)
5	31.3	1.94 (m, 1H), 1.44 (m, 1H)
6	54.5	3.24 (m, 1H)
7	19.5	1.38 (d, 3H, *J* = 6.57 Hz)
8	172	

HRMS (ESI, $M+H^+$) calculated for $C_7H_{14}NO_2$ 144.1024; found 144.1019.

$[\alpha]_D^{21}$ = -8 (c=0.01, MeOH).

Table S4. Spectroscopic data of [5, 7-^{13}C]-**1** in CD_3OD.

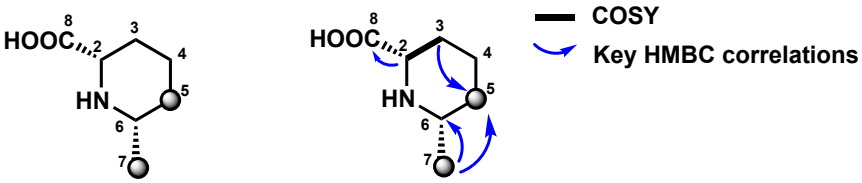

Position	δ_C	δ_H (mult.)
2	60.1	3.90 (m, 1H)
3	27.9	1.65 (m,1H), 2.36 (m,1H)
4	26.9	2.20 (m, 1H), 2.52(m, 1H)
5 (^{13}C)	31.9	1.96 (m, 1H), 1.68 (m, 1H)
6	55.1 (t)	3.24 (m, 1H)
7 (^{13}C)	20	1.38 (m, 3H)
8	172.2	

Table S5. Spectroscopic data of **6** in CD_3OD.

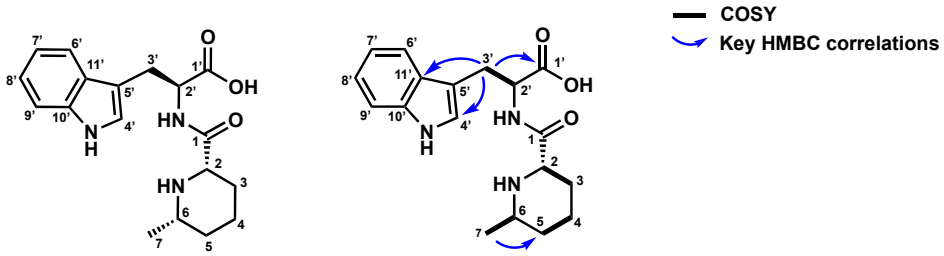

Position	δ_C	δ_H (mult.)
1	170.6	
2	60.8	3.55 (m, 1H)
3	28.7	2.12 (m, 1H), 1.33 (m, 1H)
4	24.3	1.49 (m, 1H), 1.83 (m, 1H)
5	31.9	1.76 (m, 1H), 1.31 (m, 1H)
6	54.2	2.99 (m, 1H)
7	20.2	1.25 (d, 3H, *J* = 6.5 Hz)
1‘	178.6	
2'	57.8	4.62 (m, 1H)
3'	29.4	3.39 (m, 1H), 3.23 (m, 1H)
4'	124.7	7.15 (s, 1H)
5'	112.7	
6‘	120.0	7.68 (d, 1H, J = 7.9 Hz)
7‘	119.8	7.01 (m, 1H)
8‘	122.4	7.10 (m, 1H)
9'	112.3	7.33 (d, 1H, *J* = 8.1 Hz)
10'	138.2	
11'	129.6	

HRMS (ESI, M+H$^+$) calculated for $C_{18}H_{24}N_3O_3$ 330.1818; found 330.1795.

$[\alpha]_D^{20}$ = -2 (c=0.01, MeOH).

Table S6. Spectroscopic data of **7** in CD_3OD.

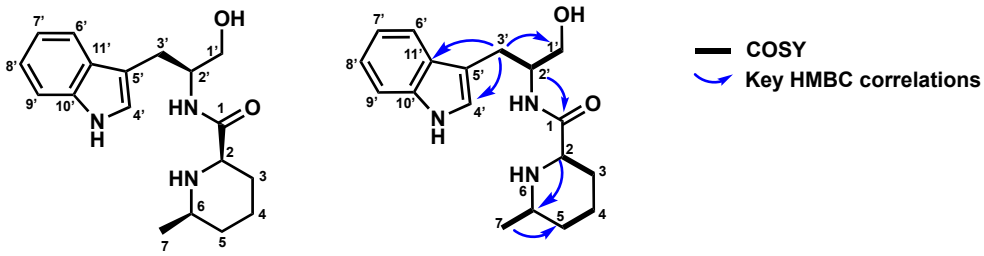

Position	δ_C	δ_H (mult.)
1	170.8	
2	61.0	3.67 (m, 1H)
3	29.4	1.64 (m, 1H), 2.21 (m, 1H)
4	24.6	1.95 (m, 1H), 1.65 (m, 1H)
5	31.9	1.93 (m, 1H), 1.45 (m, 1H)
6	54.9	3.18 (m, 1H)
7	20.1	1.33 (d, 1H, *J* = 6.3 Hz)
1'	65.0	3.62 (m, 2H)
2'	54.6	4.29 (m, 1H)
3'	28.6	3.06 (m, 1H), 2.97 (m, 1H)
4'	125.0	7.13 (s, 1H)
5'	112.9	
6'	120.3	7.65 (d, 1H, *J* = 8.1 Hz)
7'	120.5	7.03 (m, 1H)
8'	123.2	7.11 (m, 1H)
9'	113.1	7.34 (d, 1H, *J* = 8.1 Hz)
10'	139.0	
11'	129.7	

HRMS (ESI, M+H$^+$) calculated for $C_{18}H_{26}N_3O_2$ 316.2025; found 316.2025.

$[\alpha]_D^{20}$ = -16 (c=0.01, MeOH).

Table S8. Spectroscopic data of **14** in CD_3OD.

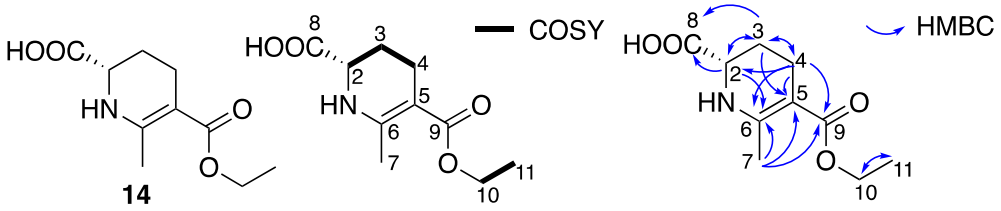

Position	δ_C	δ_H (mult.)
2	55.3	3.97 (m, 1H)
3	26.2	2.05 (m, 1H), 1.97 (m, 1H)
4	23.0	2.32 (m, 1H), 2.45 (m, 1H)
5	92.6	
6	156.1	
7	22.2	2.27 (s, 3H)
8	176.9	
9	171.9	
10	60.8	4.10 (q, 2H, 7.11 Hz)
11	15.8	1.27 (t, 3H, 7.11 Hz)

HRMS (ESI, $M+H^+$) calculated for $C_{10}H_{16}NO_4$ 214.1079; found 214.1035.

Table S9. Spectroscopic data of **22** in CD_3OD.

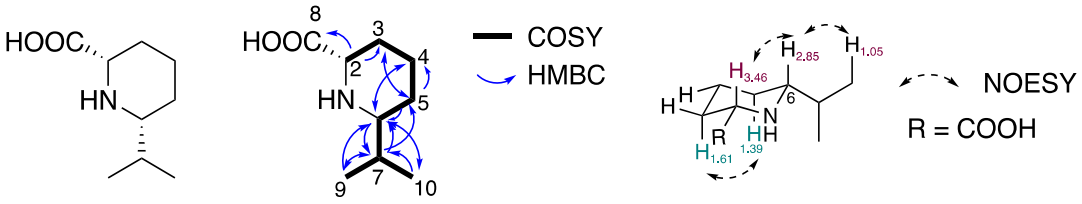

Position	δ_C	δ_H (mult.)
2	62.6[a]	3.46 (dd, 1H, *J* = 11.55 Hz, 2.35 Hz)
3	27.9	2.35 (m, 1H), 1.61 (m, 1H)
4	24.3	1.58 (m, 1H), 1.99 (m, 1H)
5	26	1.39 (m, 1H), 1.95 (m, 1H)
6	63.6	2.85 (m, 1H)
7	32.5	1.97 (m, 1H)
8	174.0[b]	
9	19.6	1.09 (d, 3H, 7.01 Hz)
10	18.3	1.05 (d, 3H, 6.81 Hz)

[a]Signal of C_2 was weak from ^{13}C spectrum, HSQC correlation was used to determine the chemical shift. [b]Signal of C_8 was weak from ^{13}C spectrum, HMBC correlation with H_2 was used to determine C_8 chemical shift.

HRMS (ESI, $M+H^+$) calculated for $C_9H_{18}NO_2$ 172.1337; found 172.1332.

$[\alpha]_D^{20}$ = -16 (c=0.01, MeOH).

Table S10. Spectroscopic data of **23** in CD_3OD.

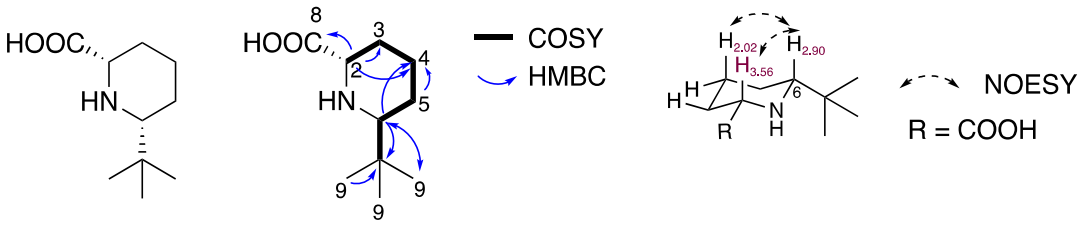

Position	δ_C	δ_H (mult.)
2	64.0[a]	3.56 (m, 1H)
3	27.6	2.31 (m, 1H), 1.63 (m, 1H)
4	24.9	2.02 (m, 2H)
5	24.5	1.59 (m, 1H), 1.48 (m, 1H)
6	67.6	2.90 (d, 1H, *J* = 11.91 Hz)
7	34.3	
8	174.7[b]	
9	26.8	1.09 (s, 9H)

[a]Signal of C_2 was weak from ^{13}C spectrum, HSQC correlation with H_2 was used to determine C_2 chemical shift. [b]Signal of C_8 was weak from ^{13}C spectrum, HMBC correlation with H_2 was used to determine C_8 chemical shift.

HRMS (ESI, M+H$^+$) calculated for $C_{10}H_{20}NO_2$ 186.1494; found 186.1489.

$[\alpha]_D^{21}$ = -16 (c=0.01, MeOH).

Table S11. Spectroscopic data of **24** in CD_3OD.

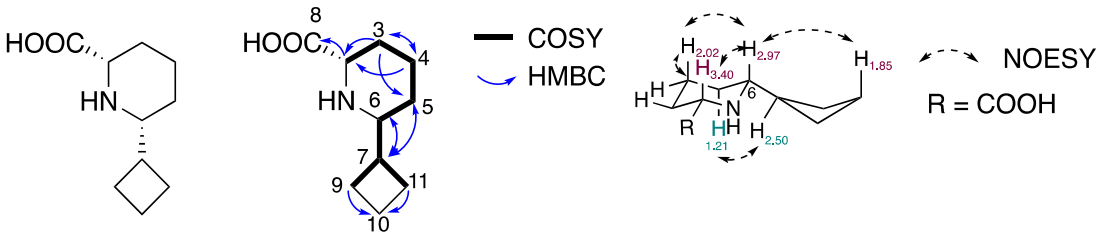

Position	δ_C	δ_H (mult.)
2	61.1[a]	3.4 (dd, 1H, *J* = 12.14 Hz, 3.19 Hz)
3	28.5	1.55 (m, 1H), 2.32 (m, 1H)
4	24.1	1.92 (m, 1H), 1.56 (m, 1H)
5	26.8	1.21 (m, 1H), 1.88 (m, 1H)
6	62.9	2.97 (ddd, 1H, J = 12.23 Hz, 8.51 Hz, 3.04 Hz)
7	39.7	2.50 (m, 1H)
8	174.5[b]	
9	26.8	1.95 (m, 1H), 2.10 (m, 1H)
10	19.1	1.85 (m, 1H), 1.99 (m, 1H)
11	26.4	2.04 (m, 1H), 2.11 (m, 1H)

[a]Signal of C_2 was weak from ^{13}C spectrum, HSQC correlation with H_2 was used to determine C_2 chemical shift. [b]Signal of C_8 was weak from ^{13}C spectrum, HMBC correlation with H_2 was used to determine C_8 chemical shift.

HRMS (ESI, M+H$^+$) calculated for $C_{10}H_{18}NO_2$ 184.1338; found 184.1332.

$[\alpha]_D^{21}$ = -22 (c=0.01, MeOH).

Table S12. Spectroscopic data of **25** in CD_3OD.

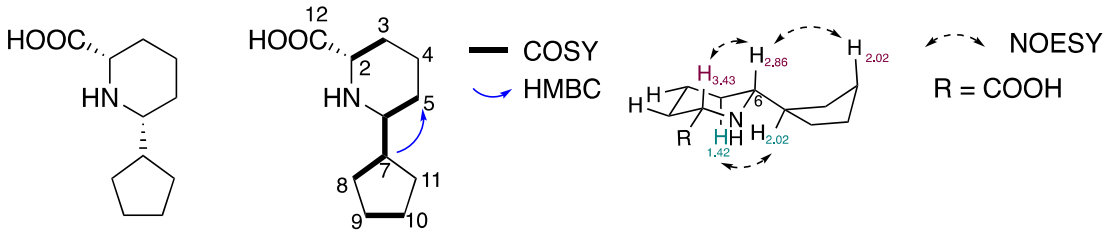

Position	δ_C	δ_H (mult.)
2	61.5[a]	3.43 (m, 1H)
3	27.2	2.32 (m, 1H), 1.58 (m, 1H)
4	23.4	1.94 (m, 1H), 1.58 (m, 1H)
5	28.3	2.01 (m, 1H), 1.41 (m, 1H)
6	63.0	2.86 (ddd, 1H, *J* = 12.23 Hz, 8.51 Hz, 3.04 Hz)
7	45.5	2.02 (m, 1H)
8	30.8	1.29 (m, 1H), 1.33 (m, 1H)
9	26.0	1.76 (m, 1H), 1.67 (m, 1H)
10	22.8	1.98 (m, 1H), 2.02 (m, 1H)
11	30.7	1.89 (m, 1H), 1.87 (m, 1H)
12	176.4	

[a]Signal of C_2 was weak from ^{13}C spectrum, HSQC correlation with H_2 was used to determine C_2 chemical shift.

HRMS (ESI, $M+H^+$) calculated for $C_{11}H_{20}NO_2$ 198.1494; found 198.1489.

$[\alpha]_D^{21}$ = -4 (c=0.01, MeOH).

Table S13. Spectroscopic data of **26$_{cis}$** in CD_3OD.

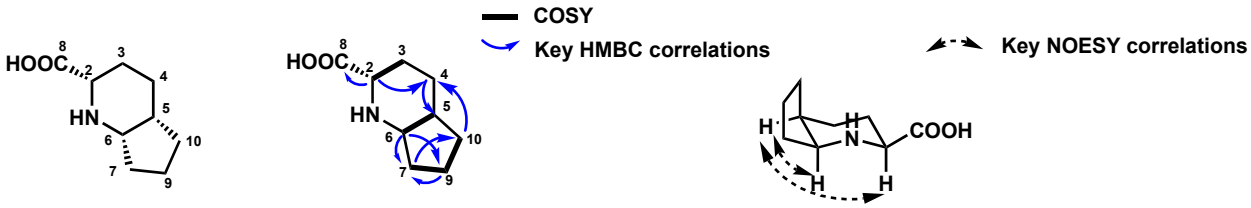

Position	δ_C	δ_H (mult.)
2	61.6[a]	3.38 (dd, 1H, *J* =12.2 Hz, 2.7 Hz)
3	31.8	1.83 (m, 1H), 2.17 (m, 1H)
4	24.0	1.99 (m, 1H), 1.68 (m, 1H)
5	39.6	2.22 (m, 1H)
6	61.4	3.54 (m, 1H)
7	28.5	1.73 (m, 1H), 1.69 (m, 1H)
8	174.3	
9	23.5	2.21 (m, 1H), 1.94 (m, 1H)
10	25.7	1.94 (m, 1H), 1.80 (m, 1H)

[a]Signal of C_2 was weak from ^{13}C spectrum, HSQC correlation with H_2 was used to determine C_2 chemical shift.

HRMS (ESI, $M+H^+$) calculated for $C_9H_{16}NO_2$ 170.1181; found 170.1175.

$[\alpha]_D^{21}$ = -16 (c=0.01, MeOH).

Table S14. Spectroscopic data of **27**$_{trans}$ in CD_3OD.

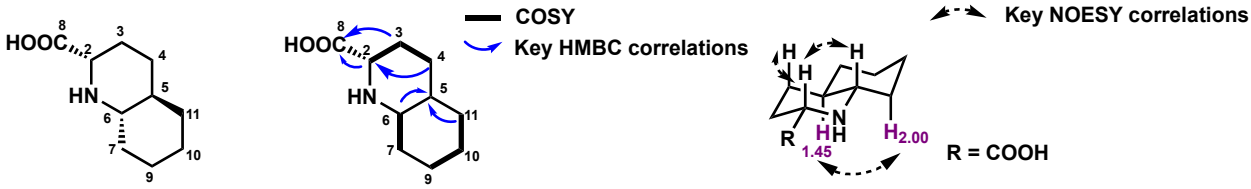

Position	δ_C	δ_H (mult.)
2	62.5[a]	3.48 (dd, 1H, *J* = 12.5, 3.5 Hz)
3	29.1	2.34 (m, 1H), 1.68 (m, 1H)
4	27.1	1.86 (m, 1H), 1.36 (m, 1H)
5	40.9	1.45 (m, 1H)
6	62.0	2.72 (td, 1H, *J* = 10.9, 3.8 Hz)
7	31.6	2.00 (m, 1H), 1.50 (m, 1H)
8	174.6[b]	
9	26.6	1.84 (m, 1H), 1.43 (m, 1H)
10	33.6	1.11 (m, 1H), 1.79 (m, 1H)
11	32.3	1.84 (m, 1H), 1.34 (m, 1H)

[a]Signal of C_2 was weak from ^{13}C spectrum, HSQC correlation with H_2 was used to determine C_2 chemical shift. [b]Signal of C_8 was weak from ^{13}C spectrum, HMBC correlation with H_2 was used to determine C_8 chemical shift.

HRMS (ESI, M+H$^+$) calculated for $C_{10}H_{18}NO_2$ 184.1337; found 184.1333.

$[\alpha]_D^{21}$ = -12 (c=0.01, MeOH).

Table S15. Spectroscopic data of **27$_{cis}$** in CD_3OD.

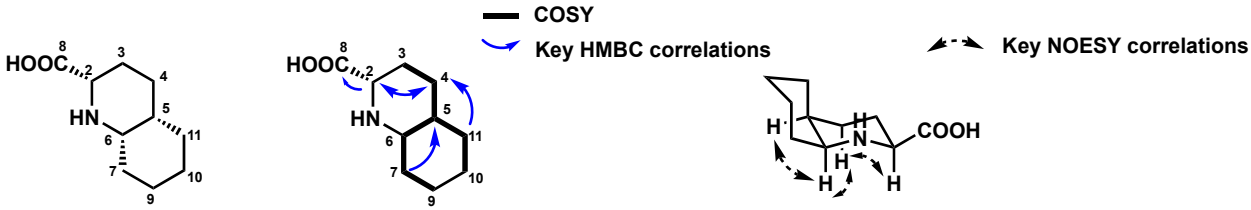

Position	δ_C	δ_H (mult.)
2	63.8[a]	3.49 (dd, 1H, *J* = 12.5, 3.5 Hz)
3	30.5	2.01 (m, 1H), 1.53 (m, 1H)
4	24.1	2.14 (m, 1H), 1.77 (m, 1H)
5	35.2	1.96 (m, 1H)
6	57.8	3.41 (m, 1H)
7	30.9	1.85 (m, 1H), 1.76 (m, 1H)
8	174.7[b]	
9	27.0	1.42 (m, 2H)
10	21.0	1.60 (m, 1H), 1.55 (m, 1H)
11	26.4	1.69 (m, 2H)

[a]Signal of C_2 was weak from ^{13}C spectrum, HSQC correlation with H_2 was used to determine C_2 chemical shift. [b]Signal of C_8 was weak from ^{13}C spectrum, HMBC correlation with H_2 was used to determine C_8 chemical shift.

HRMS (ESI, M+H$^+$) calculated for $C_{10}H_{18}NO_2$ 184.1337; found 184.1333.

$[\alpha]_D^{21}$ = -2 (c=0.01, MeOH).

4. Supplementary Figures

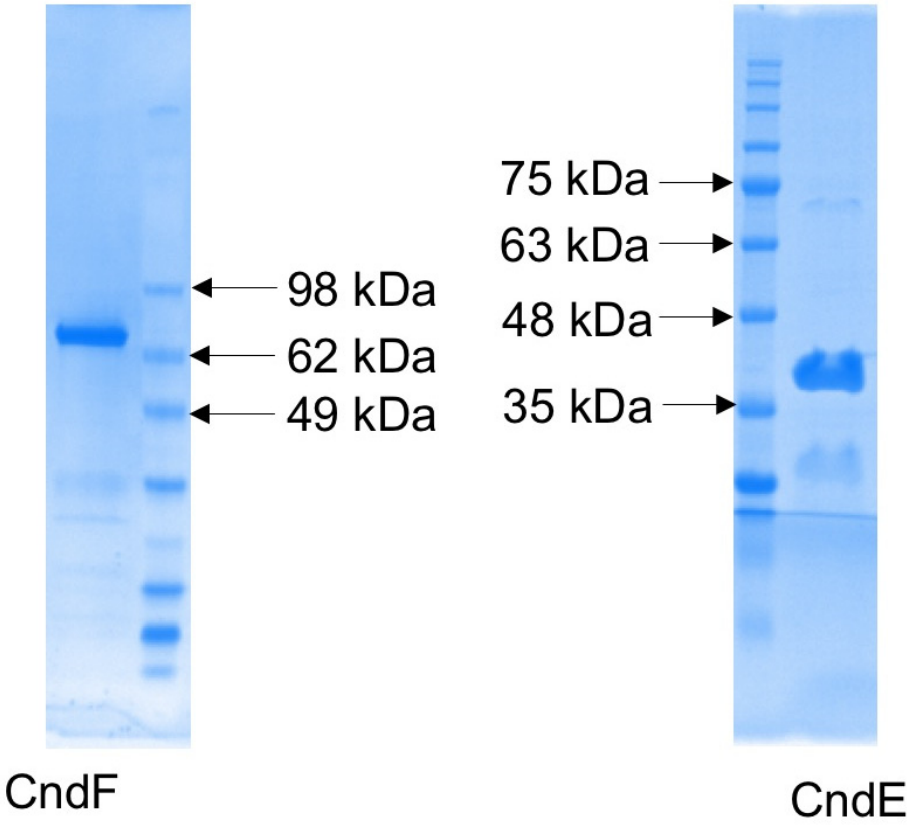

Fig S1. SDS-PAGE gels of purified proteins used in this study.

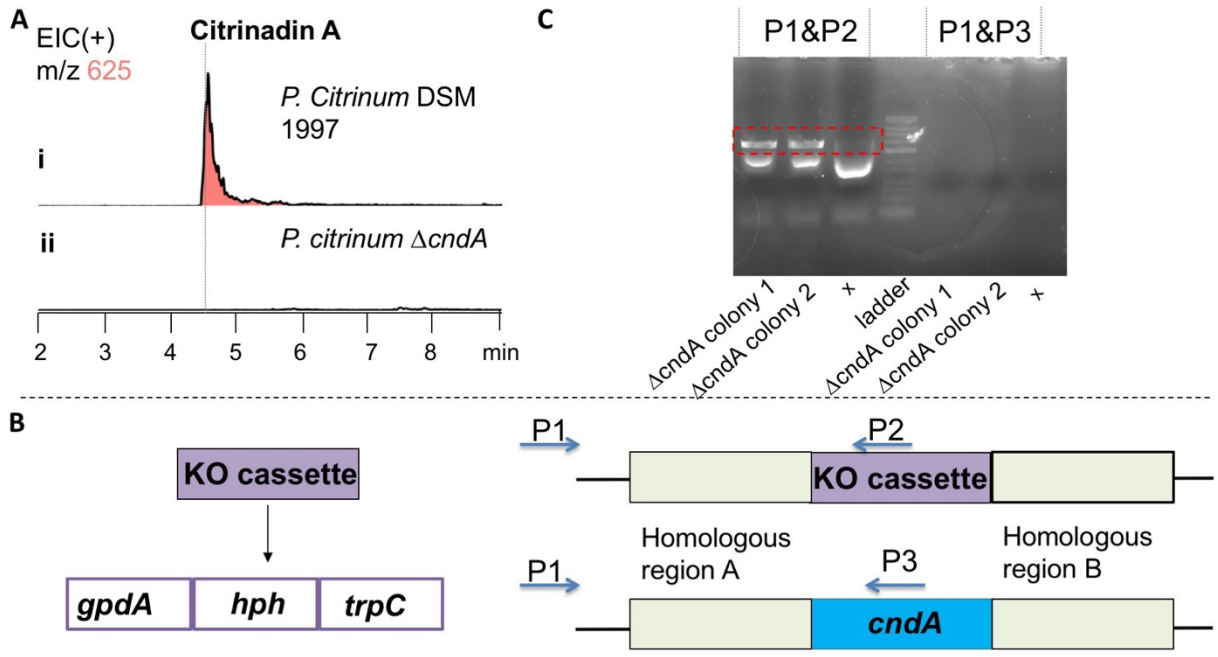

Fig S2. Identification *cnd* cluster from citrinadin A producing strain *Penicillium citrinum* DSM 1997. (**A**) Citrinadin A is produced by *P. citrinum* DSM 1997. (i) Citrinadin A can be detected from culture of *P. citrinum* DSM 1997. (ii) NRPS gene *cndA* knockout strain *P. citrinum* Δ*cndA* does not produce citrinadin A anymore, confirming *cnd* is the responsible biosynthetic cluster. (**B**) Primer design for examining *cndA* knockout. KO cassette contains a hygromycin resistance gene (*hph*), which is driven by promoter gpdA and controlled by terminator trpC. Once KO cassette is incorporated by protoplast transformation, *hph* will confer hygromycin resistance for selection. To examine the incorporation of KO cassette, three primers will be used: P1 binds to a genomic region, P2 binds to KO cassette, and P3 binds to *cndA*. P1-P2 primer pair recognizes the KO cassette, P1-P3 primer pair recognizes wild type *P. citrinum* DSM 1997. (**C**) Confirmation of knockout of NRPS gene *cndA* by PCR. Two transformant colonies were selected for PCR examination. A Δ*cndA* transformant should have the KO cassette replace a partial region of *cndA*. Therefore, P1-P2 primer pair that recognizes the KO cassette can lead to an amplification band, P1-P3 primer pair should not have a PCR amplification band.

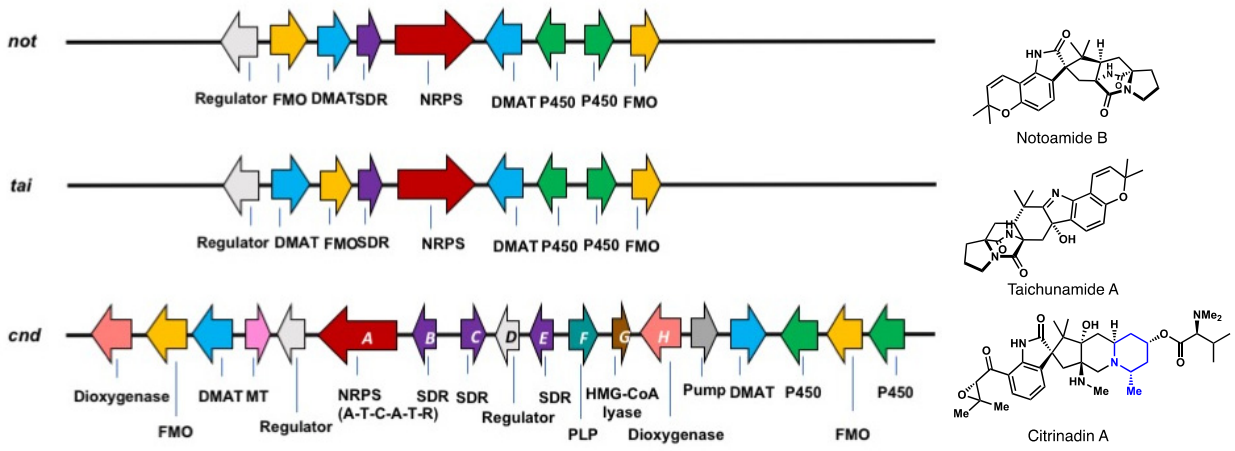

Fig S3. Compilation of clusters biosynthesizing related indole alkaloids. The amino acid precursors of notoamide B and taichunamide A are L-tryptophan and L-proline, both of which are readily available from primary metabolism. On the contrary, citrinadin A contains an unusual (2*S*, 6*S*)-6-methyl-pipecolate, which is not a primary metabolite and requires efforts of dedicated enzymes. Genomic comparison across these three clusters can yield insights on unique genes *cndE-cndG* for citrinadin A biosynthesis, which are likely to be involved in the biosynthesis of (2*S*, 6*S*)-6-methyl-pipecolate.

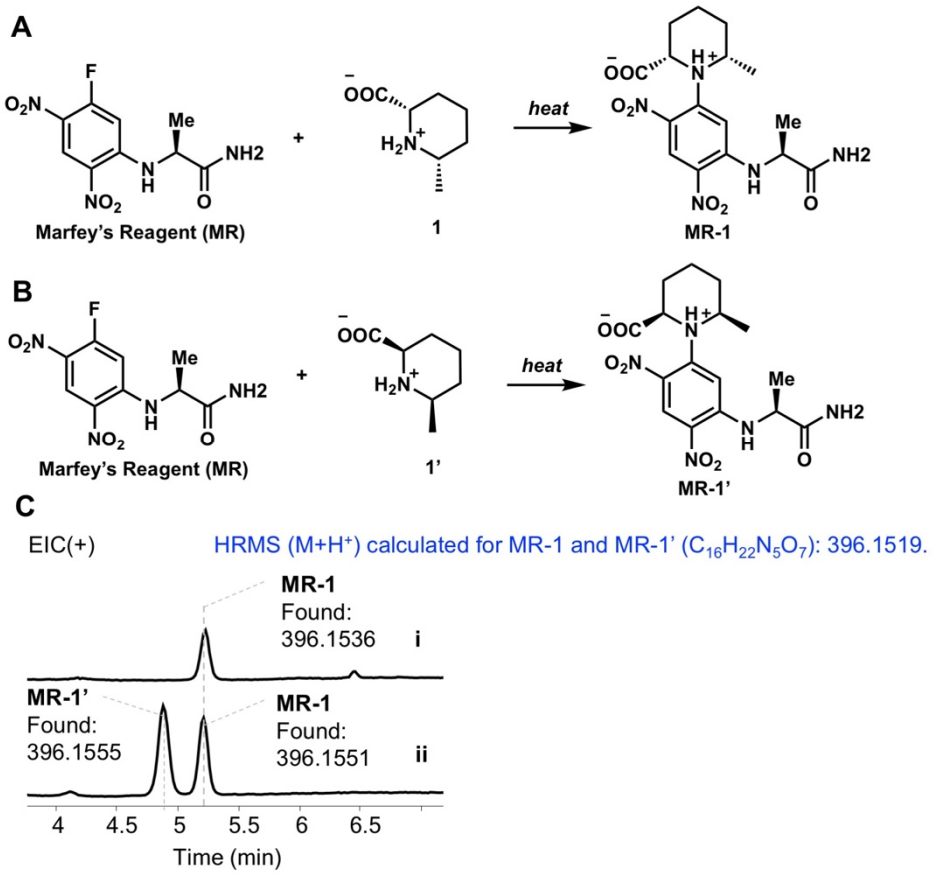

Fig S4. Chiral derivatization showed that **1** is a single enantiomer. (**A**) Marfey's reagent modified (2*S*, 6*S*)-6-methyl pipecolate **MR-1**. (**B**) Marfey's reagent modified (2*R*, 6*R*)-6-methyl pipecolate **MR-1'**. (**C**) **1** is a single enantiomer. (**i**) Derivatization of **1** purified from heterologous production by Marfey's reagent. (**ii**) Derivatization of (±)-*cis*-6-methyl pipecolate standard has two peaks, one is derived (2*R*, 6*R*)-6-methyl pipecolate **MR-1'**, the other is (2*S*, 6*S*)-6-methyl pipecolate **MR-1**. Relative stereochemistry of **1** was determined by NMR (Table S3). Absolute stereochemistry assignment was based on previous reports of total synthesis on citrinadin A, which have determined the absolute stereochemistry of C6 to be *S*.[5-6]

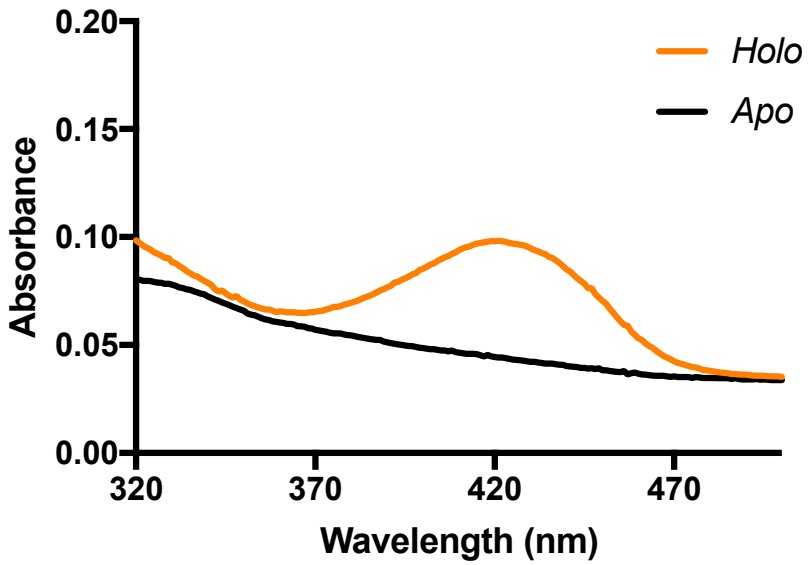

Fig S5. CndF is a PLP-containing enzyme. Purified CndF is in *holo* form, exhibiting a characteristic λ_{max} of internal aldimine at 420 nm (orange line). CndF becomes *apo* after extensive treatment with hydroxylamine, the disappearance of λ_{max} at 420 nm indicates that CndF lacks PLP to form internal aldimine with (black plot).

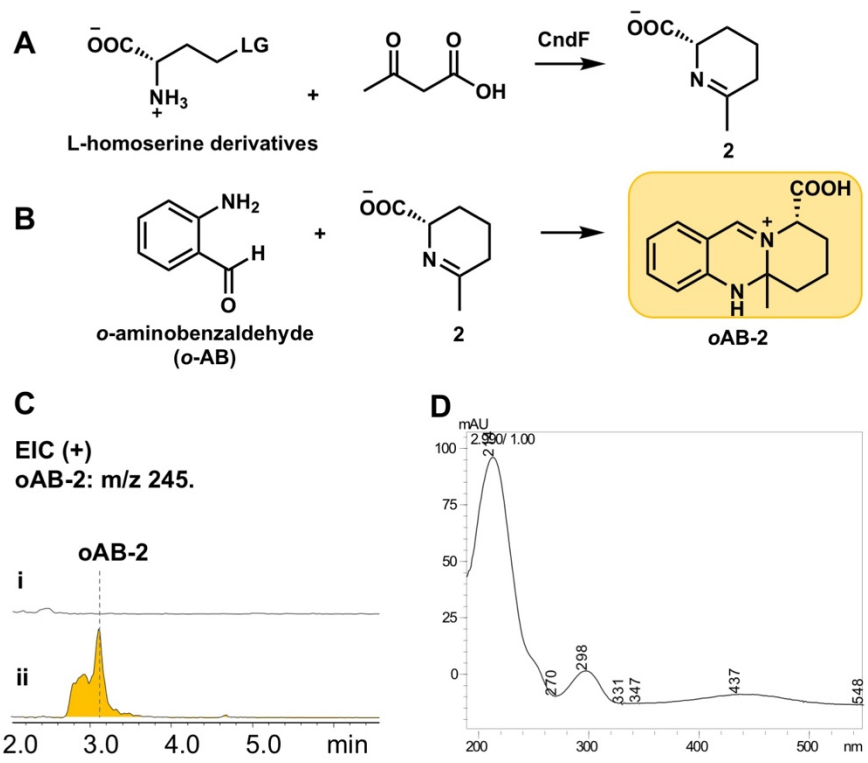

Fig S6. Measurement of amount of imine **2** was used to determine the native amino acid substrate of CndF. (**A**) The amino acid substrate of CndF should possess a good leaving group at γ position for γ-substitution reaction. (**B**) Imine **2** can be derivatized by o-aminobenzaldehyde (o-AB) to facilitate detection. (**C**) o-AB derivatized **2** can be detected by MS. (**i**) Control reaction with denatured CndF did not show oAB-**2** EIC(+) peak; (**ii**) oAB-**2** EIC(+) peak can be detected post-derivatization in reaction mixture of CndF with *O*-acetyl L-homoserine and acetoacetate. (**D**) The characteristic UV absorbance of dihydroquinazolinium derivative at 440 nm facilitates identification of the iminium product.

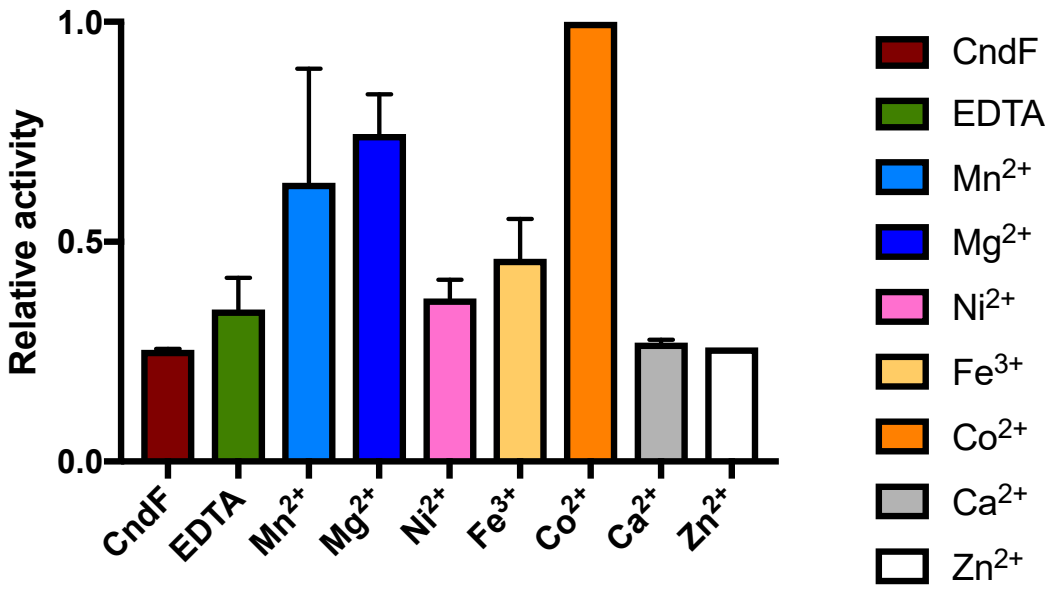

Fig S7. Co^{2+} facilitates CndF catalysis. A variety of metal ions were tested to evaluate their effects on CndF catalysis. The concentration of each metal ion was 2.5 mM. Reactions were carried out in 50 mM phosphate buffer (pH 6.5) in the presence of 1.9 mM O-acetyl L-homoserine and 1.9 mM lithium acetoacetate. 80 μM (final concentration) CndF was added to initiate reactions. The reactions were incubated at room temperature for 1 hr. Protein was separated from the reaction mixture by Amicon centrifugation filters, and resulting protein-free reactions were derivatized with o-aminobenzaldehyde. The amount of oAB-**2** produced was used to gauge the activity of CndF in the presence of different metal ions. Relative activity of highest production of oAB-**2** in the presence of Co^{2+} was set to 1.0.

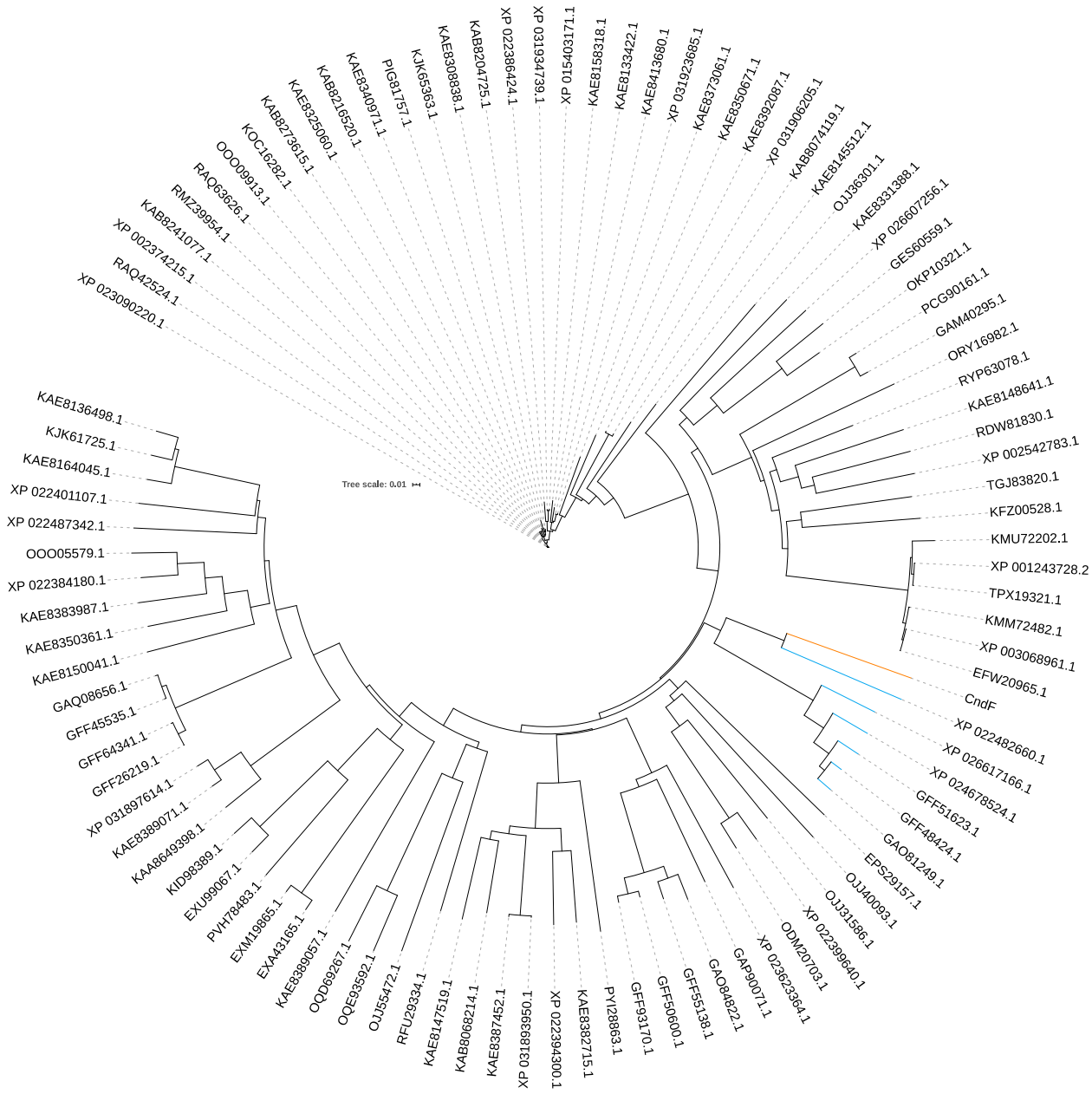

Fig S8. Phylogenetic analysis of CndF and its uncharacterized homologues. CndF is highlighted in orange, and its closest homologues are highlighted in blue. Phylogenetic analysis was carried out by Clustal Omega, and tree was displayed by iTOL (https://itol.embl.de/).

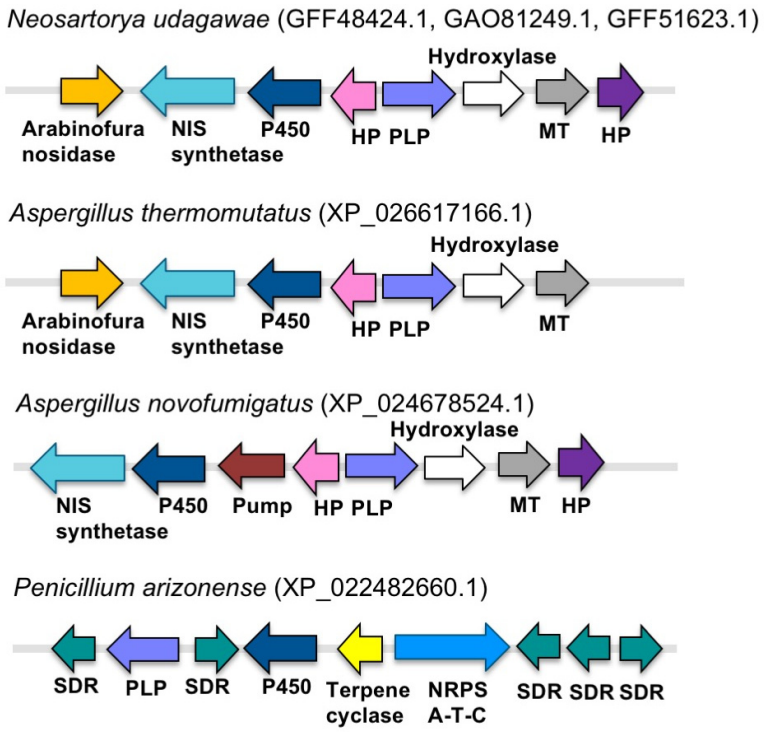

Fig S9. Biosynthetic clusters in which closest homologues to CndF are found. These cryptic clusters encode a PLP-dependent enzyme similar to CndF, and the presence of a NRPS gene or a NIS gene implies that these CndF homologues may participate in synthesis of noncanonical amino acids.

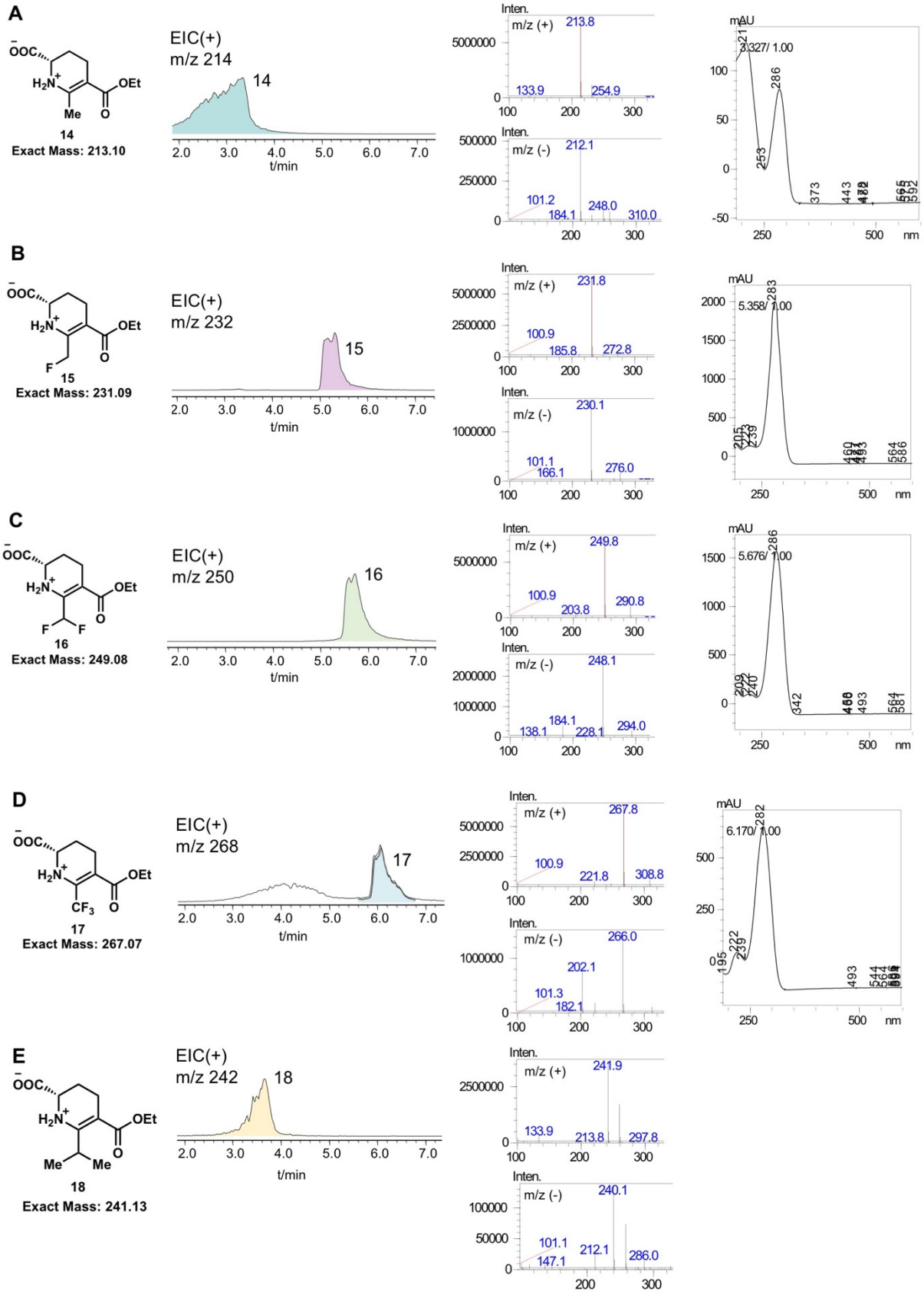
A
14
Exact Mass: 213.10
EIC(+)
m/z 214
14
t/min
Inten.
m/z (+)
213.8
133.9
254.9
m/z (-)
212.1
101.2
184.1
248.0
310.0
mAU
3.327/ 1.00
286
253
373
nm
B
15
Exact Mass: 231.09
EIC(+)
m/z 232
15
231.8
100.9
185.8
272.8
230.1
101.1
166.1
276.0
5.358/ 1.00
283
C
16
Exact Mass: 249.08
EIC(+)
m/z 250
16
249.8
100.9
203.8
290.8
248.1
184.1
138.1
228.1
294.0
5.676/ 1.00
286
342
D
17
Exact Mass: 267.07
EIC(+)
m/z 268
17
267.8
100.9
221.8
308.8
266.0
202.1
101.3
182.1
6.170/ 1.00
282
E
18
Exact Mass: 241.13
EIC(+)
m/z 242
18
241.9
133.9
213.8
297.8
240.1
101.1
212.1
147.1
286.0

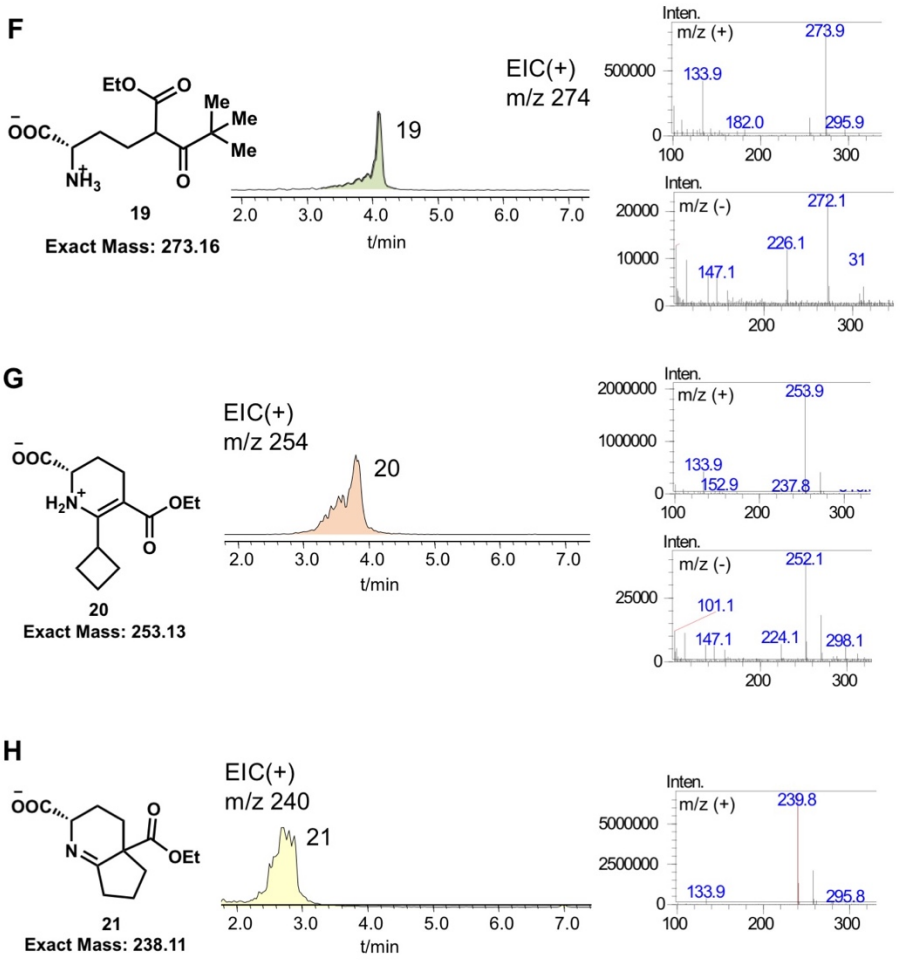

Fig S10. CndF catalyzes C-C bond formation between *O*-acetyl L-homoserine and β-keto esters. (**A**) LC-MS and UV data for compound **14** from CndF *in vitro* assay. (**B**) LC-MS and UV data for compound **15** from CndF *in vitro* assay. (**C**) LC-MS and UV data for compound **16** from CndF *in vitro* assay. (**D**) LC-MS and UV data for compound **17** from CndF *in vitro* assay. (**E**) LC-MS data for compound **18** from CndF *in vitro* assay. (**F**) LC-MS data for compound **19** from CndF *in vitro* assay. (**G**) LC-MS data for compound **20** from CndF *in vitro* assay. (**H**) LC-MS data for compound **21** from CndF *in vitro* assay.

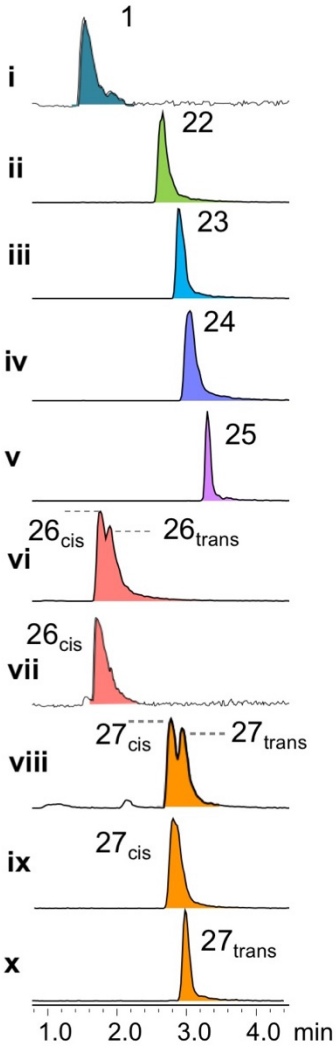

Fig S11. LC-MS traces of 6-alkyl pipecolates in this study. (**i**) Purified compound **1**. (**ii**) Purified compound **22**. (**iii**) Purified compound **23**. (**iv**) Purified compound **24**. (**v**) Purified compound **25**. (**vi**) Compounds **26_{cis} and 26_{trans}**. (**vii**) Purified compound **26_{cis}**. (**viii**) Compounds **27_{cis} and 27_{trans}**. (**ix**) Purified compound **27_{cis}**. (**x**) Purified compound **27_{trans}**.

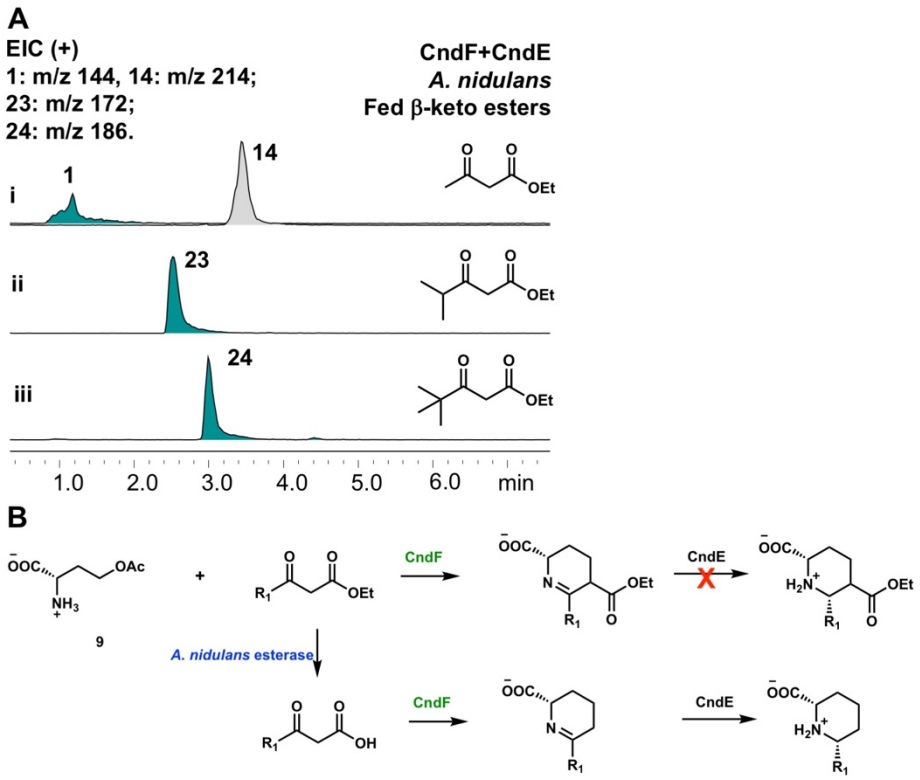

Fig S12. The competition for β-keto esters between esterase hydrolysis and CndF condensation determines product profiles *in vivo*. (**A**) Effects of R_1 substituent size on product profiles *in vivo*. (**i**) Feeding ethyl acetoacetate to *A. nidulans* transformant harboring CndF and CndE led to production of both enamine ester **14** and pipecolate **1**, with **14** as the major product. (**ii**) Feeding isopropyl acetoacetate ethyl ester to *A. nidulans* transformant harboring CndF and CndE led to production of pipecolate **23**, while enamine ester **18** was not detected. (**iii**) Feeding t-butyl acetoacetate ethyl ester to *A. nidulans* transformant harboring CndF and CndE led to production of pipecolate **24**, while enamine ester **19** was not detected. When feeding β-keto esters to *A. nidulans*, the product ratio of enamine ester and 6-alkyl pipecolate varies with the size of R_1 substituent. Smaller R_1 substituent in β-keto esters leads to the production of enamine ester as the major product; Bulkier R_1 β-keto esters results in the dominant production of 6-alkyl pipecolates. (**B**) Esterase hydrolysis competes with CndF condensation for β-keto esters in *A. nidulans*. When β-keto ester with a small R_1 substituent is fed into *A. nidulans*, it can be directly converted to enamine ester, which cannot be further hydrolyzed by esterase or reduced by CndE. However, when R_1 is considerably bulky, esterase hydrolysis rate will outcompete condensation rate, leading to the generation of β-keto acid *in situ* and dominant production 6-alkyl pipecolates.

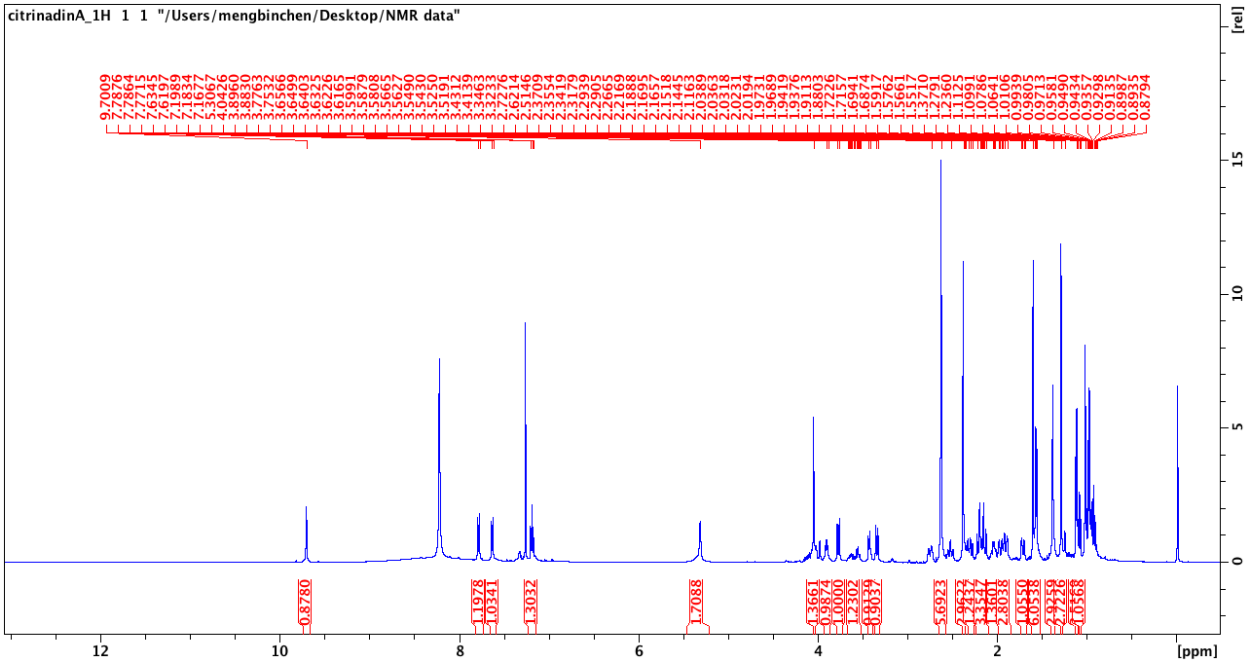

Fig S13. ^{1}H spectrum of citrinadin A in $CDCl_3$.

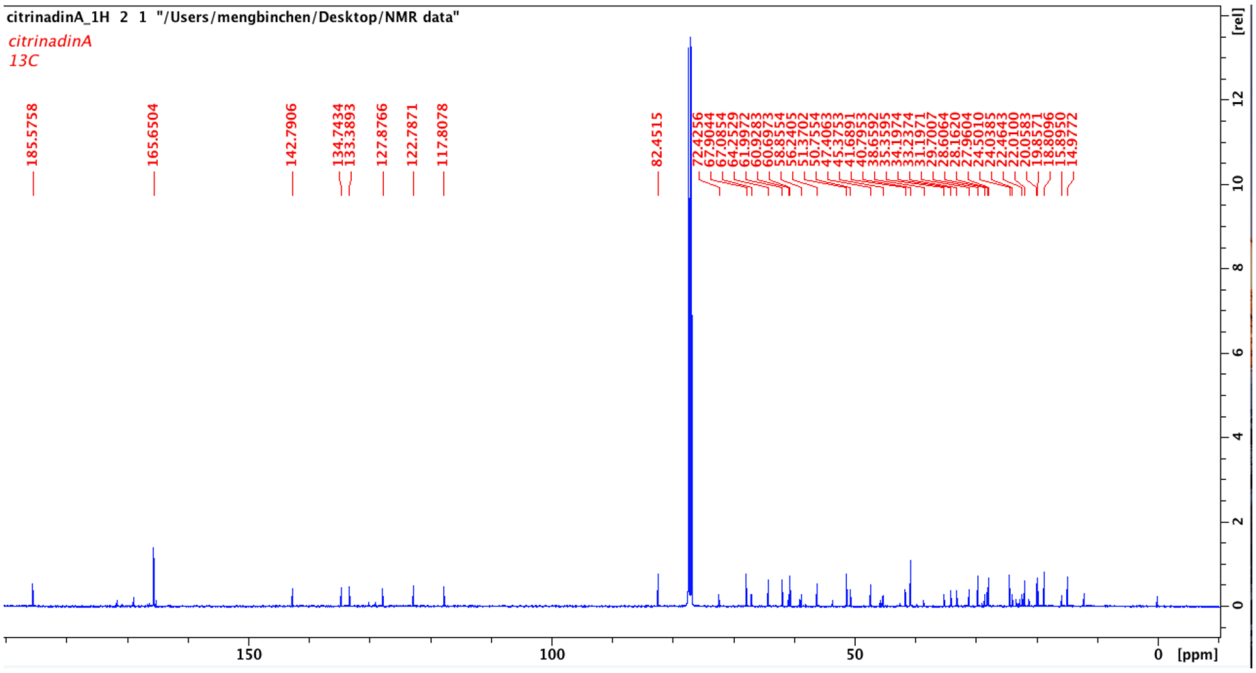

Fig S14. ^{13}C spectrum of citrinadin A in $CDCl_3$.

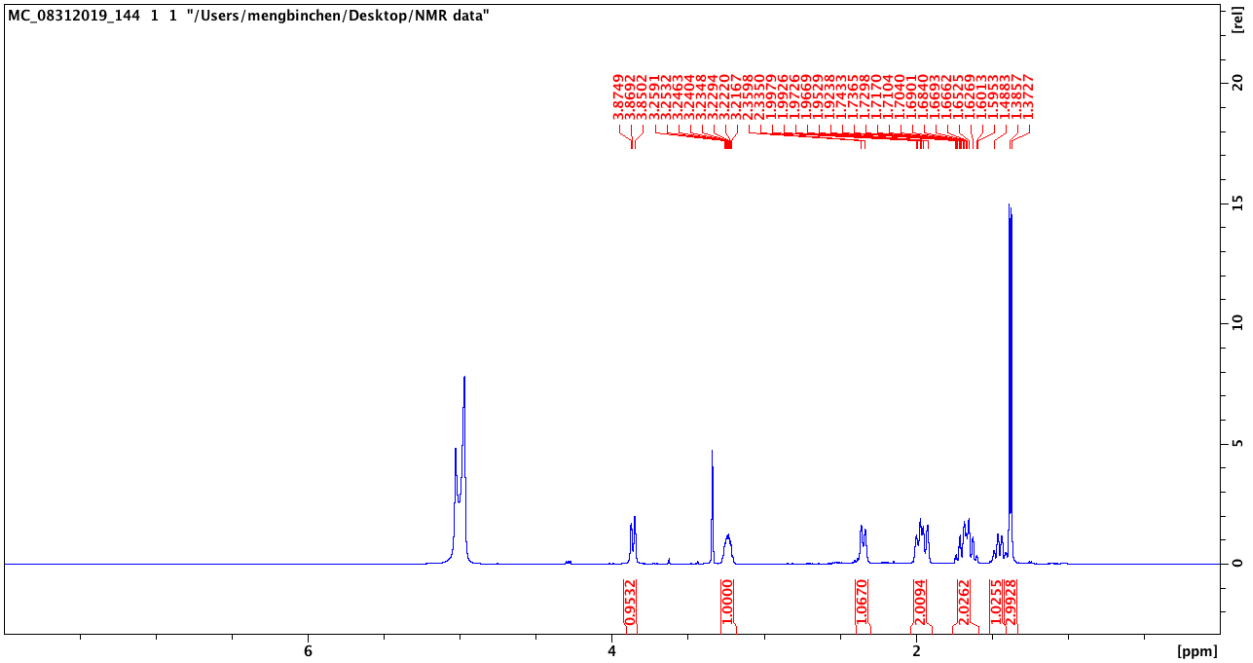

Fig S15. ^{1}H spectrum of compound **1** in CD_3OD, 500 MHz.

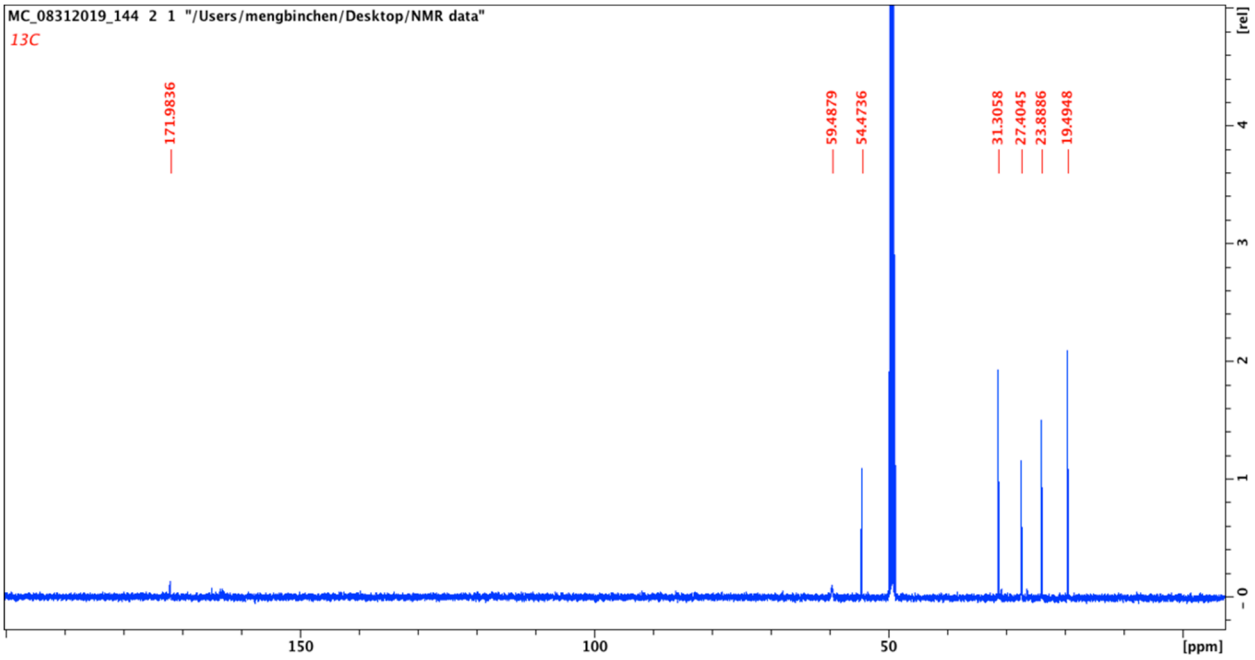

Fig S16. ^{13}C spectrum of compound **1** in CD_3OD, 125 MHz.

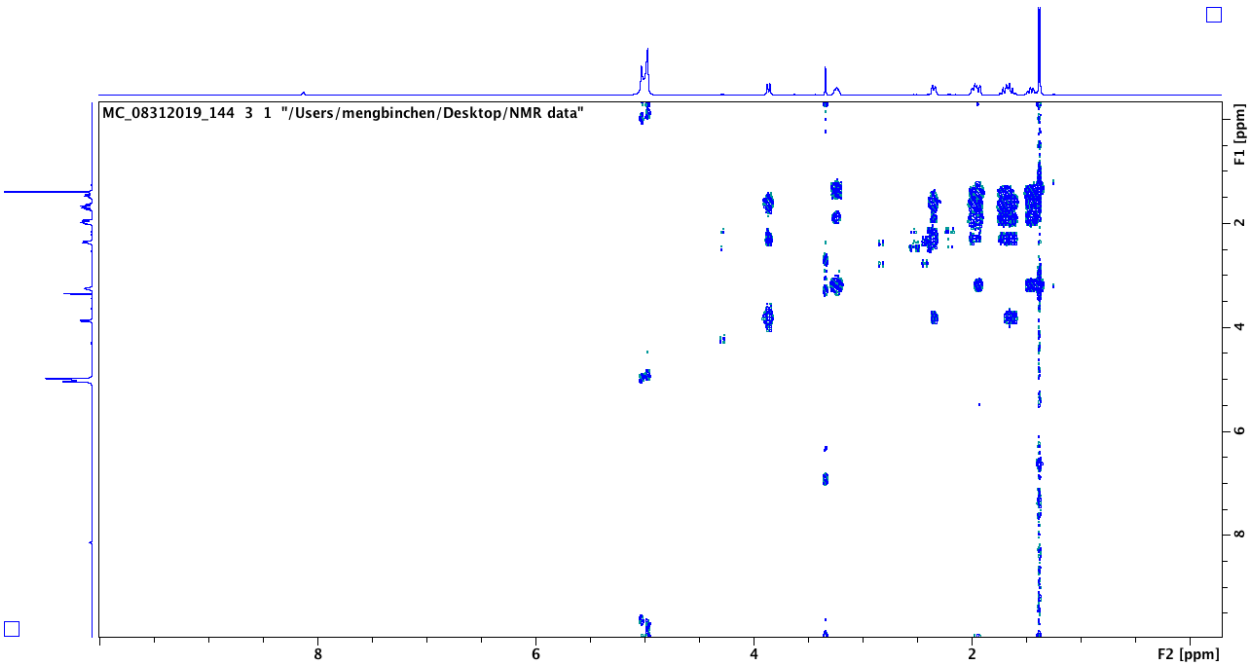

Fig S17. COSY spectrum of compound **1** in CD_3OD.

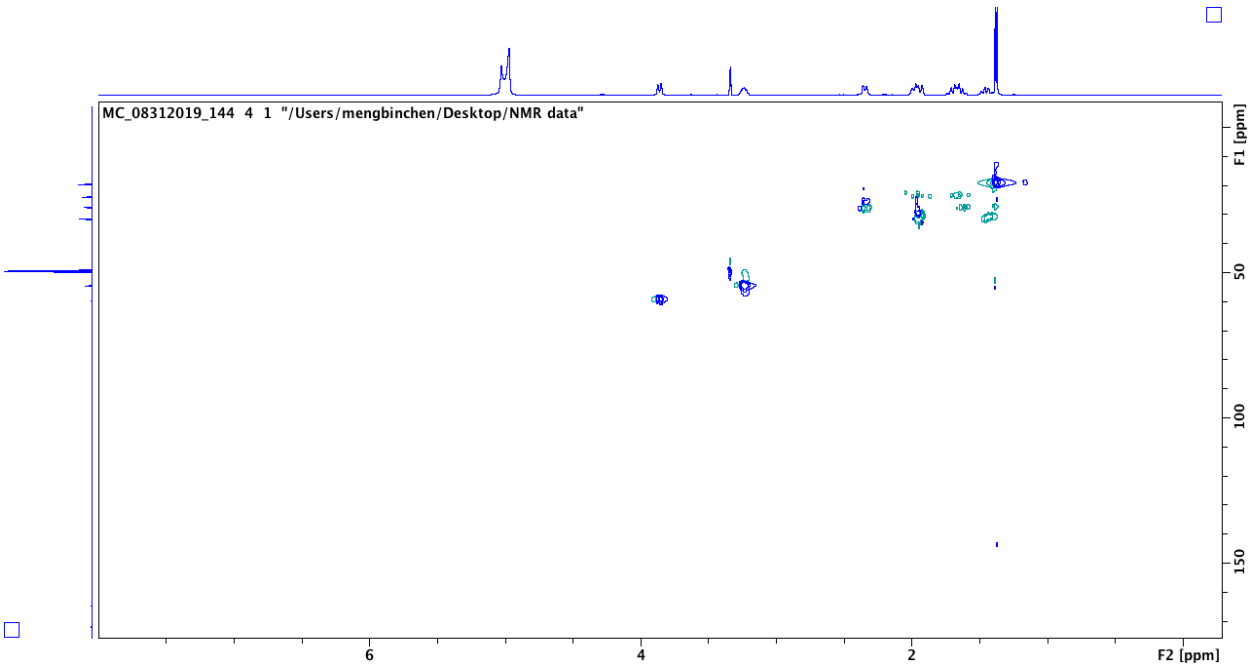

Fig S18. HSQC spectrum of compound **1** in CD_3OD.

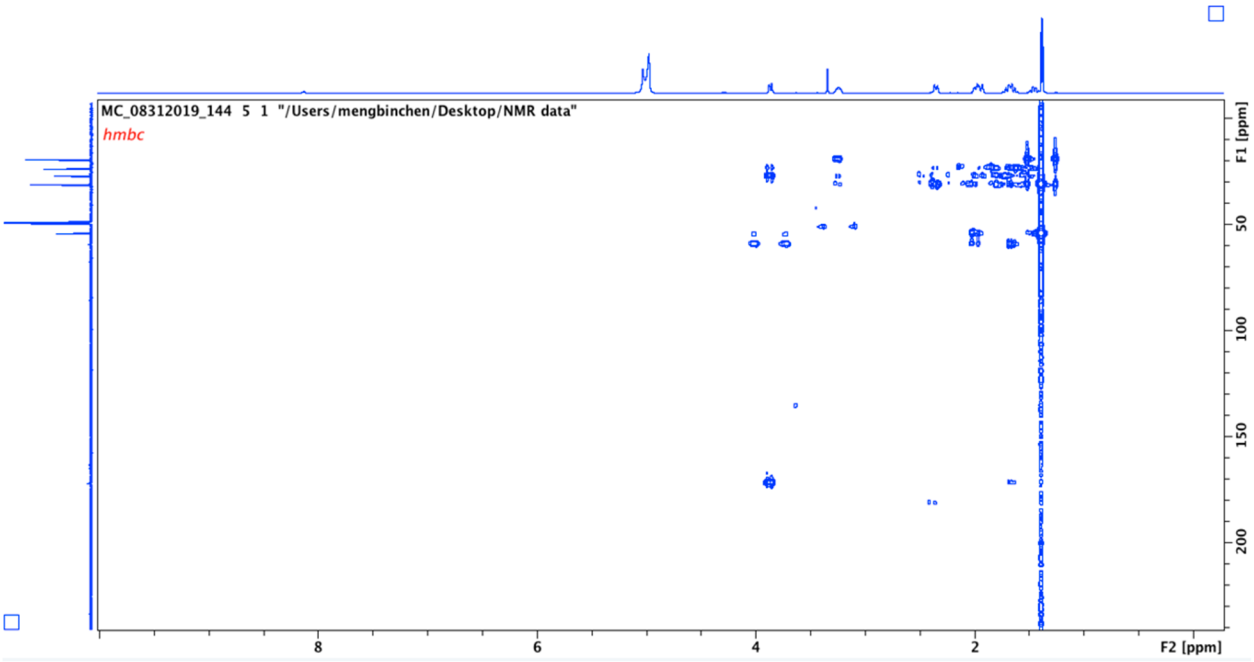

Fig S19. HMBC spectrum of compound **1** in CD_3OD.

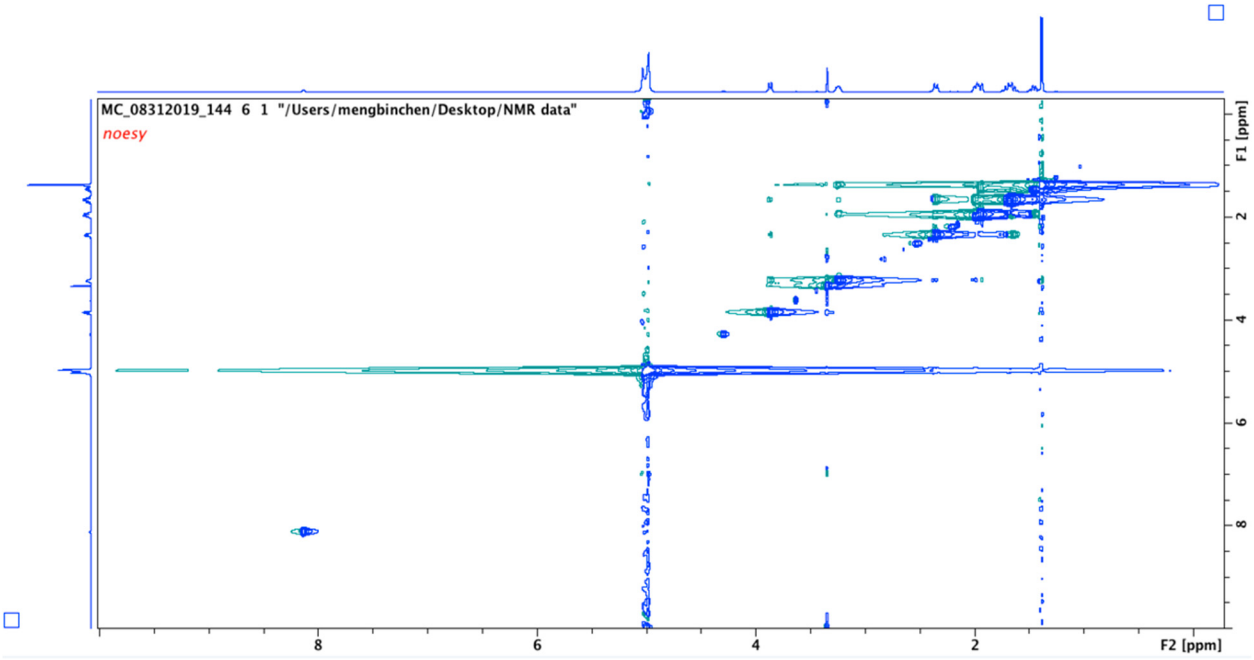

Fig S20. NOESY spectrum of compound **1** in CD_3OD

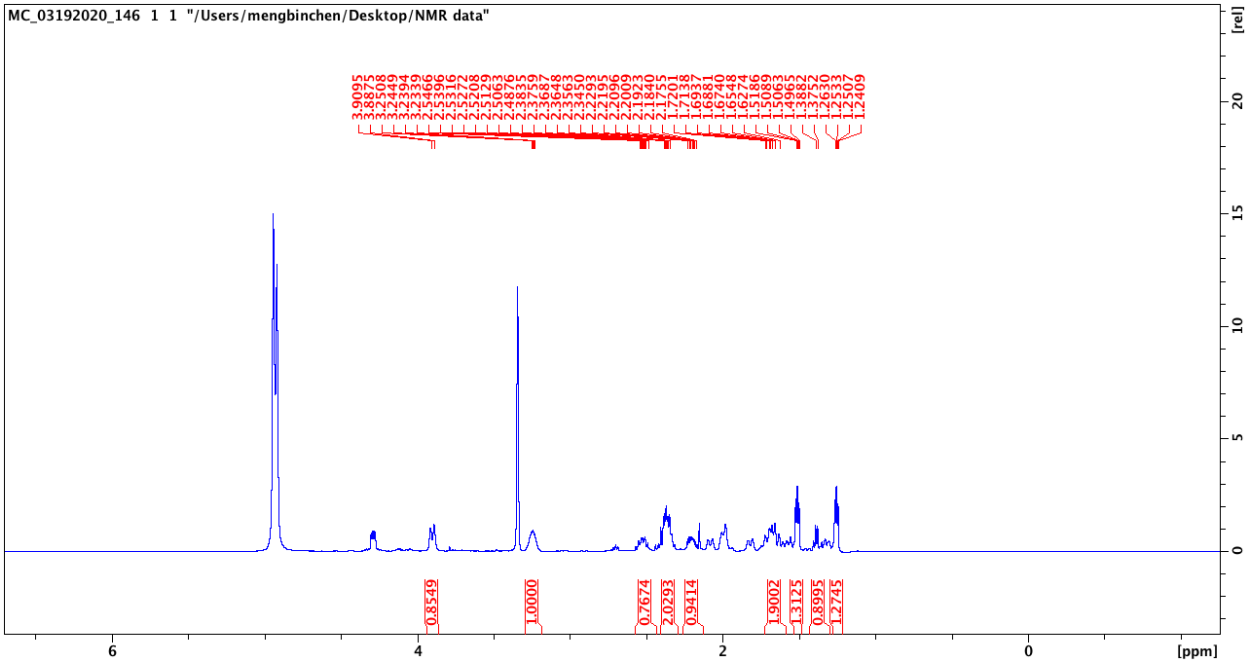

Fig S21. ^{1}H spectrum of [5, 7-^{13}C]-**1** in CD_3OD, 500 MHz.

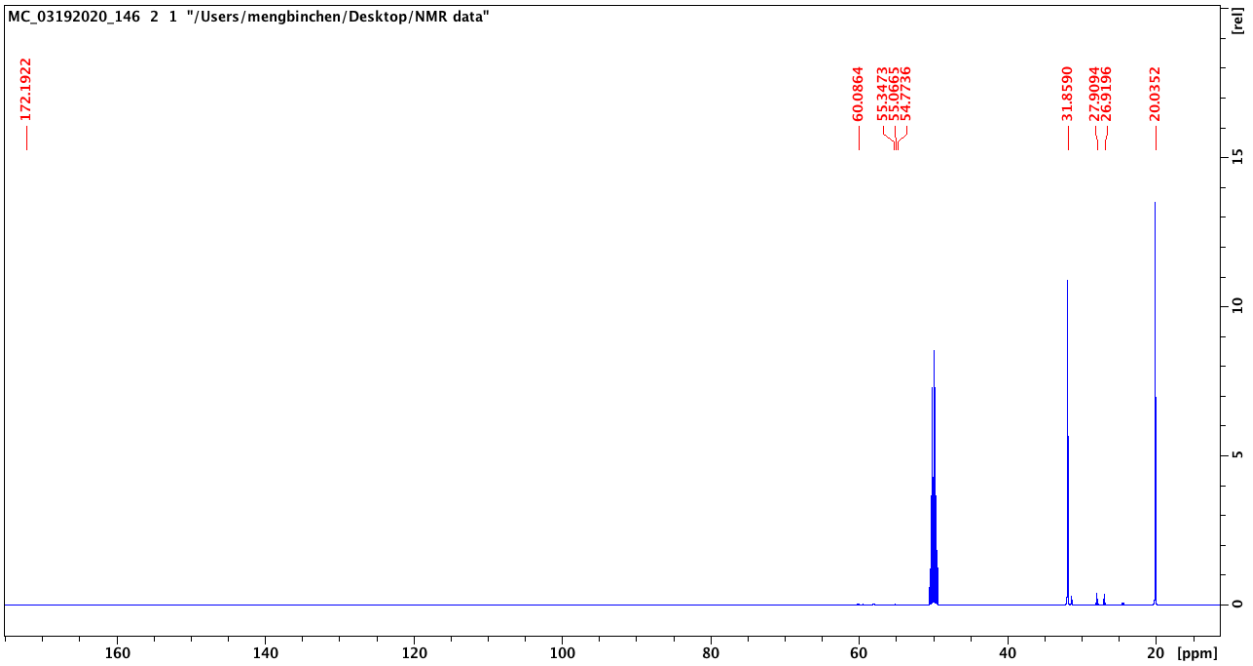

Fig S22. ^{13}C spectrum of [5, 7-^{13}C]-**1** in CD_3OD, 125 MHz.

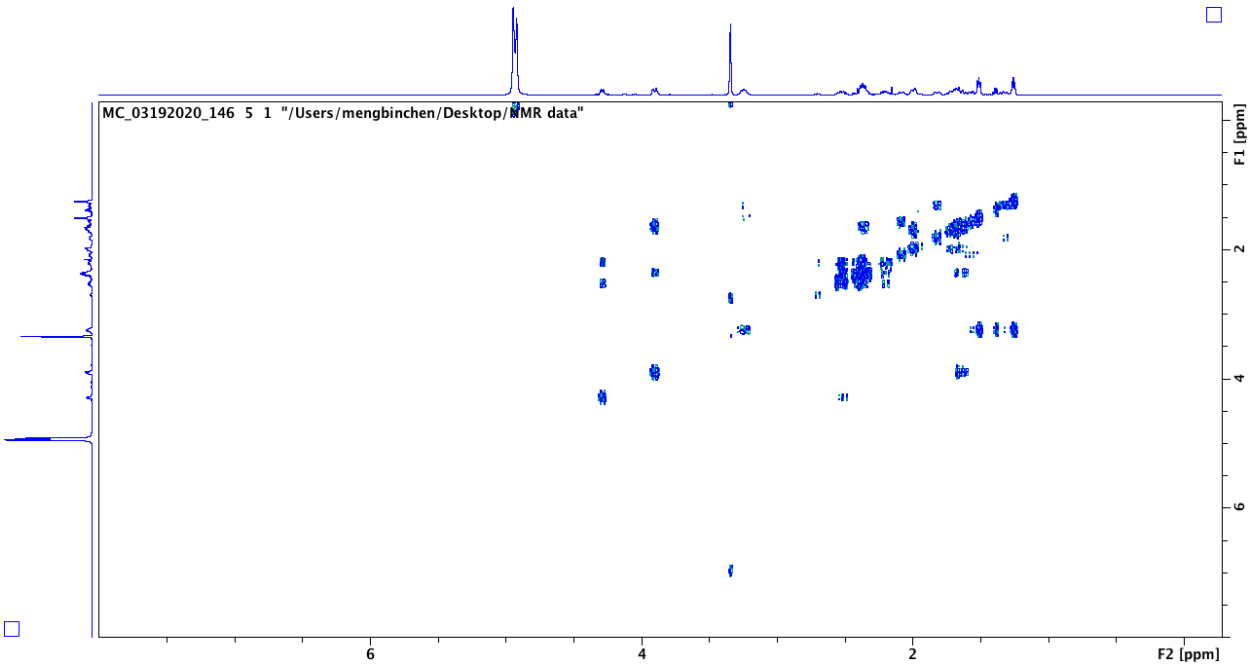

Fig S23. COSY spectrum of [5, 7-^{13}C]-**1** in CD_3OD.

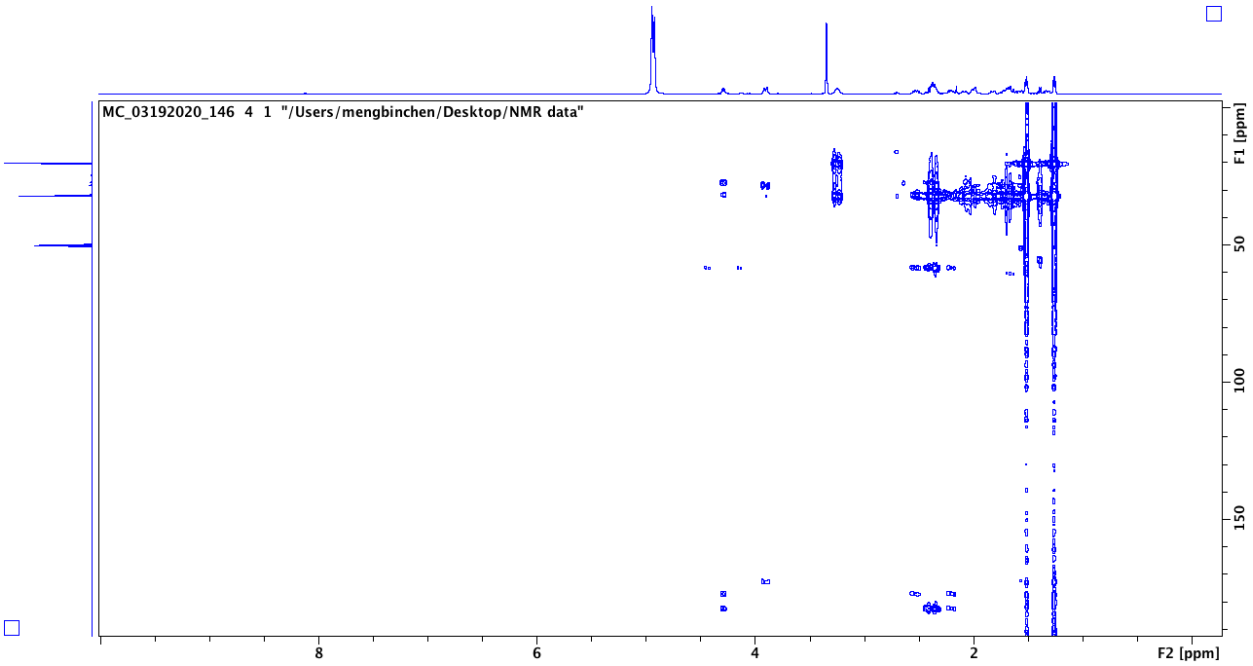

Fig S24. HMBC spectrum of [5, 7-^{13}C]-**1** in CD_3OD.

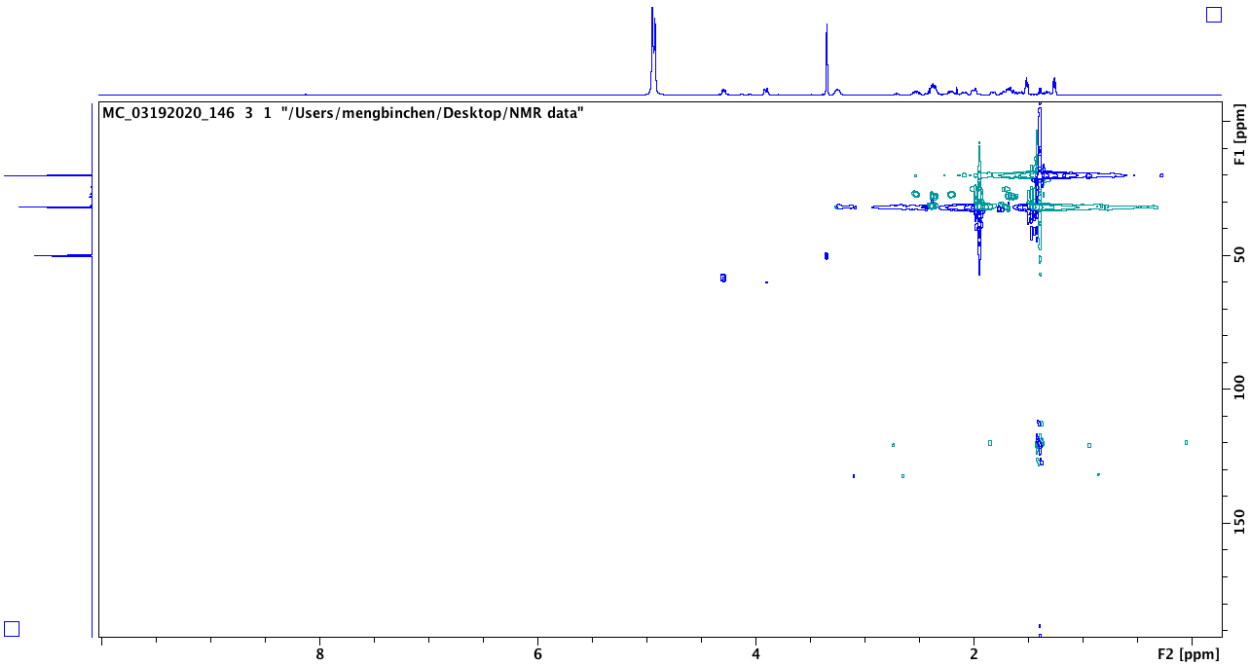

Fig S25. HSQC spectrum of [5, 7-^{13}C]-**1** in CD_3OD.

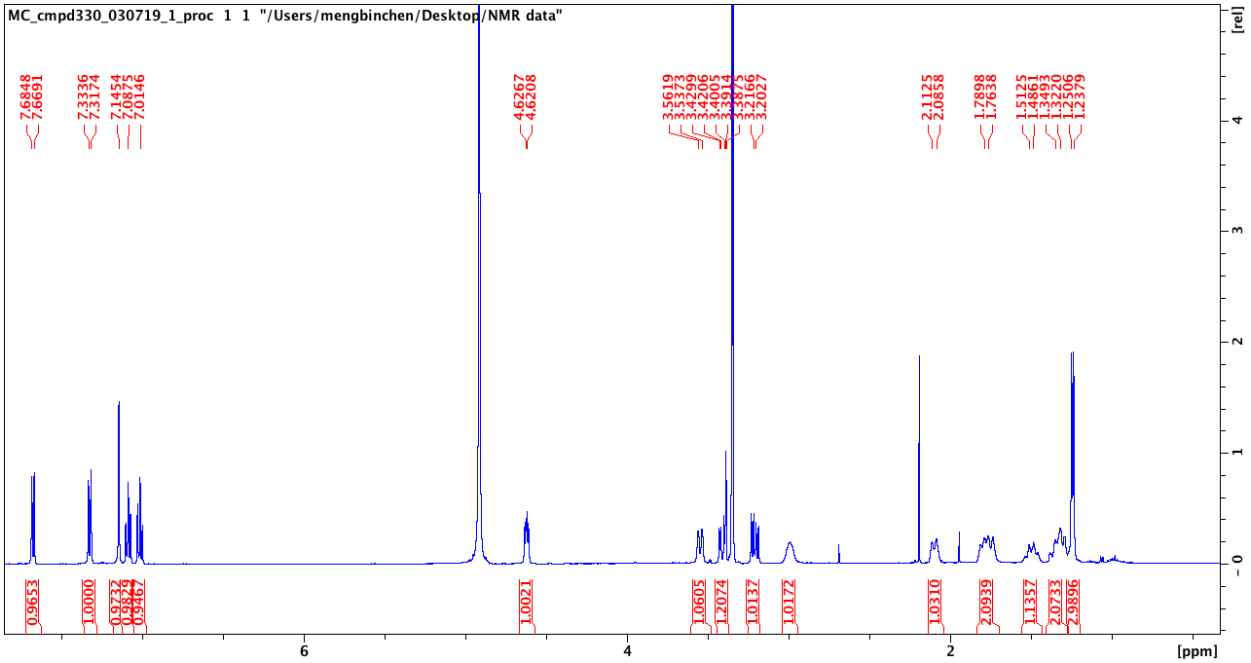

Fig S26. ^{1}H spectrum of compound **6** in CD_3OD, 500 MHz.

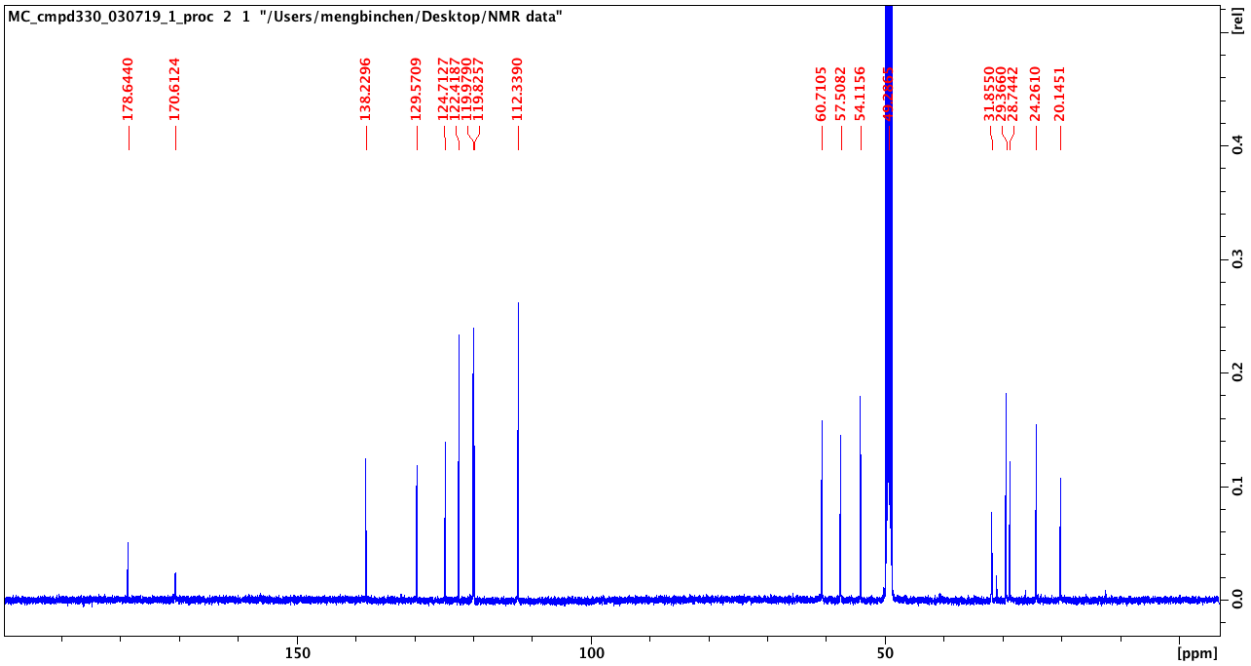

Fig S27. ^{13}C spectrum of compound **6** in CD_3OD, 125 MHz.

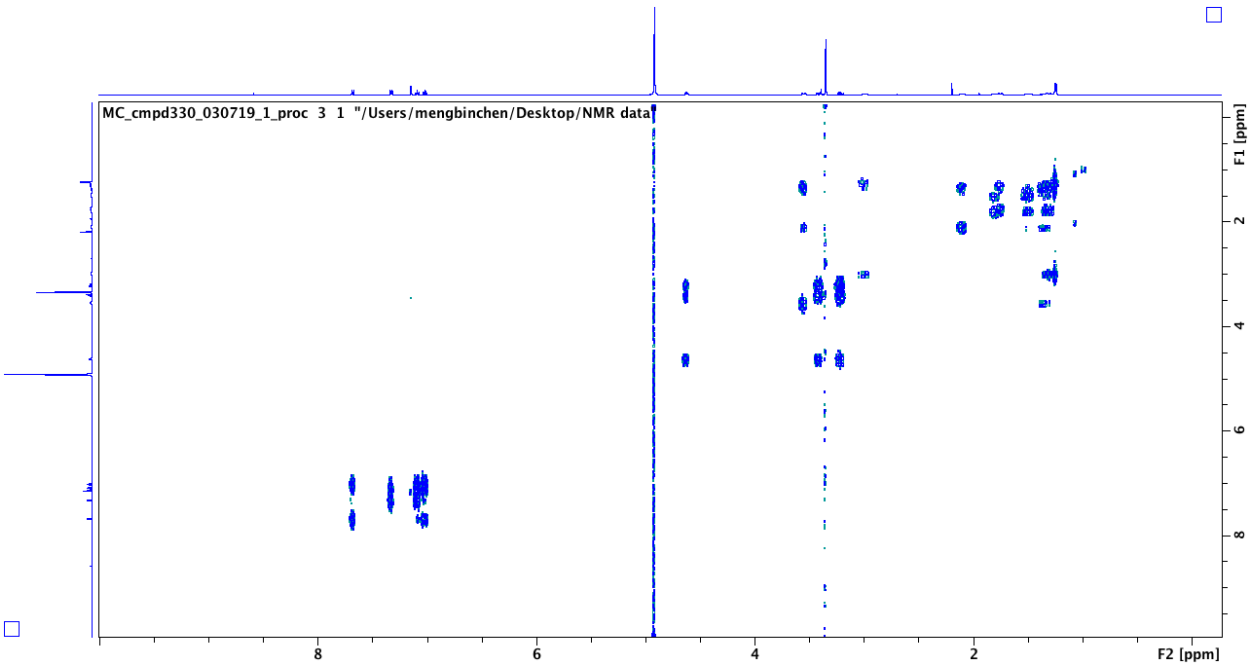

Fig S28. COSY spectrum of compound **6** in CD_3OD.

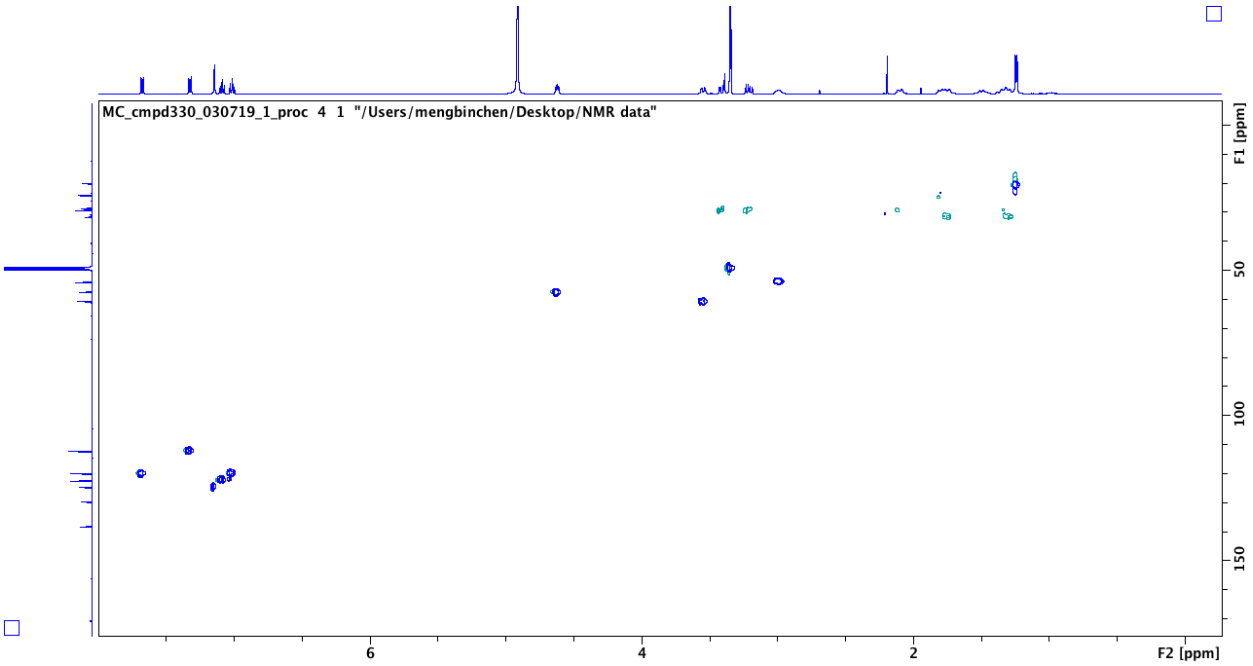

Fig S29. HSQC spectrum of compound **6** in CD_3OD.

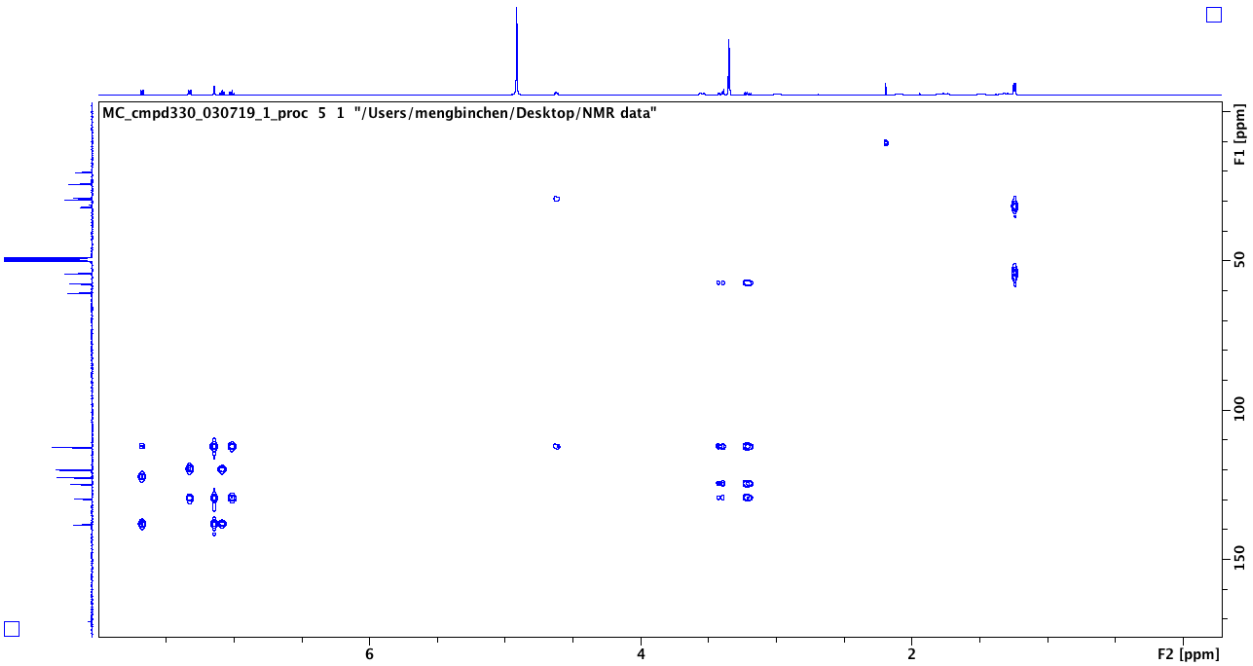

Fig S30. HMBC spectrum of compound **6** in CD_3OD.

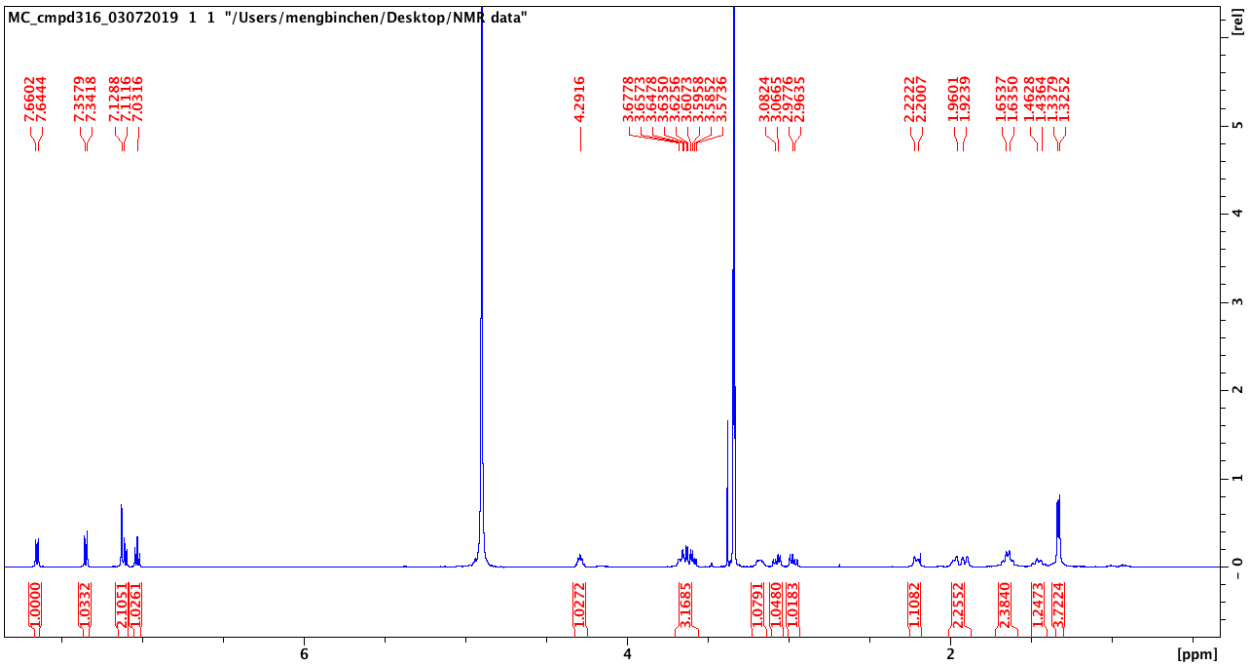

Fig S31. ^{1}H spectrum of compound **7** in CD_3OD, 500 MHz.

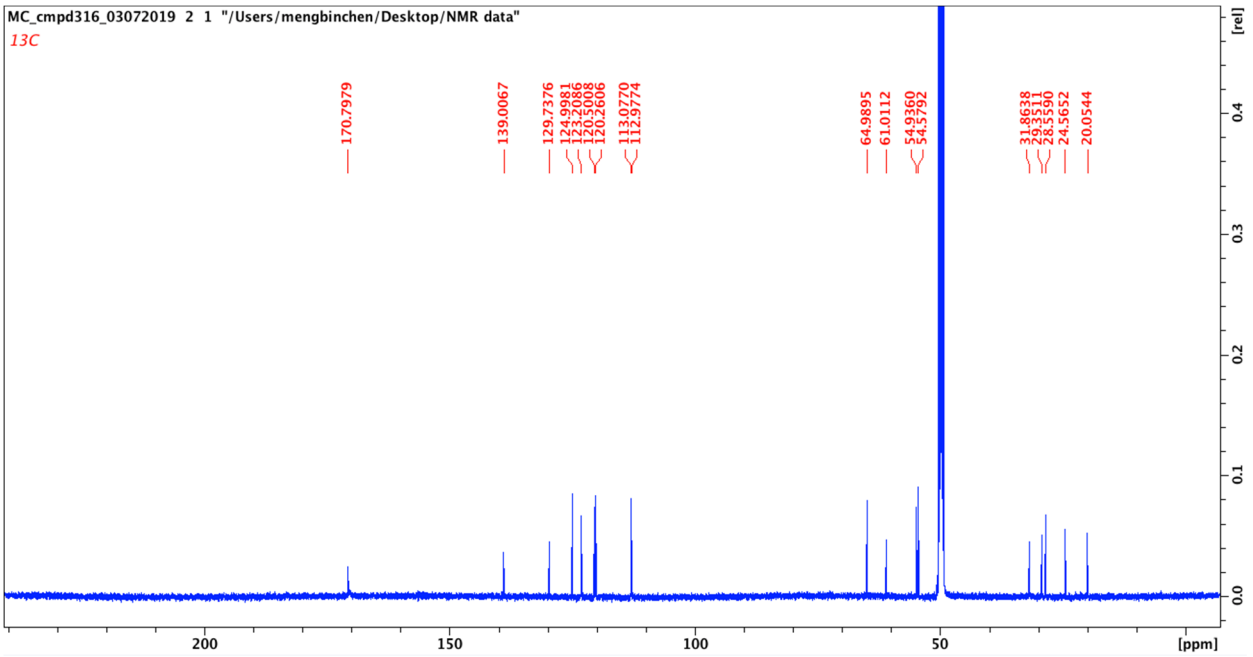

Fig S32. ^{13}C spectrum of compound **7** in CD_3OD, 125 MHz.

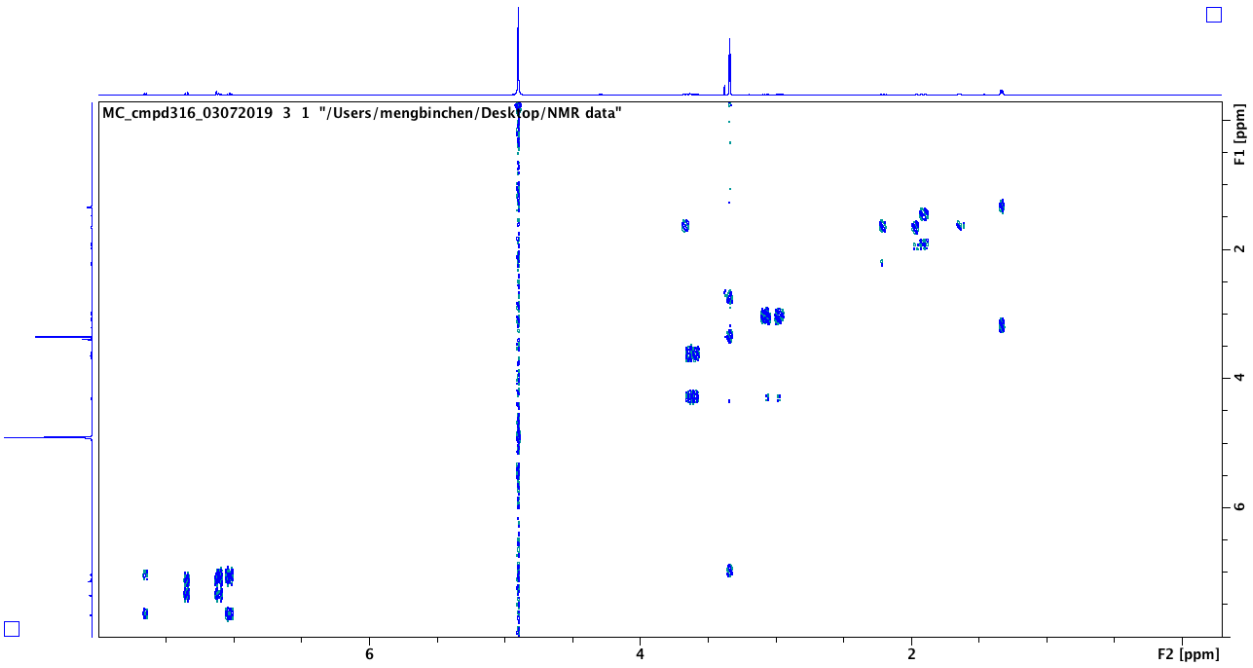

Fig S33. COSY spectrum of compound **7** in CD_3OD.

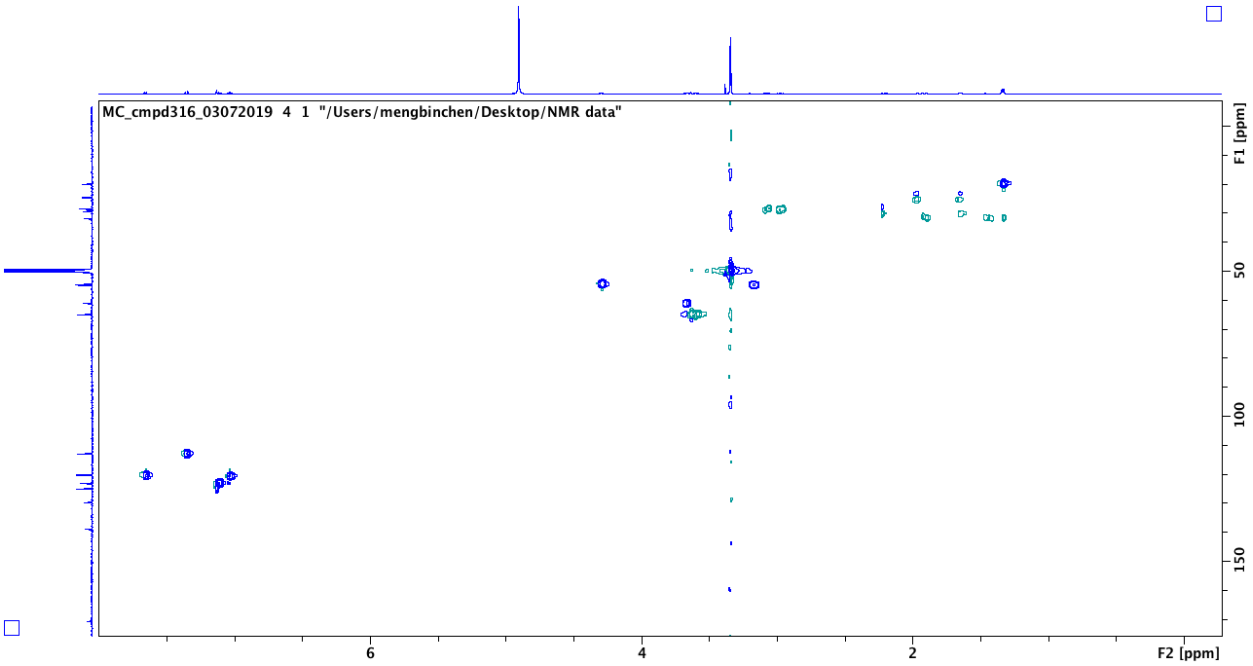

Fig S34. HSQC spectrum of compound **7** in CD_3OD.

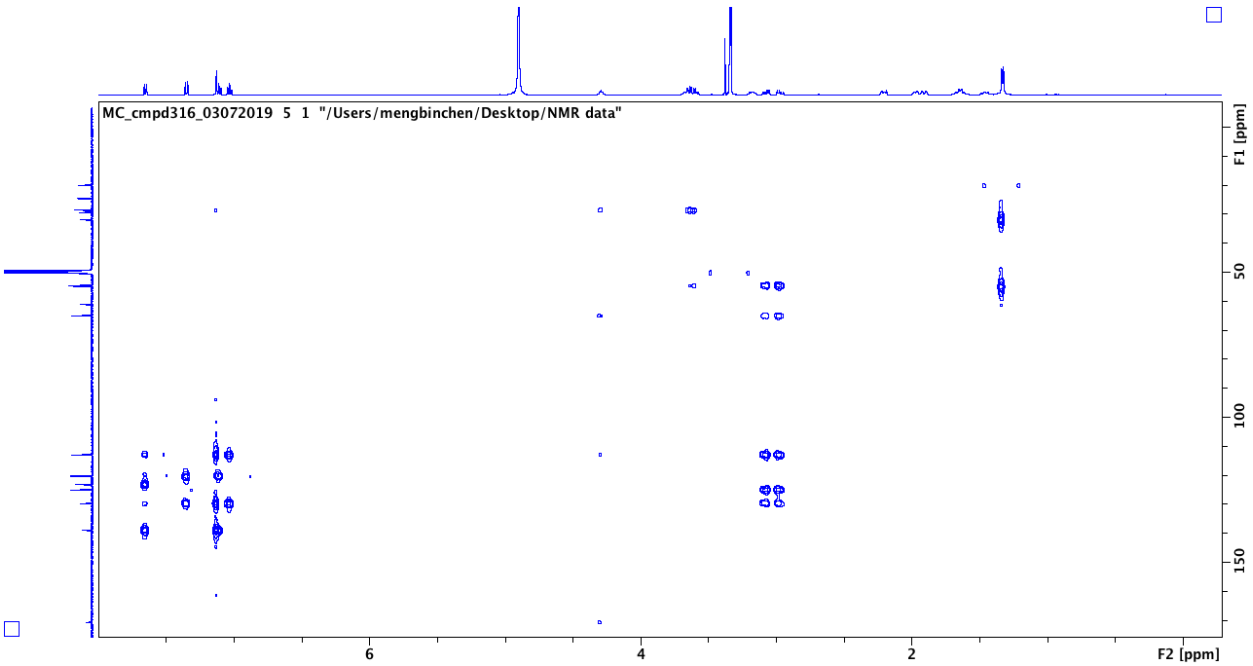

Fig S35. HMBC spectrum of compound **7** in CD_3OD.

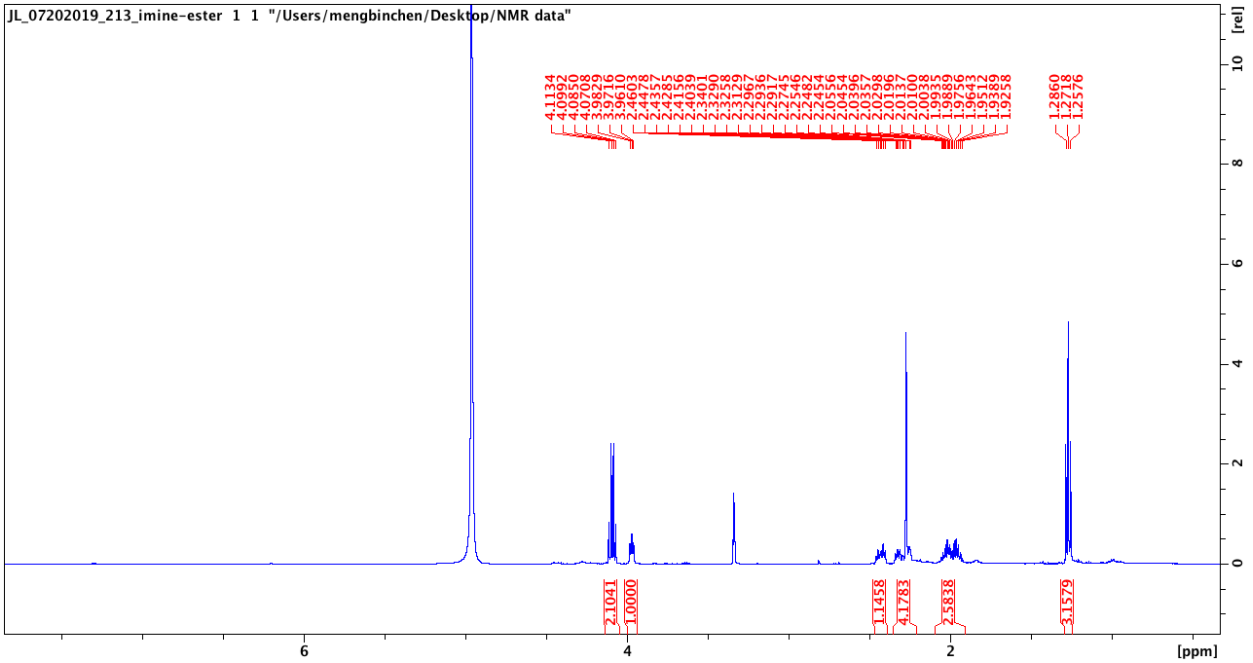

Fig S36. ^{1}H spectrum of compound **14** in CD_3OD, 500 MHz.

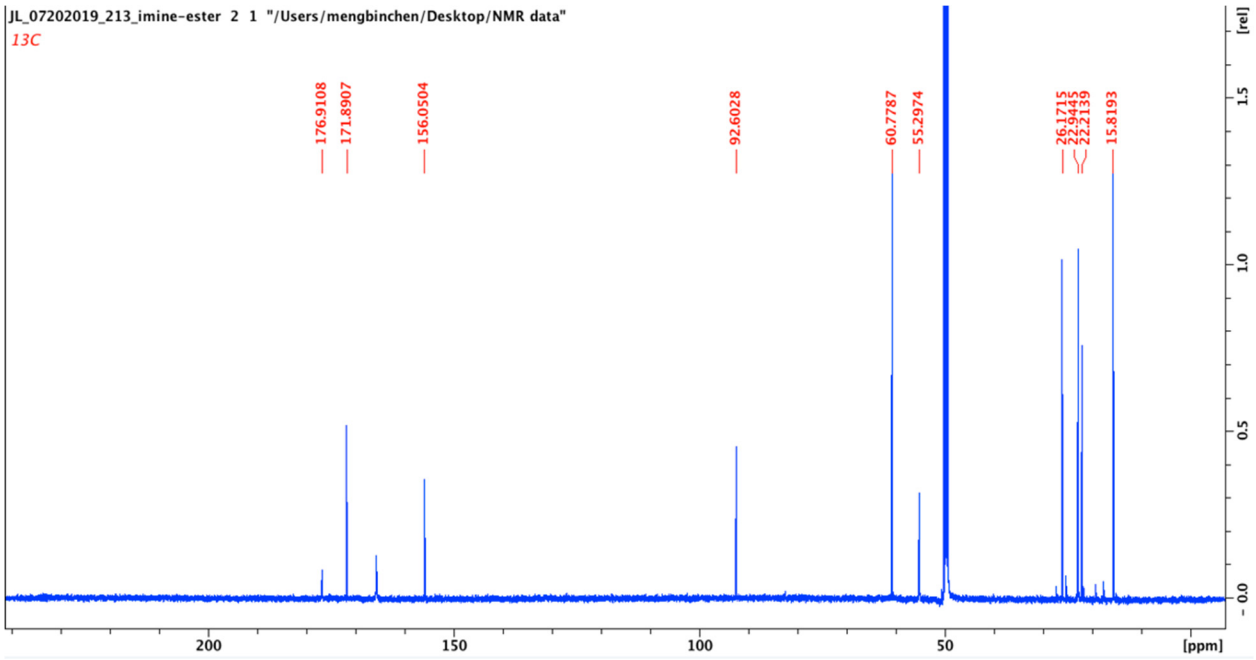

Fig S37. ^{13}C spectrum of compound **14** in CD_3OD, 125 MHz.

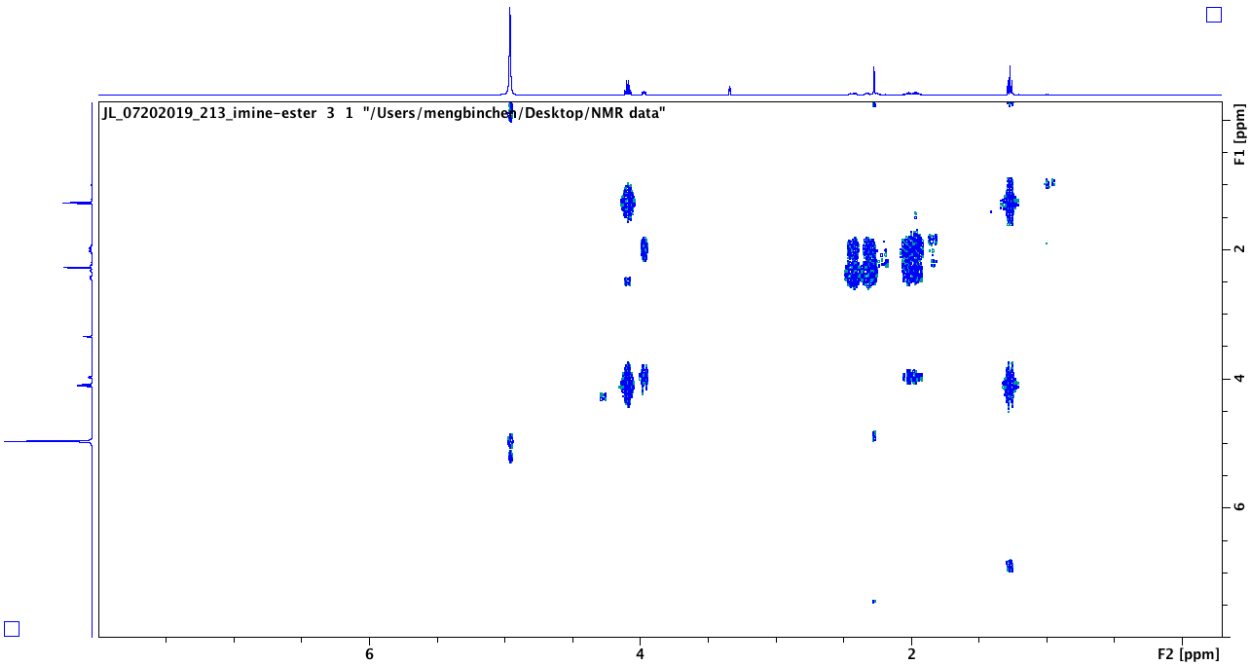

Fig S38. COSY spectrum of compound **14** in CD_3OD.

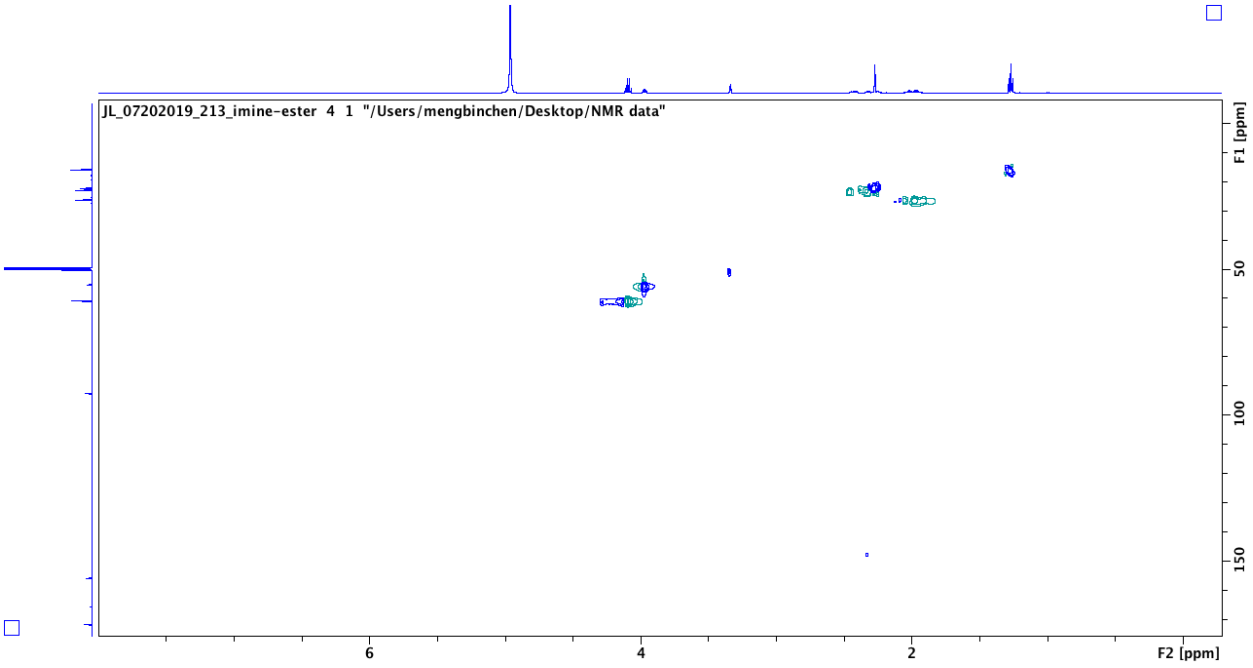

Fig S39. HSQC spectrum of compound **14** in CD_3OD.

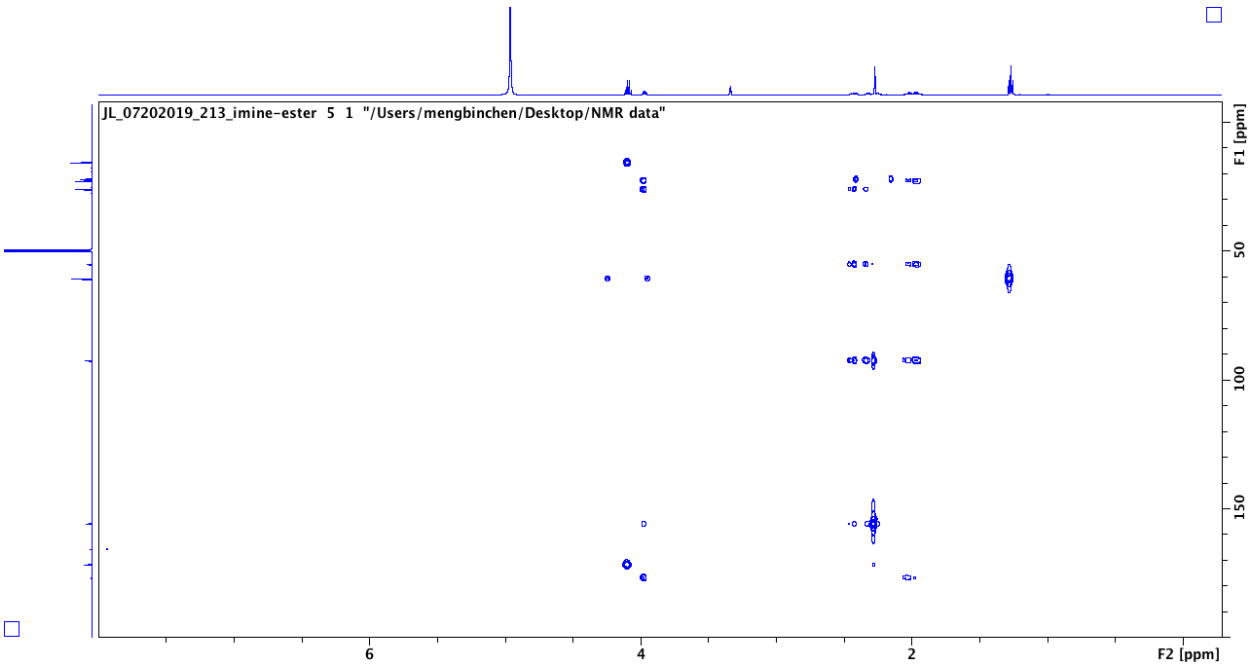

Fig S40. HMBC spectrum of compound **14** in CD_3OD.

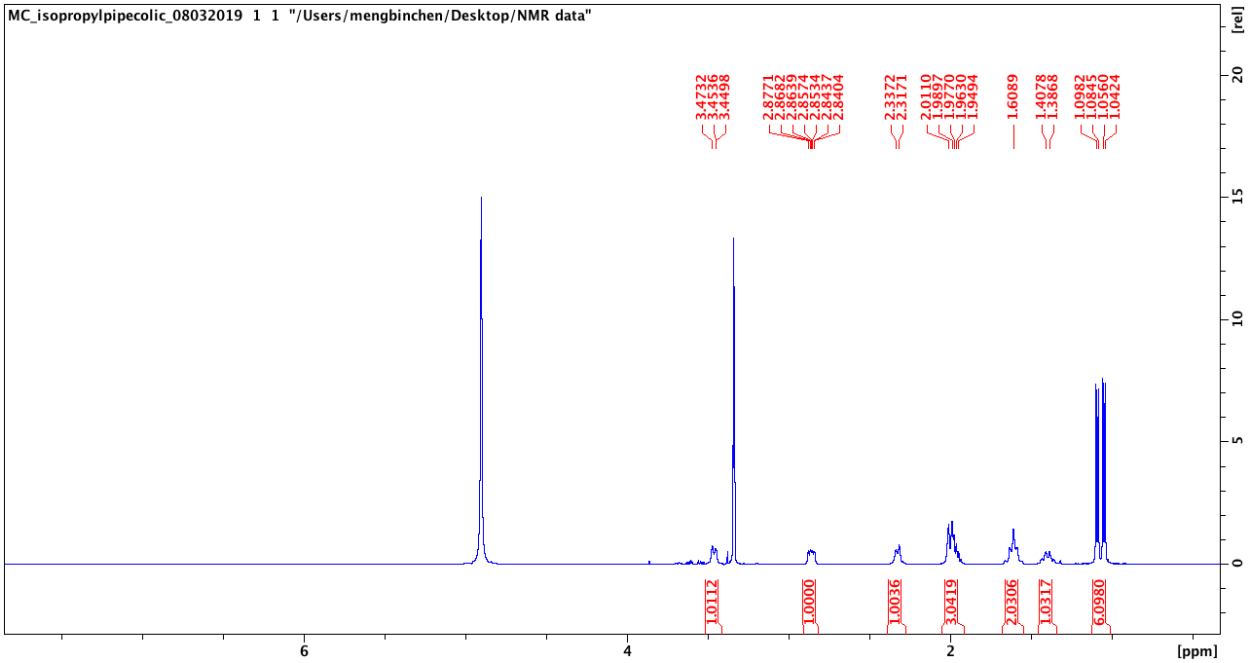

Fig S41. ^{1}H spectrum of compound **22** in CD_3OD, 500 MHz.

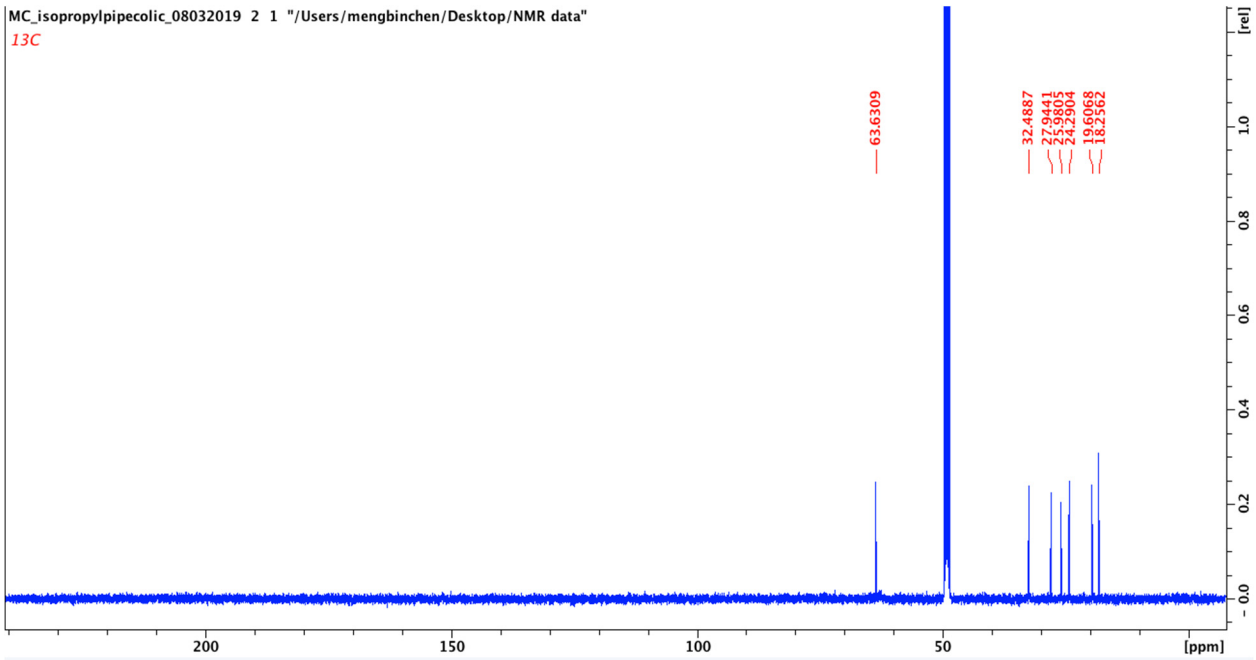

Fig S42. ^{13}C spectrum of compound **22** in CD_3OD, 125 MHz.

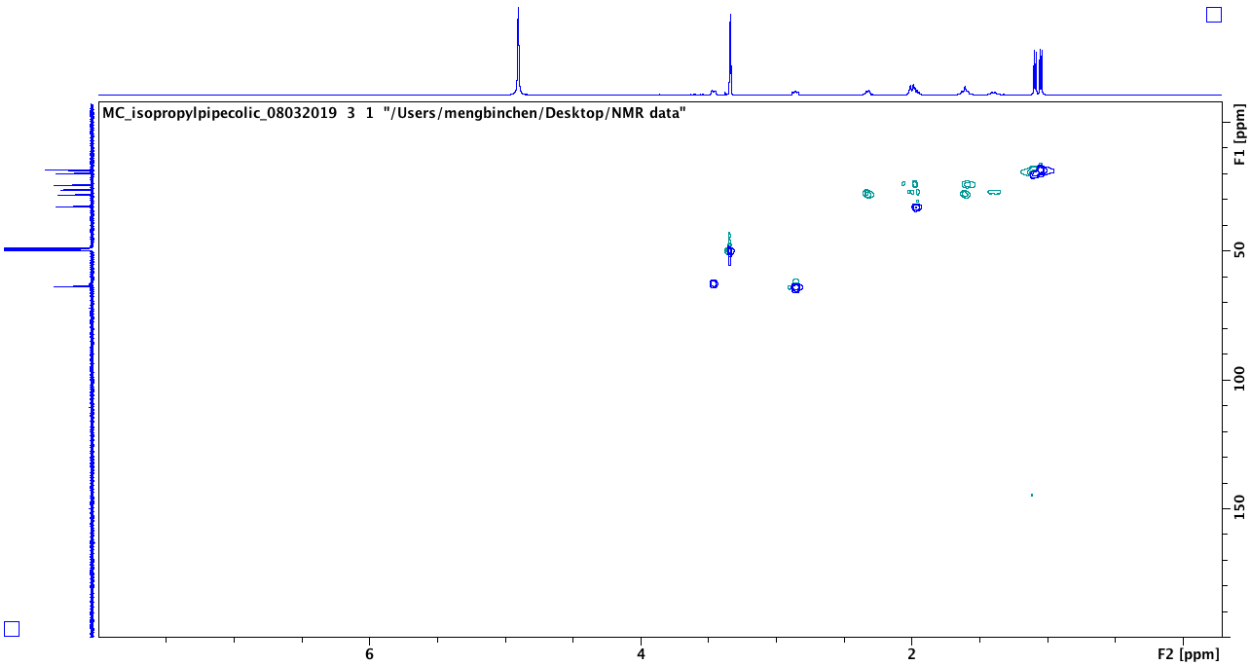

Fig S43. HSQC spectrum of compound **22** in CD_3OD.

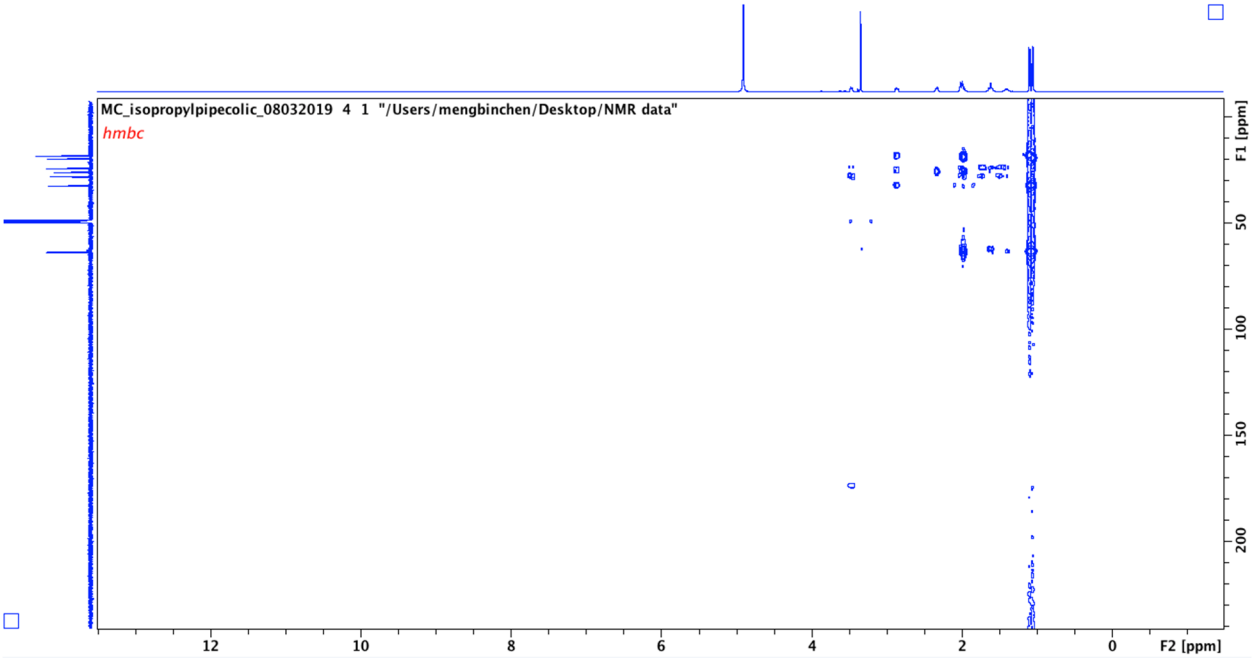

Fig S44. HMBC spectrum of compound **22** in CD_3OD.

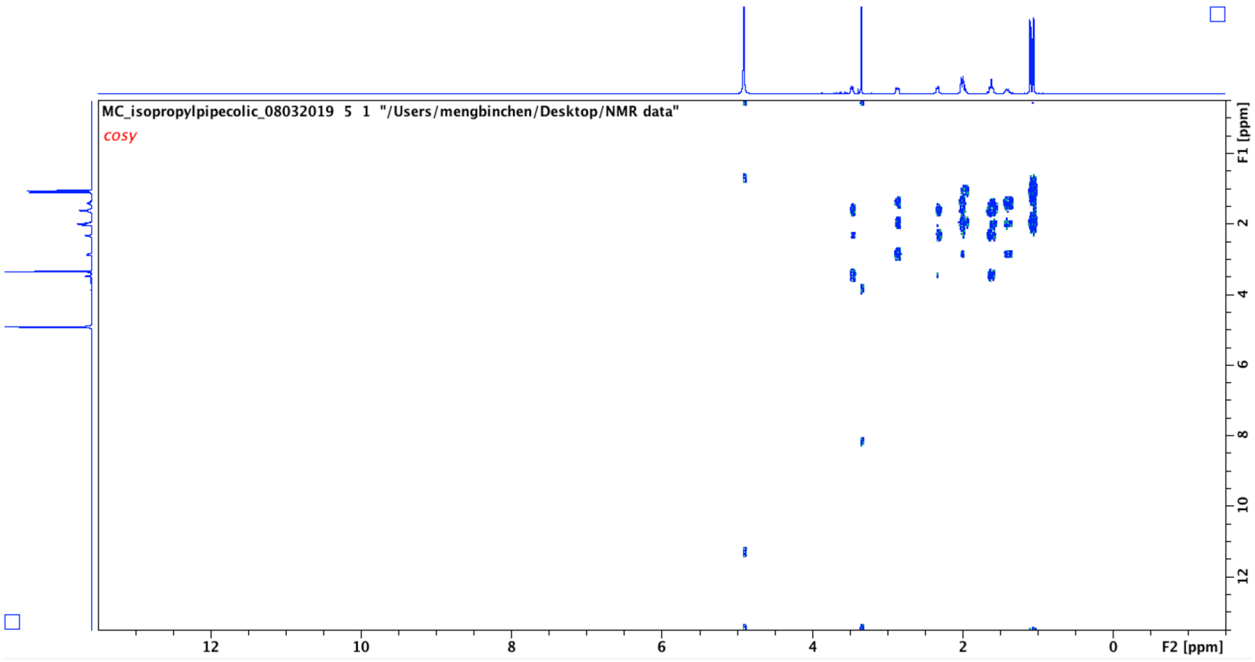

Fig S45. COSY spectrum of compound **22** in CD_3OD.

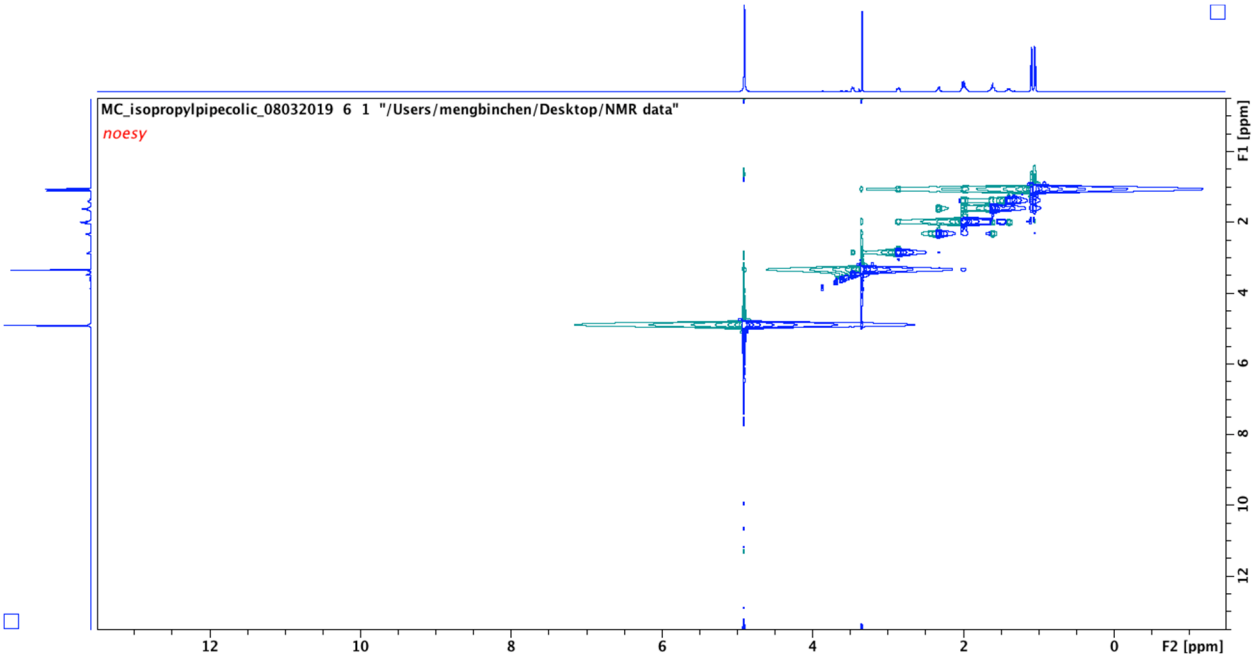

Fig S46. NOESY spectrum of compound **22** in CD_3OD.

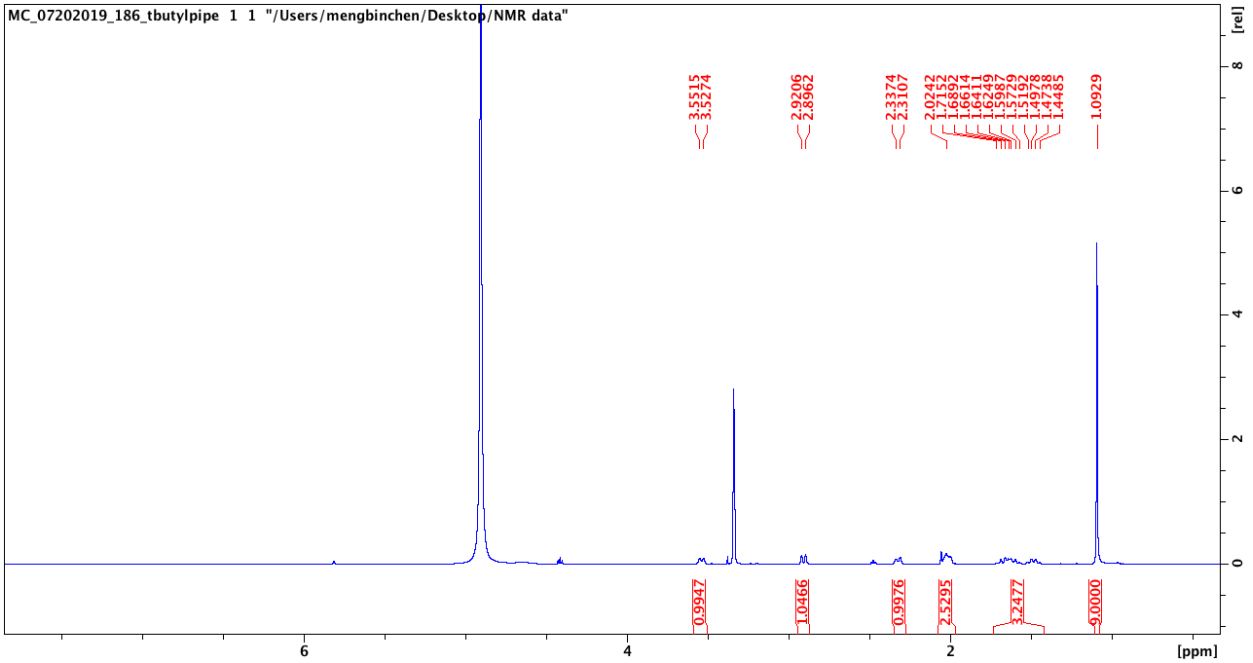

Fig S47. ^{1}H spectrum of compound **23** in CD_3OD, 500 MHz.

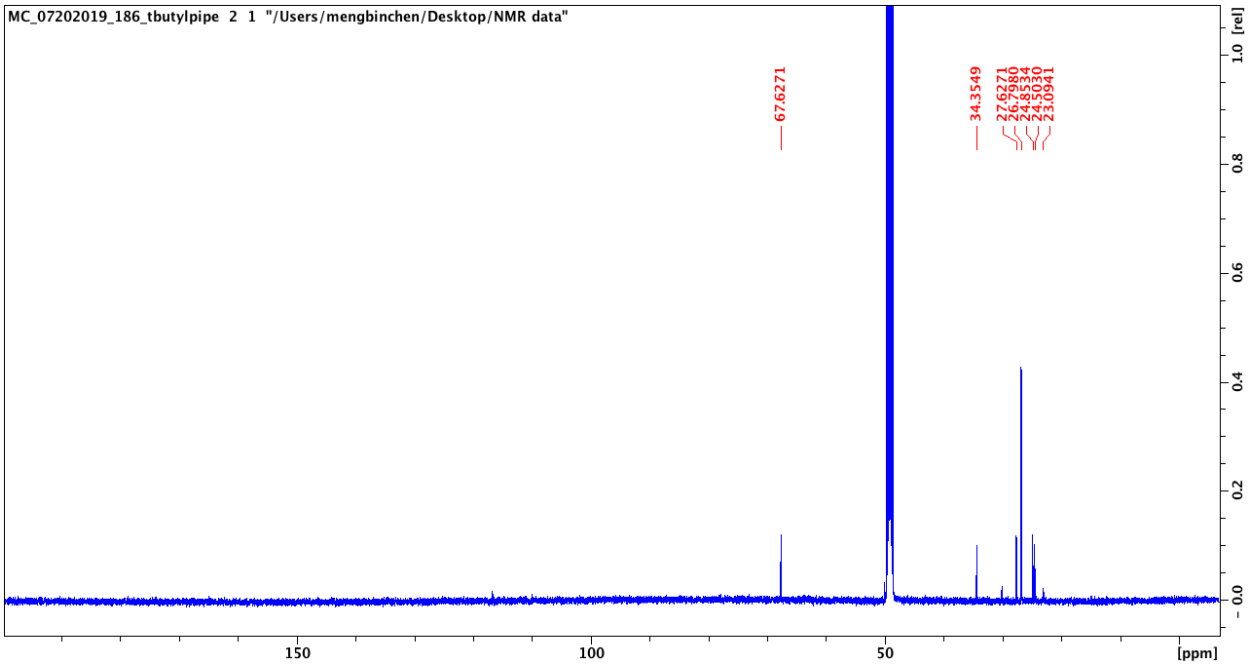

Fig S48. ^{13}C spectrum of compound **23** in CD_3OD, 125 MHz.

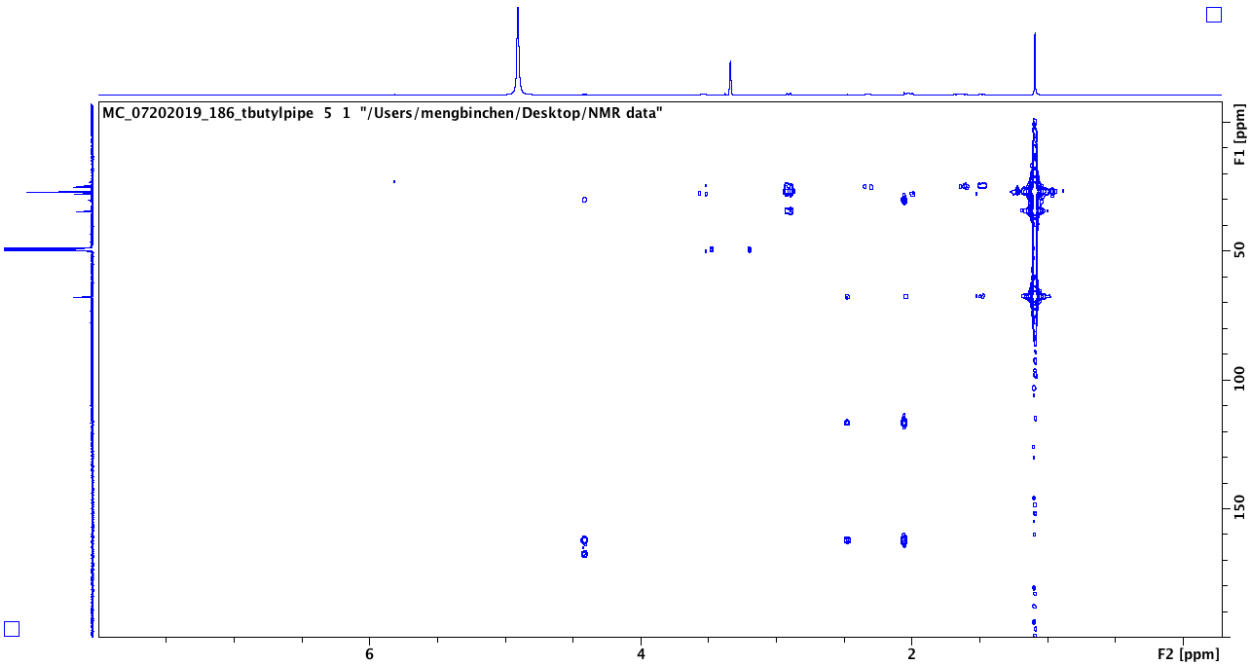

Fig S49. HMBC spectrum of compound **23** in CD_3OD.

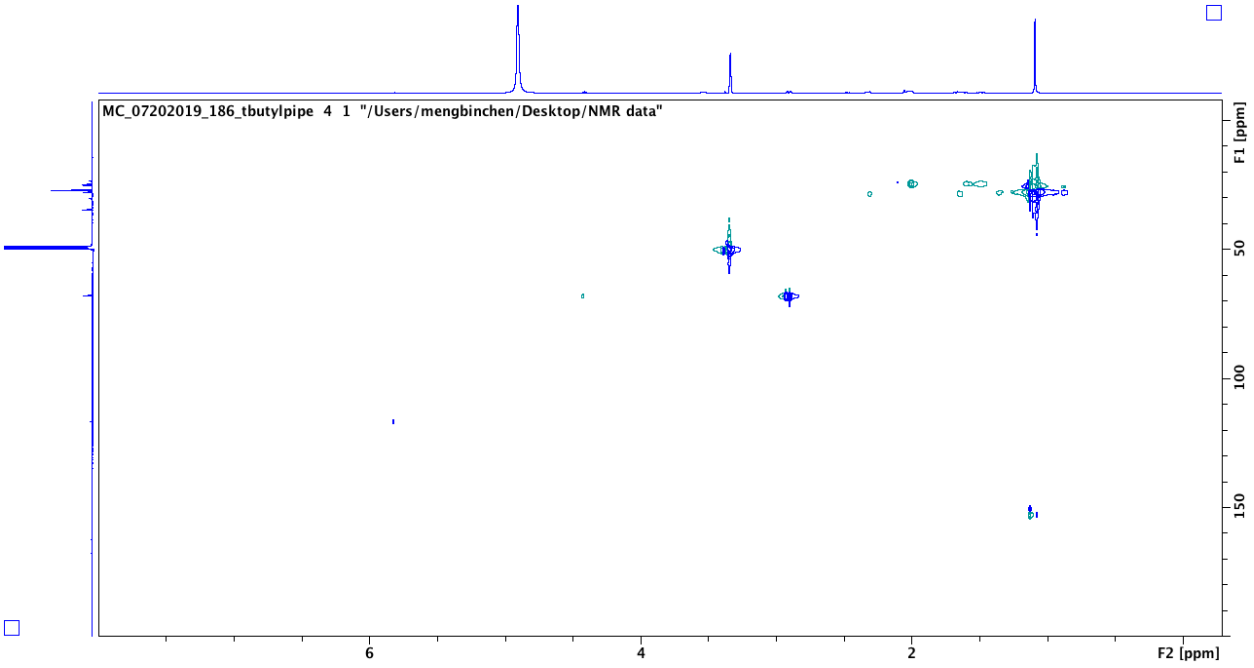

Fig S50. HSQC spectrum of compound **23** in CD_3OD.

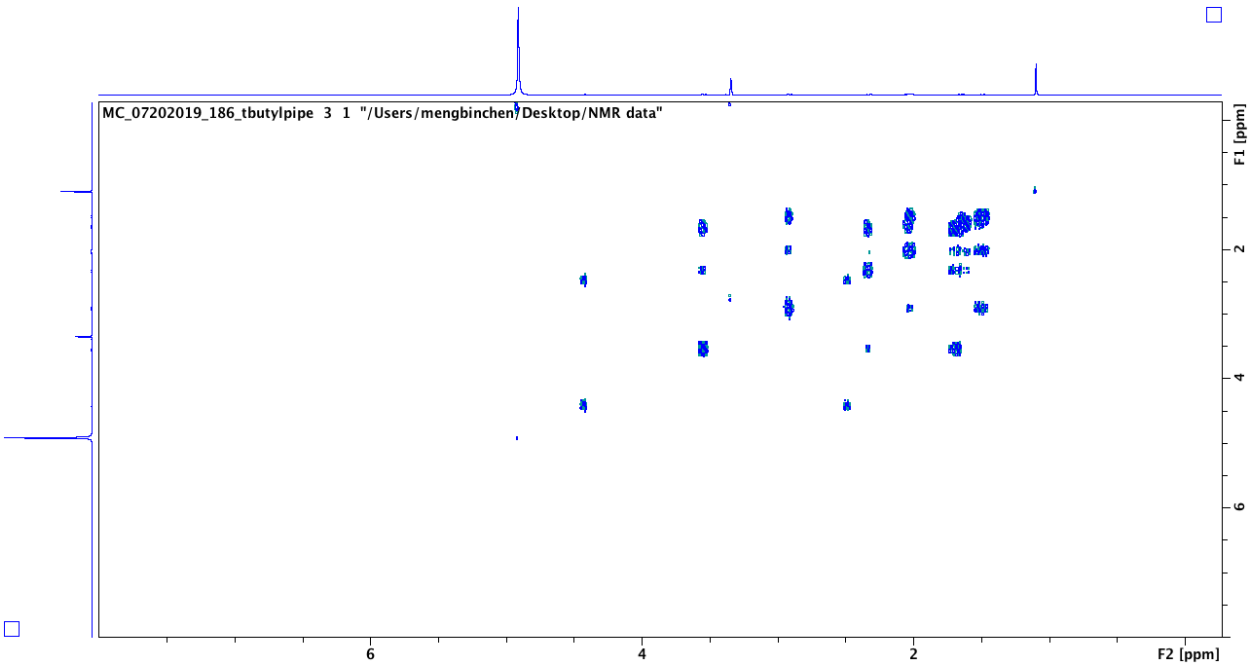

Fig S51. COSY spectrum of compound **23** in CD_3OD.

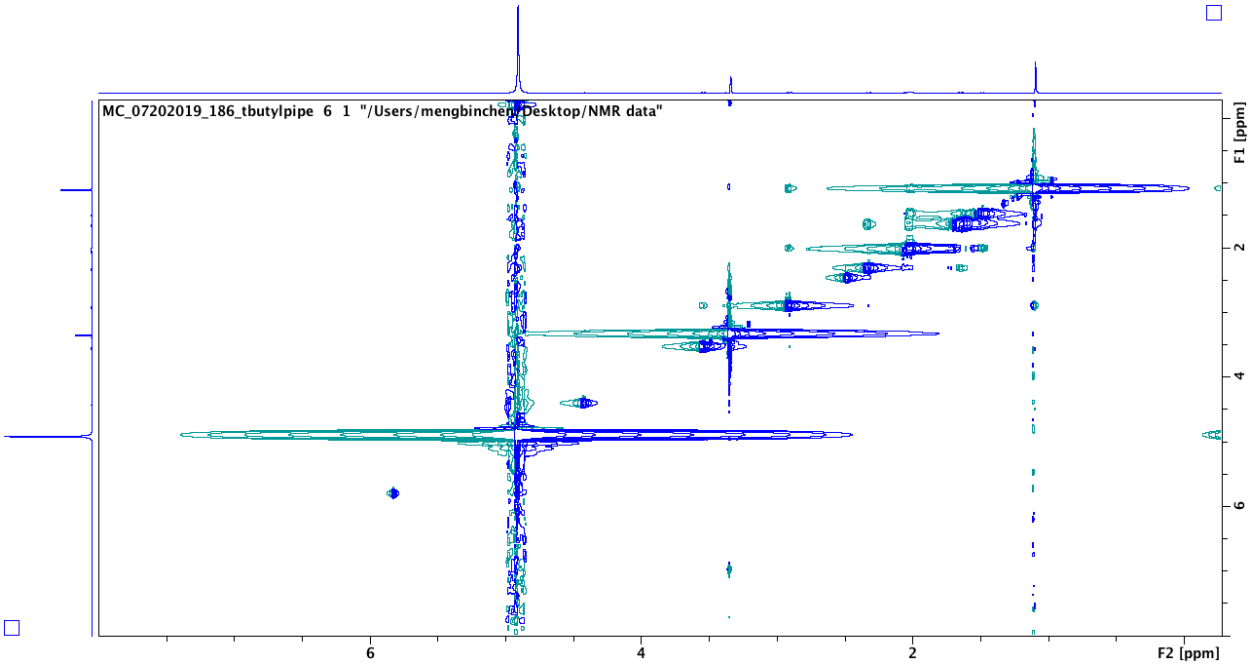

Fig S52. NOESY spectrum of compound **23** in CD_3OD.

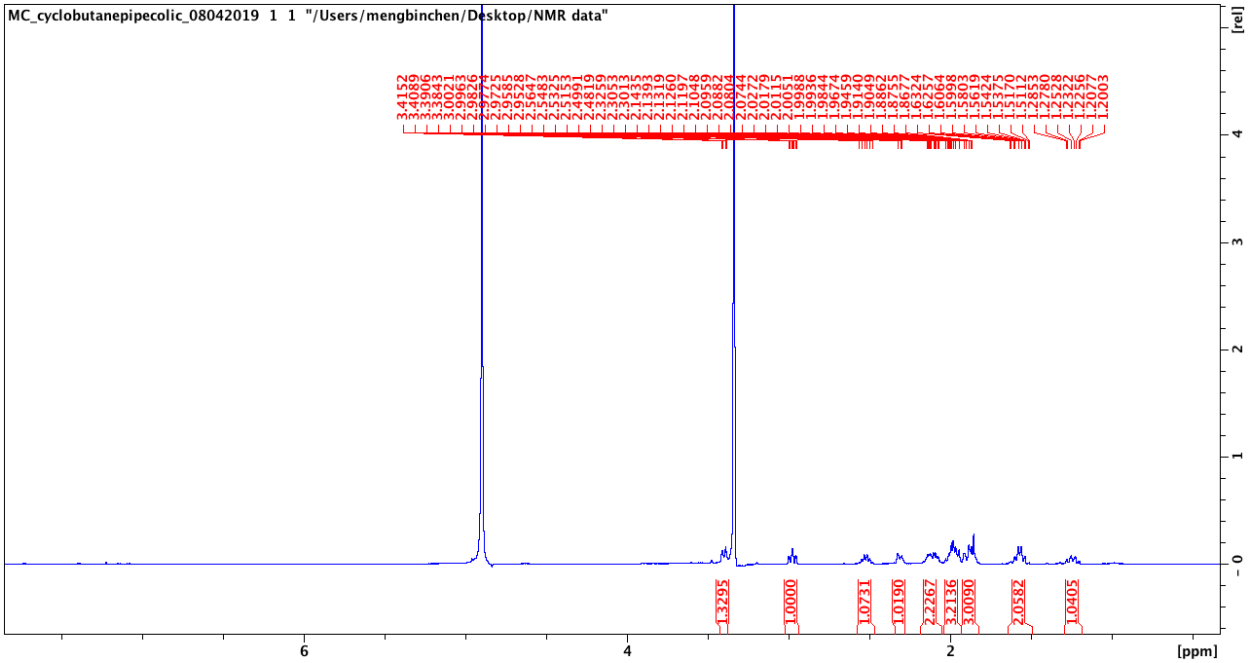

Fig S53. ^{1}H spectrum of compound **24** in CD_3OD, 500 MHz.

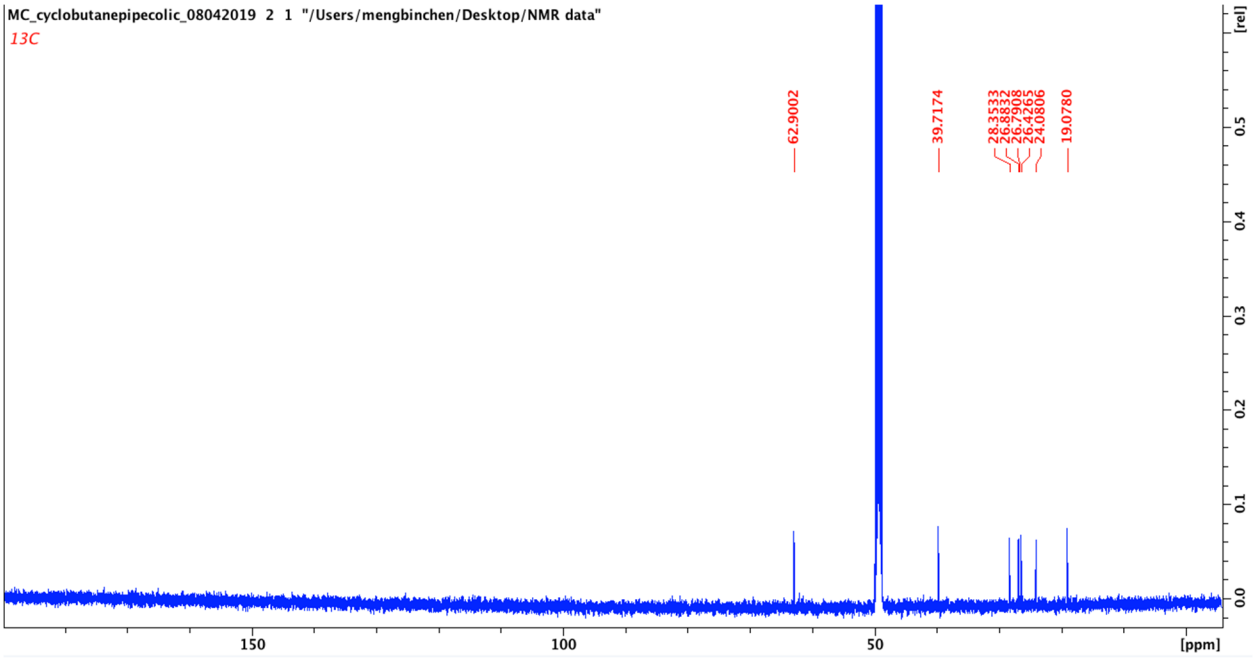

Fig S54. ^{13}C spectrum of compound **24** in CD_3OD, 125 MHz.

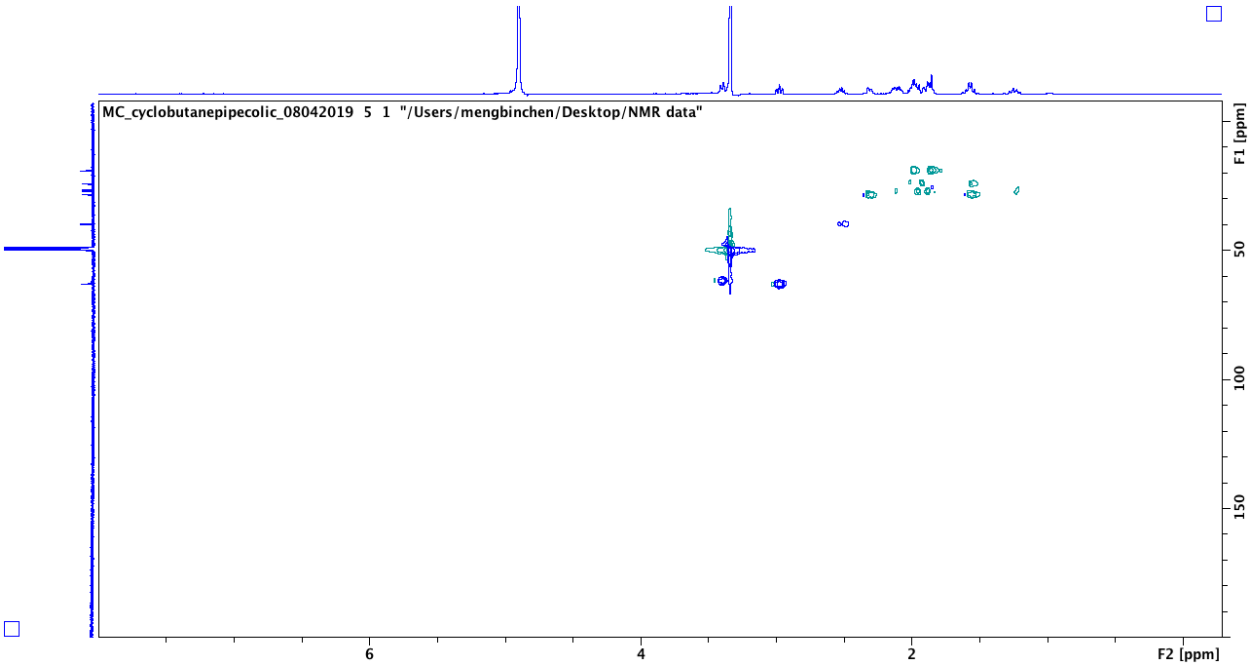

Fig S55. HSQC spectrum of compound **24** in CD_3OD.

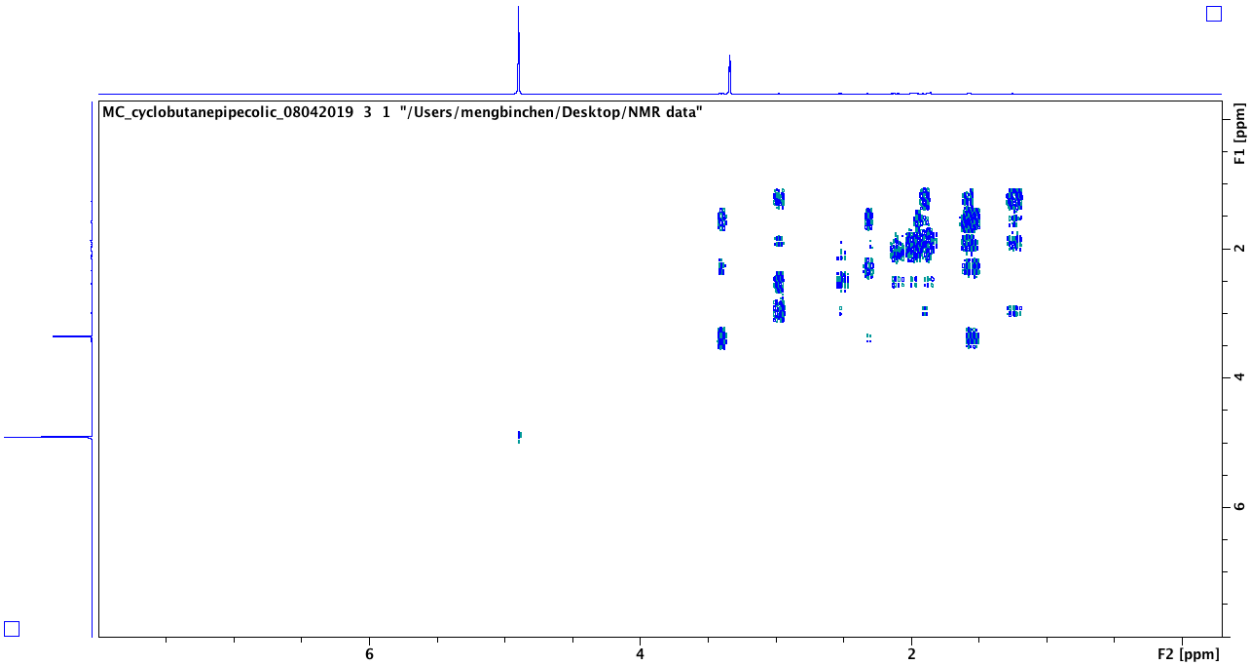

Fig S56. COSY spectrum of compound **24** in CD_3OD.

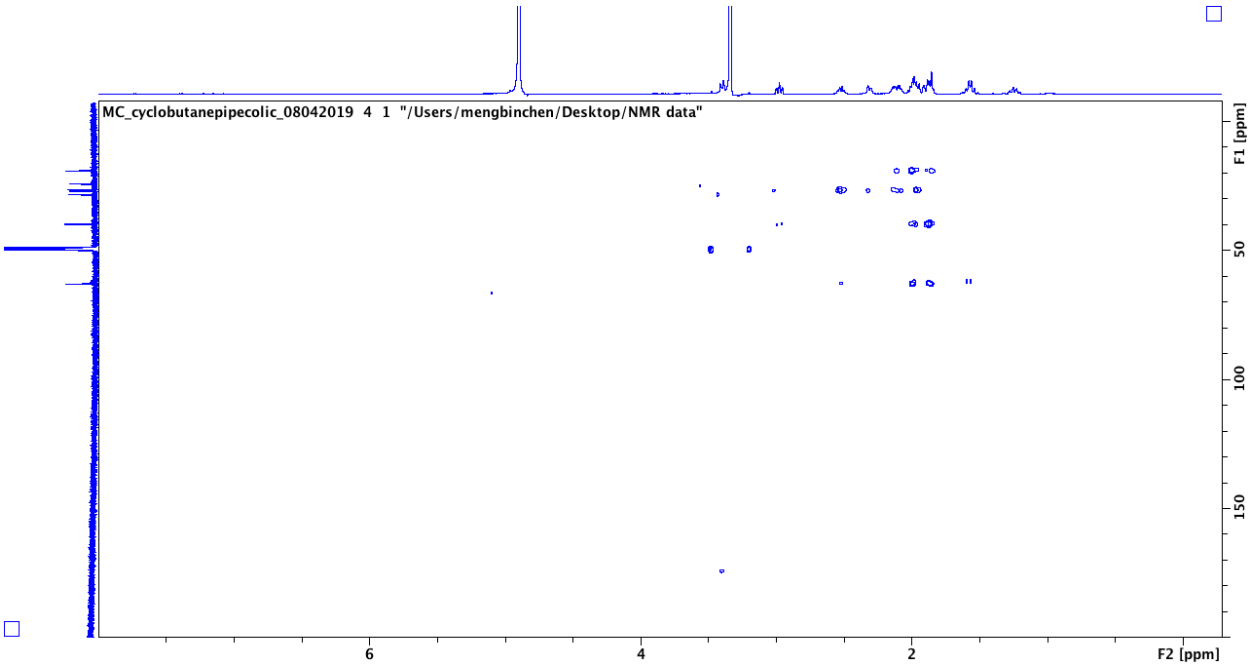

Fig S57. HMBC spectrum of compound **24** in CD_3OD.

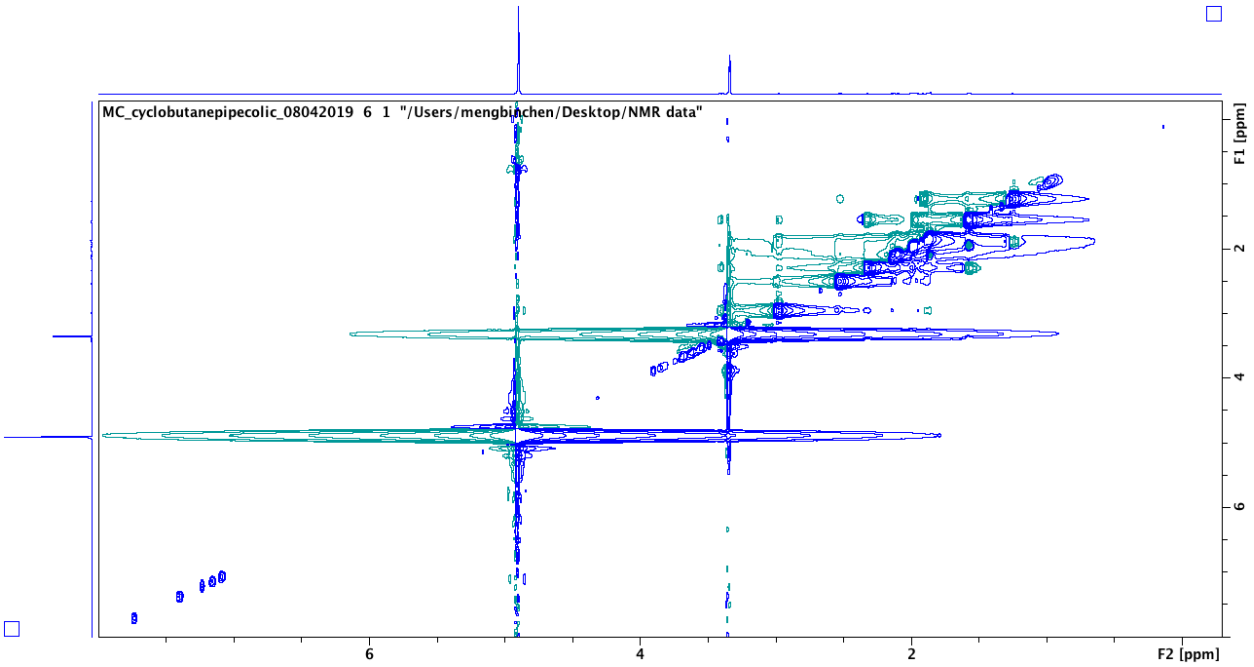

Fig S58. NOESY spectrum of compound **24** in CD_3OD.

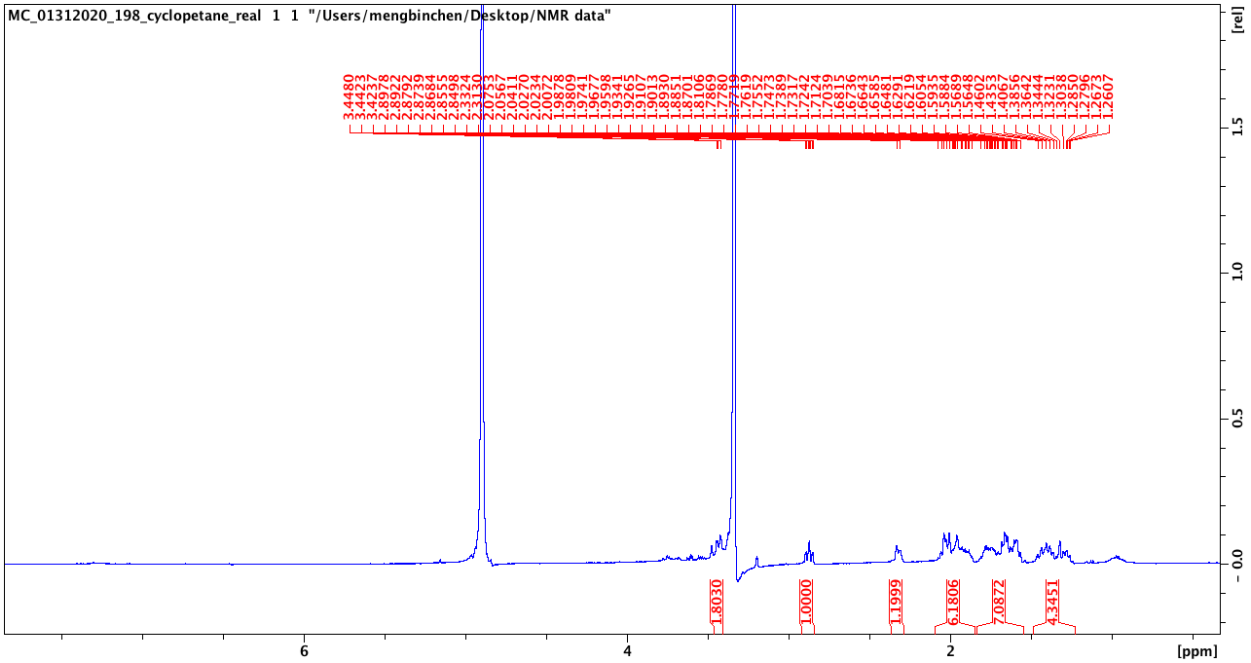

Fig S59. ^{1}H spectrum of compound **25** in CD_3OD, 500 MHz.

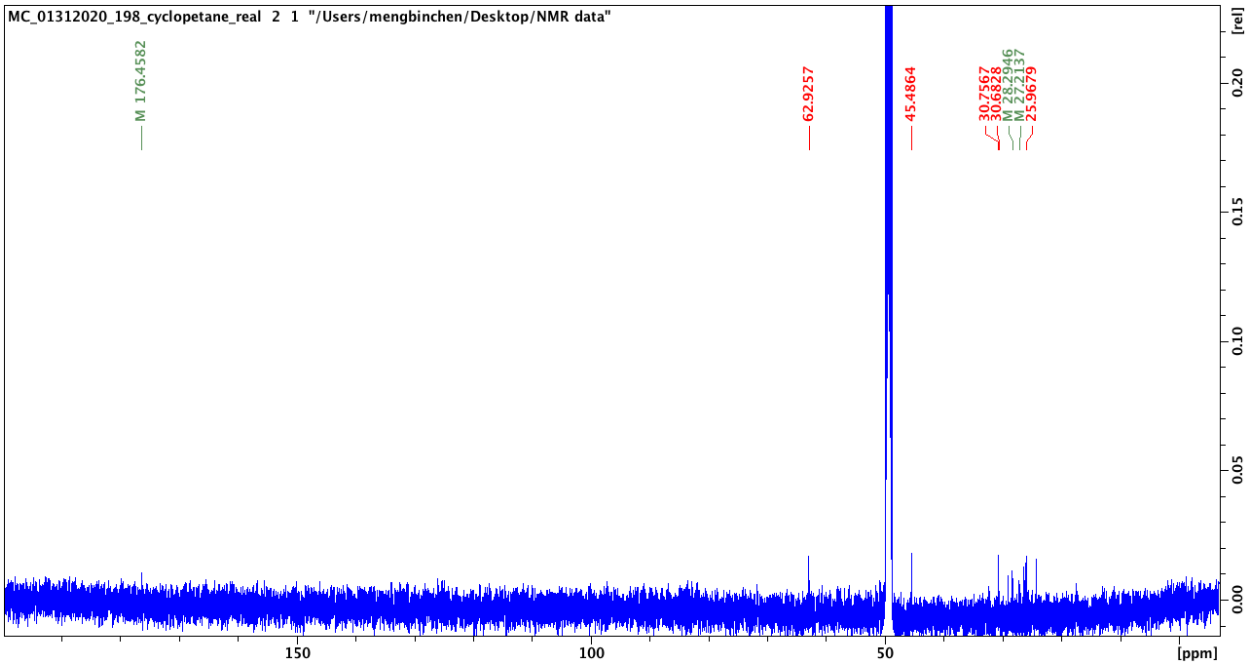

Fig S60. ^{13}C spectrum of compound **25** in CD_3OD, 125 MHz.

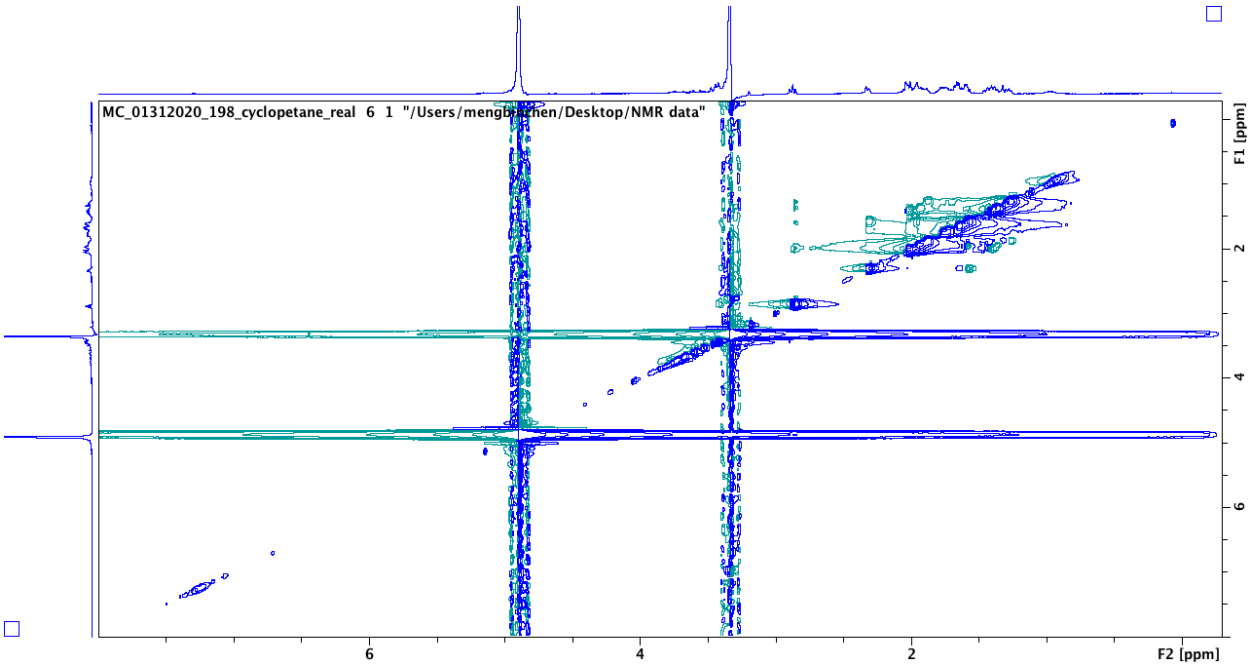

Fig S61. NOESY spectrum of compound **25** in CD_3OD.

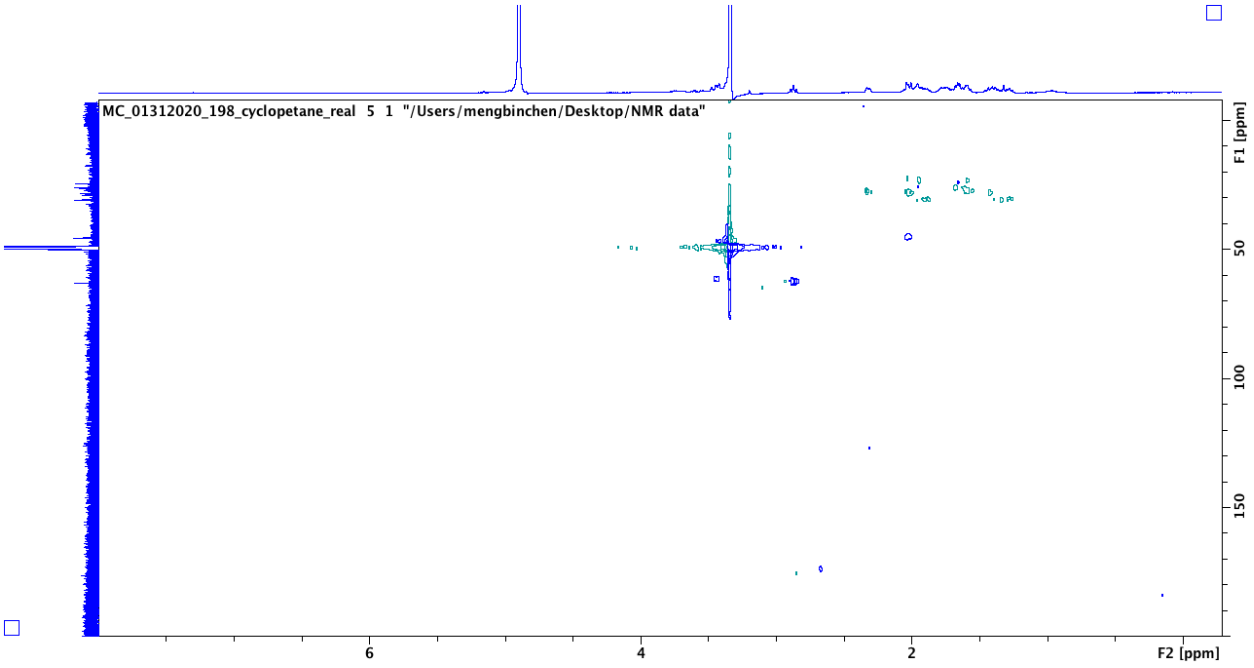

Fig S62. HSQC spectrum of compound **25** in CD_3OD.

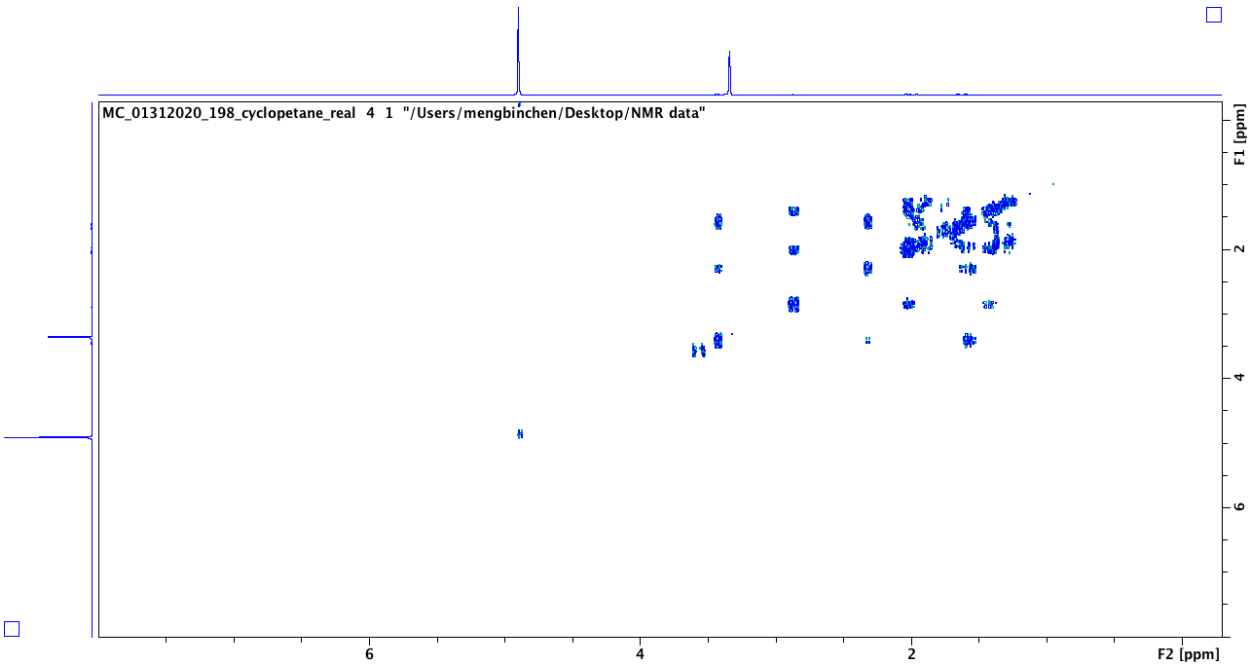

Fig S63. COSY spectrum of compound **25** in CD_3OD.

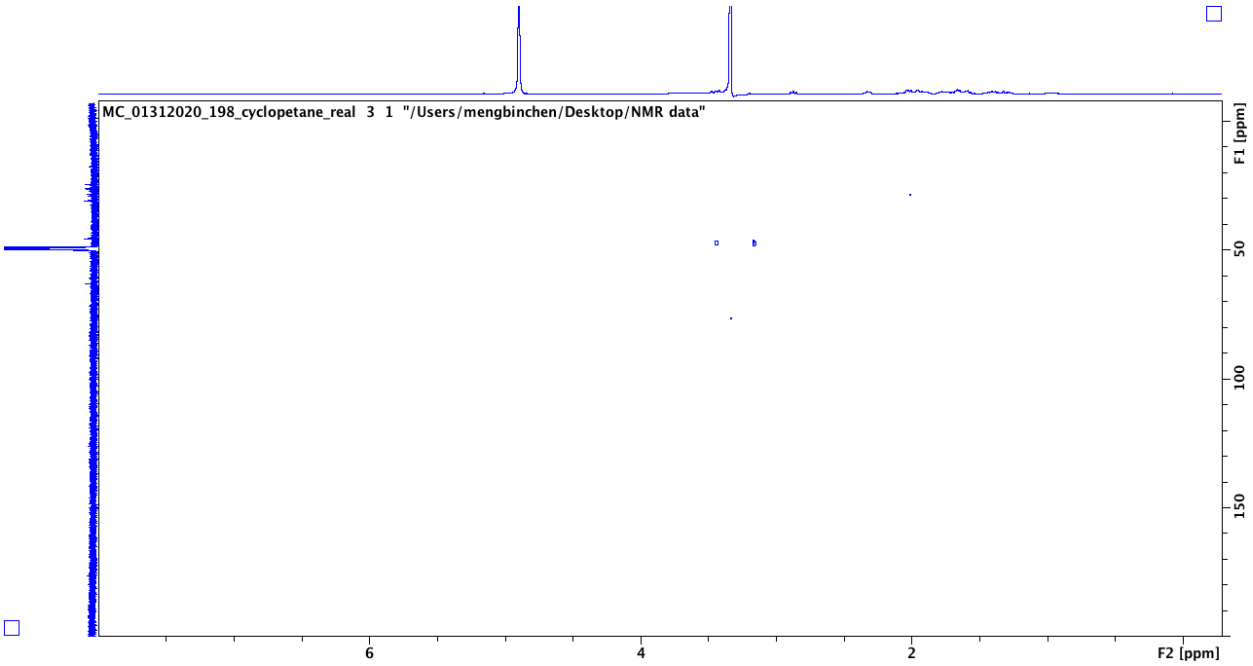

Fig S64. HMBC spectrum of compound **25** in CD_3OD.

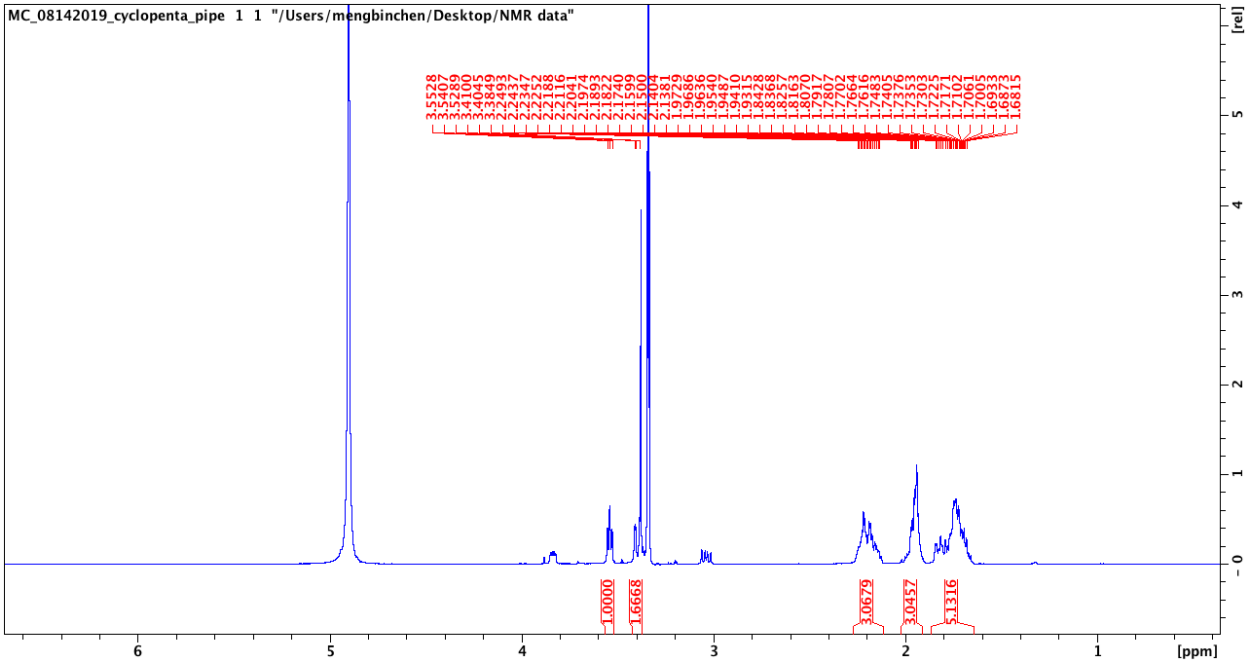

Fig S65. ^{1}H spectrum of compound **26$_{cis}$** in CD_3OD, 500 MHz.

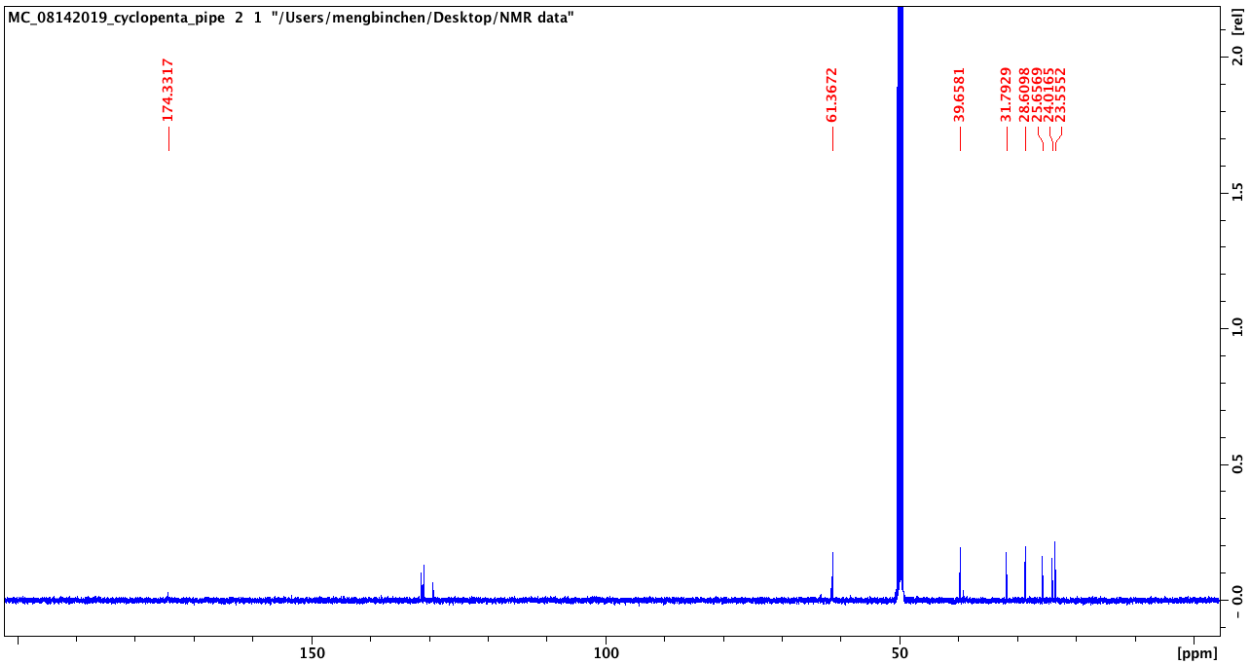

Fig S66. ^{13}C spectrum of compound **26$_{cis}$** in CD_3OD, 125 MHz.

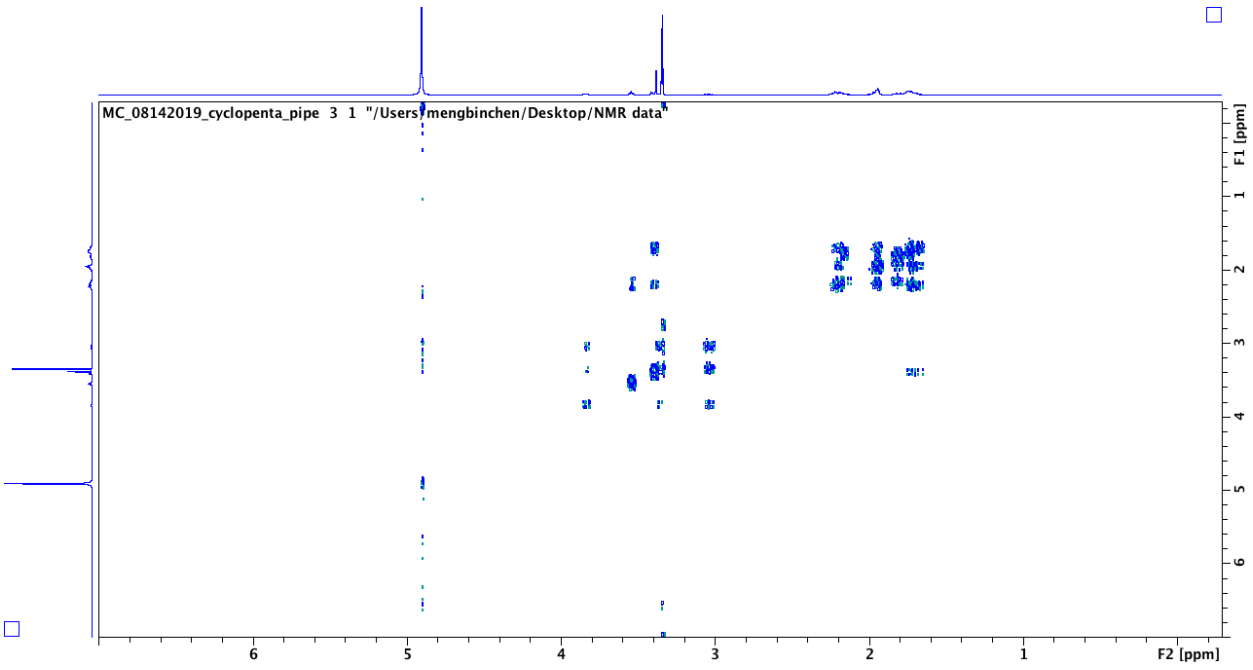

Fig S67. COSY spectrum of compound **26$_{cis}$** in CD_3OD.

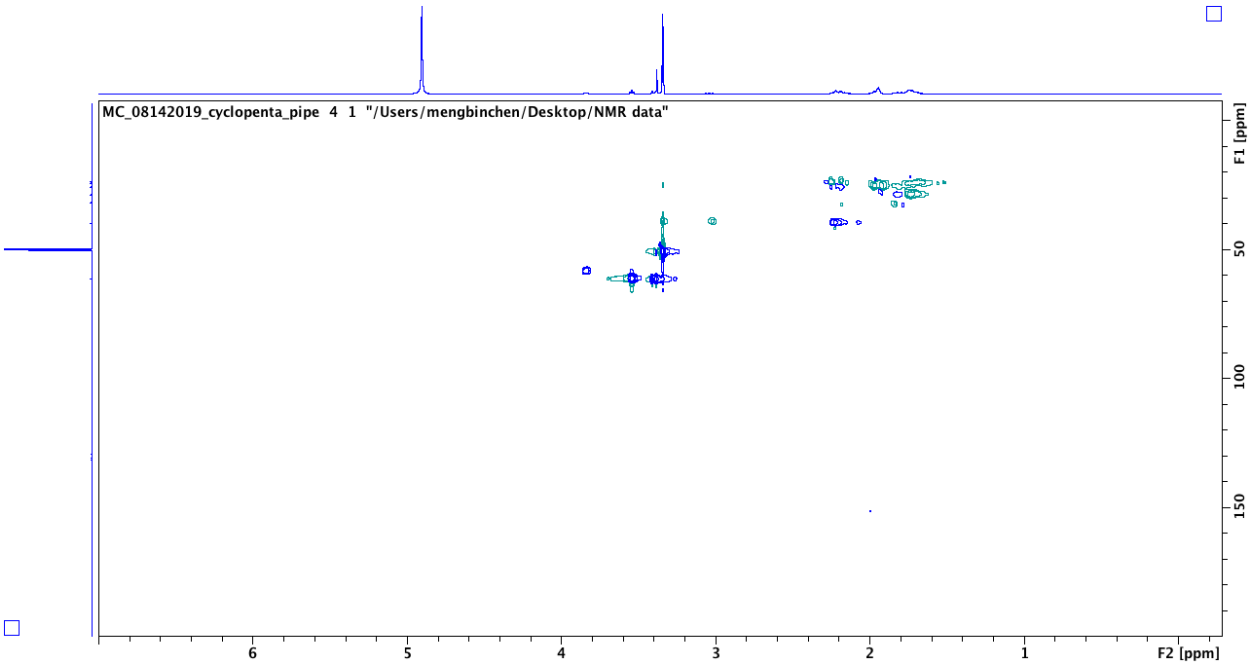

Fig S68. HSQC spectrum of compound **26$_{cis}$** in CD_3OD.

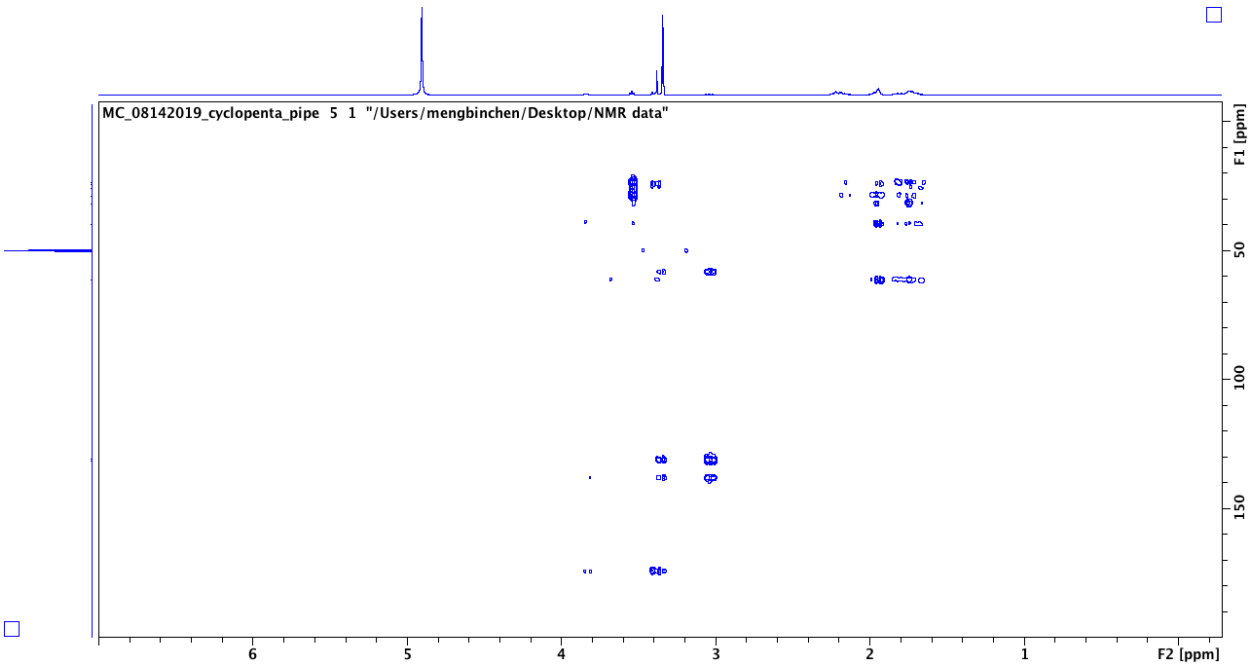

Fig S69. HMBC spectrum of compound **26_{cis}** in CD_3OD.

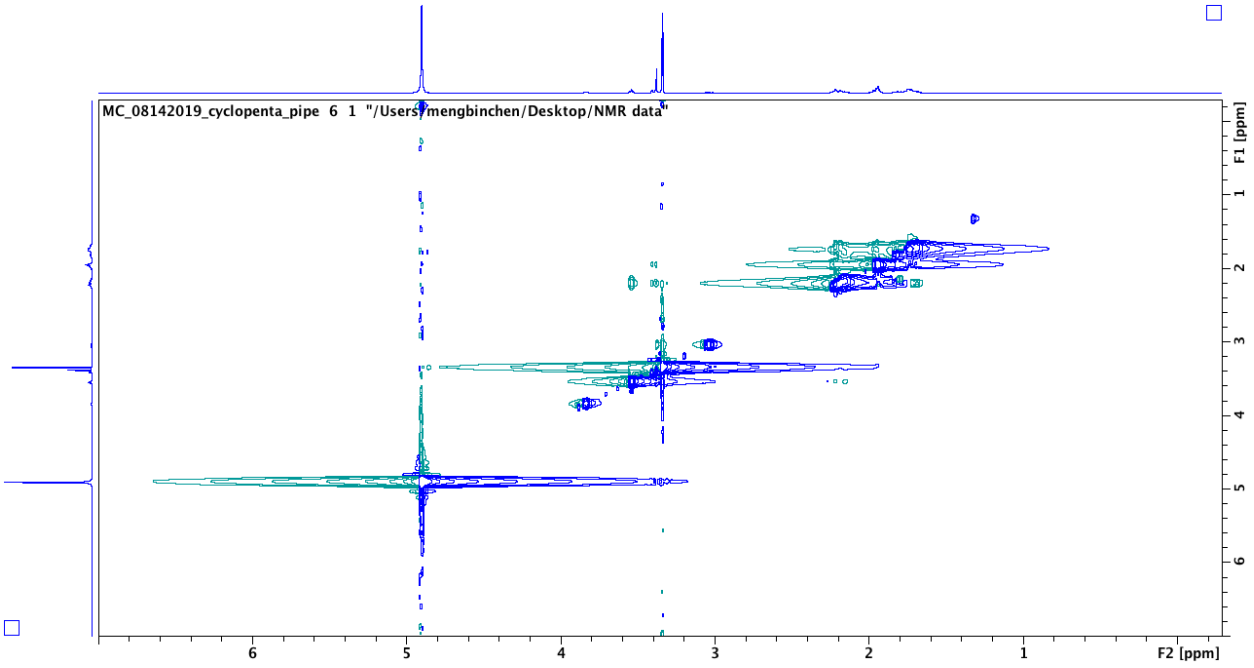

Fig S70. NOESY spectrum of compound **26_{cis}** in CD_3OD.

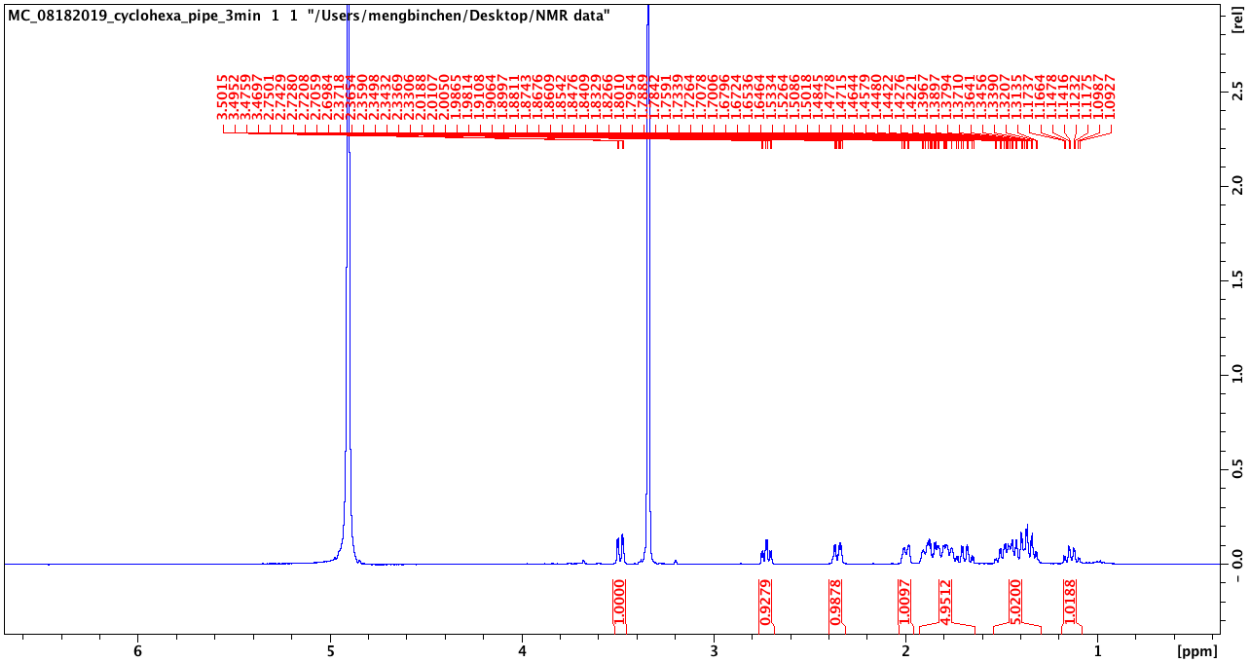

Fig S71. ^{1}H spectrum of compound **27$_{trans}$** in CD_3OD, 500 MHz.

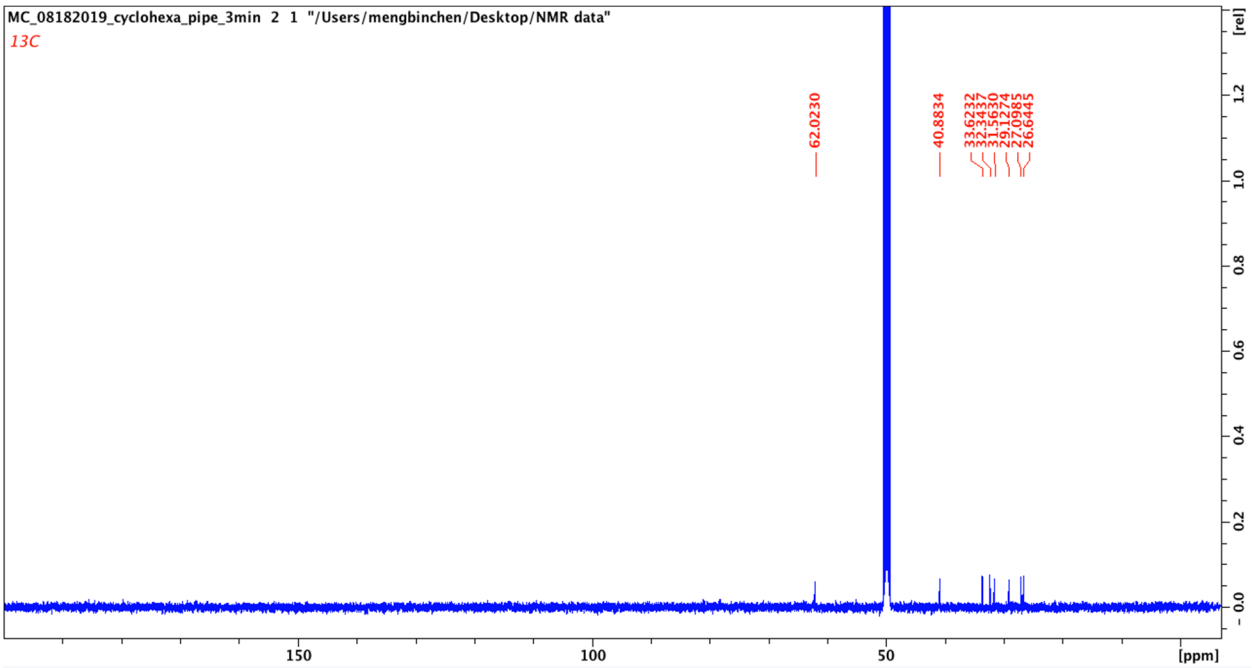

Fig S72. ^{13}C spectrum of compound **27$_{trans}$** in CD_3OD, 125 MHz.

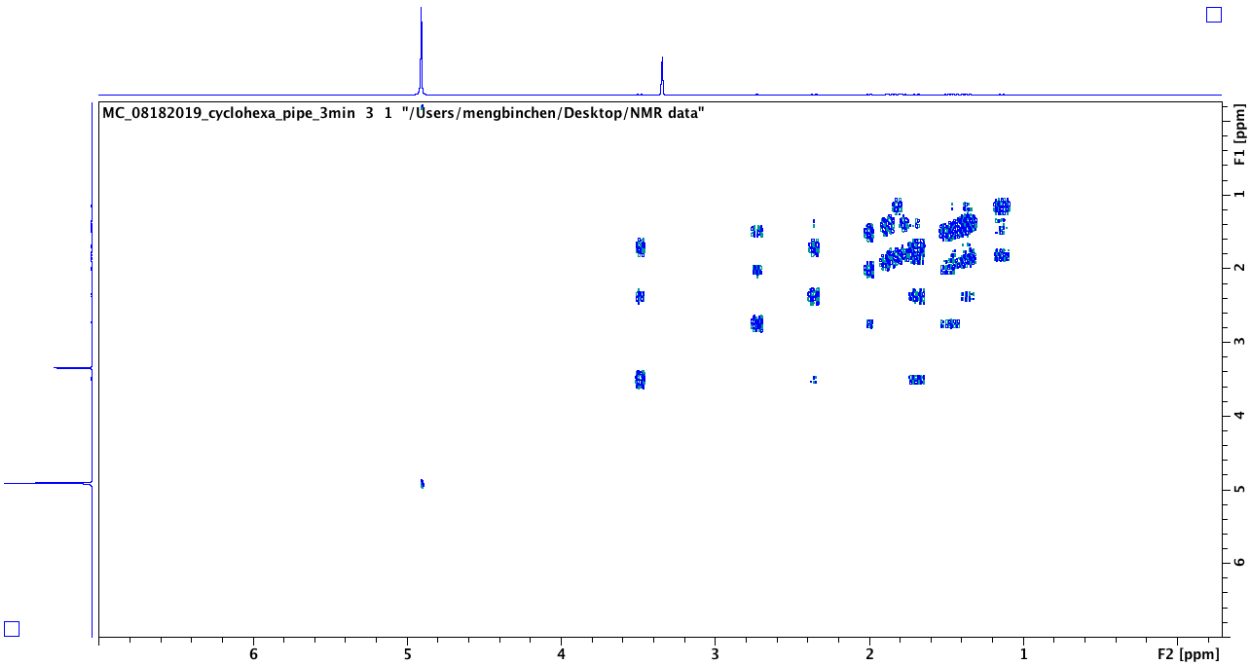

Fig S73. COSY spectrum of compound **27**$_{trans}$ in CD_3OD.

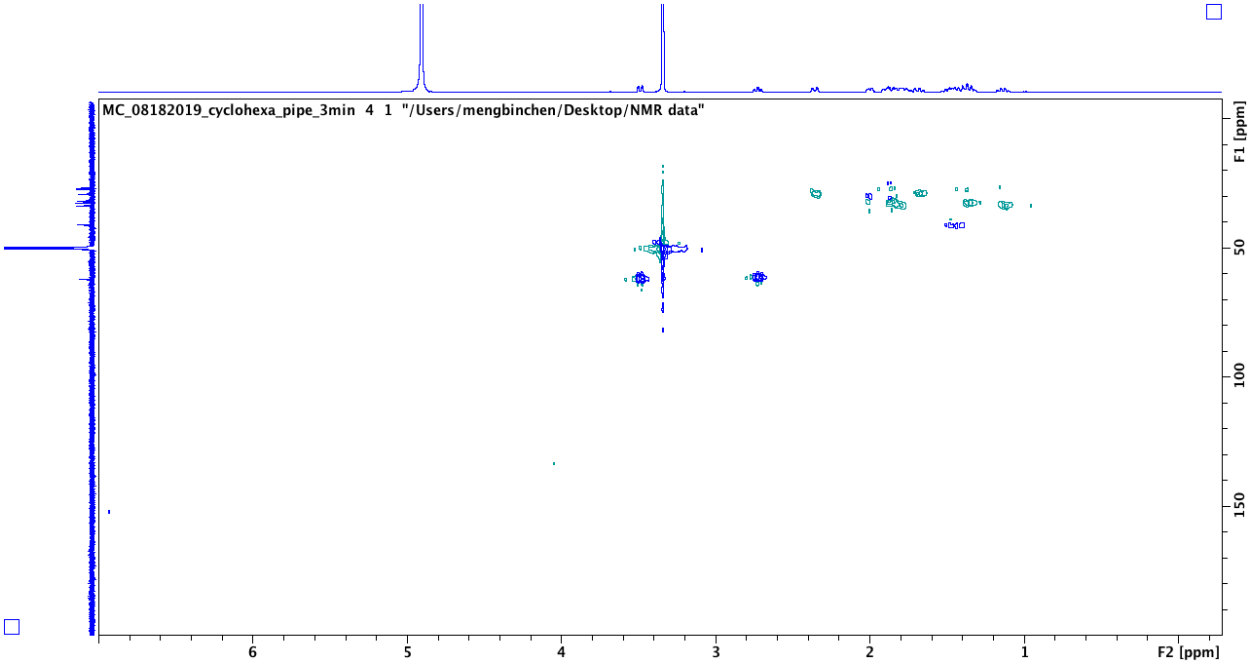

Fig S74. HSQC spectrum of compound **27**$_{trans}$ in CD_3OD.

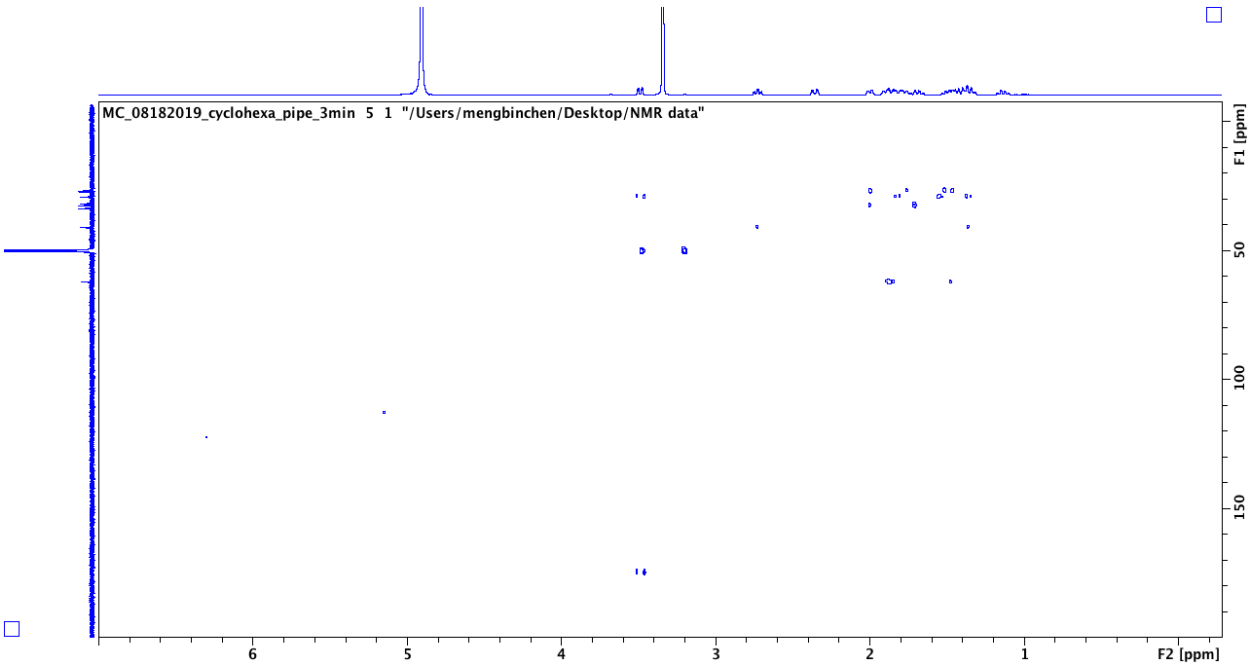

Fig S75. HMBC spectrum of compound **27**$_{\textbf{trans}}$ in CD_3OD.

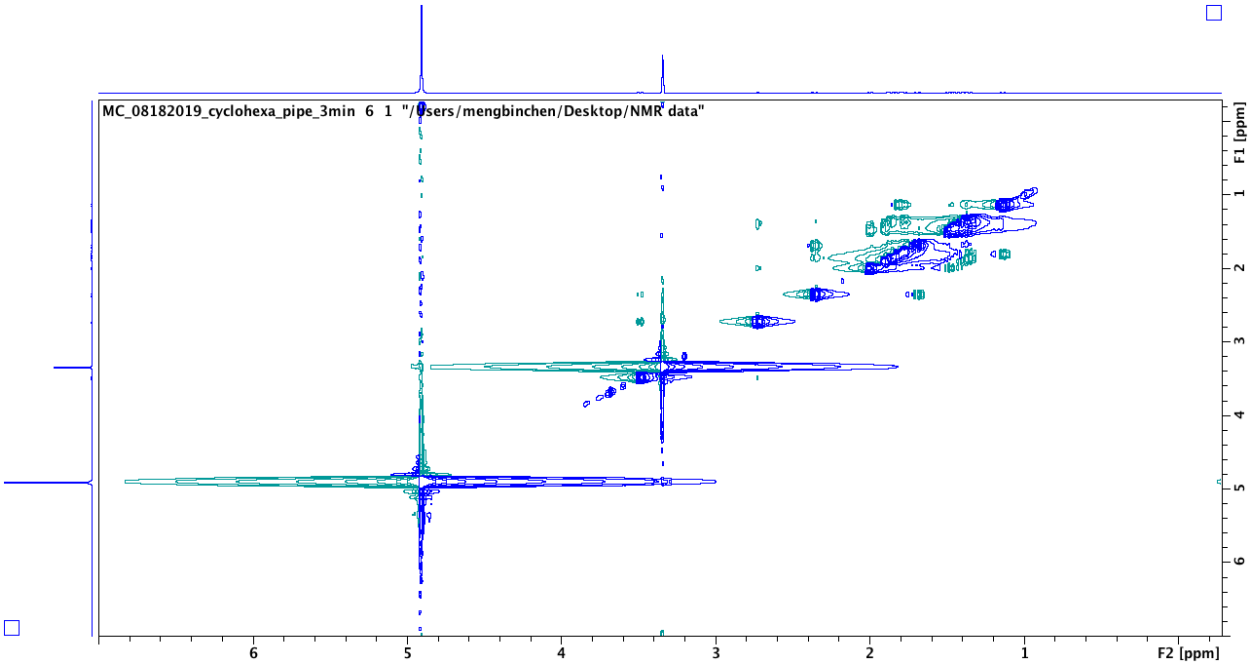

Fig S76. NOESY spectrum of compound **27**$_{\textbf{trans}}$ in CD_3OD.

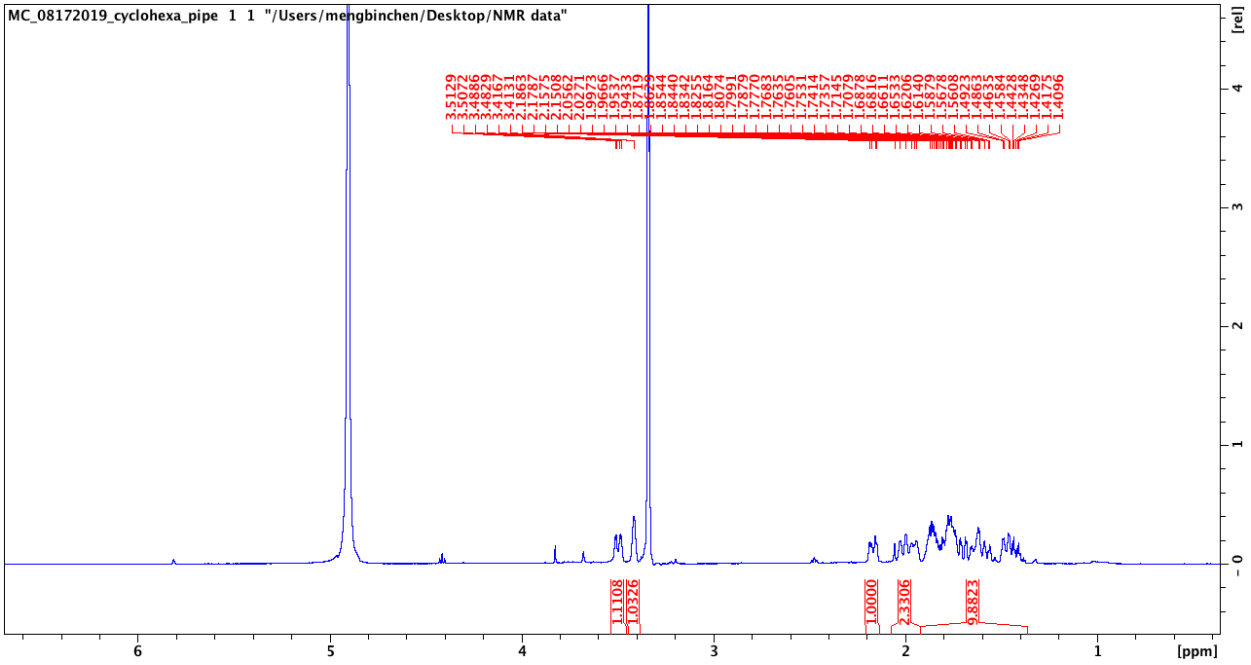

Fig S77. ^{1}H spectrum of compound **27$_{cis}$** in CD_3OD, 500 MHz.

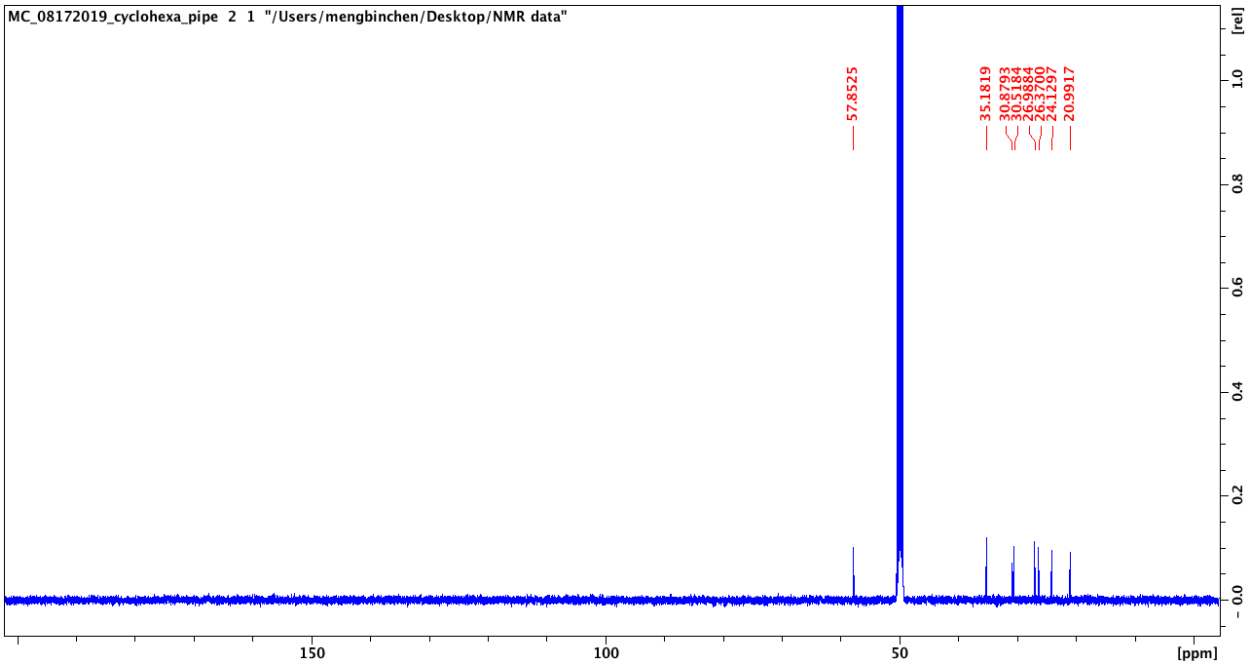

Fig S78. ^{13}C spectrum of compound **27$_{cis}$** in CD_3OD, 125 MHz.

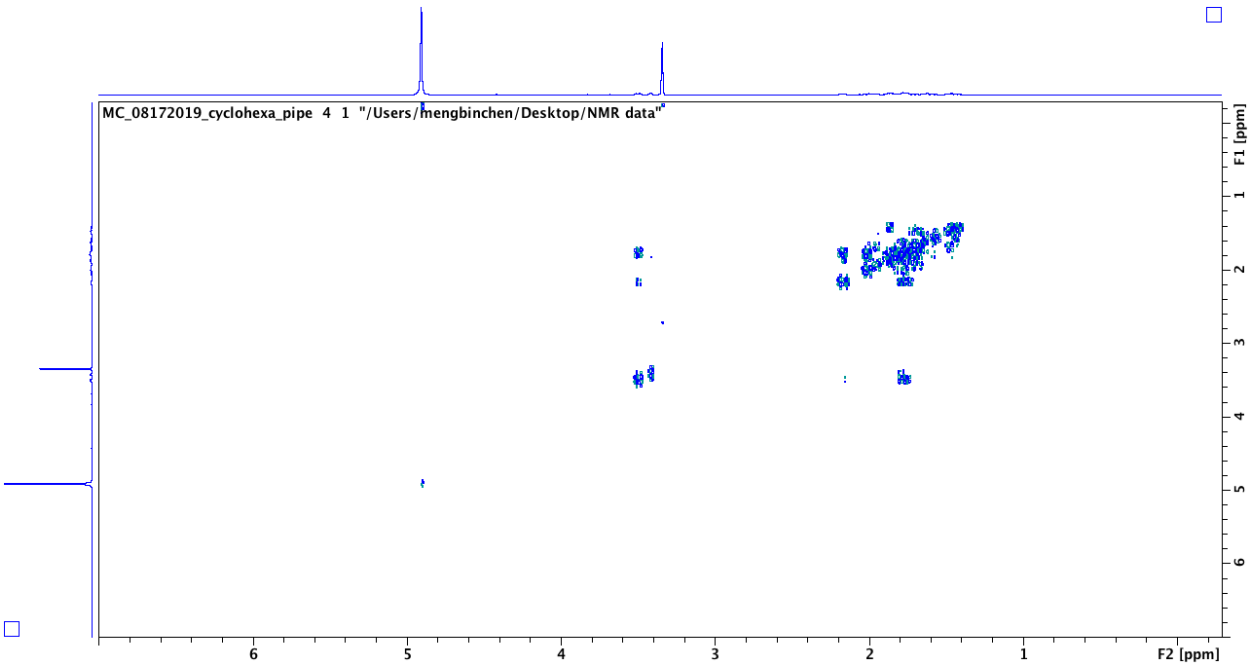

Fig S79. COSY spectrum of compound **27$_{cis}$** in CD_3OD.

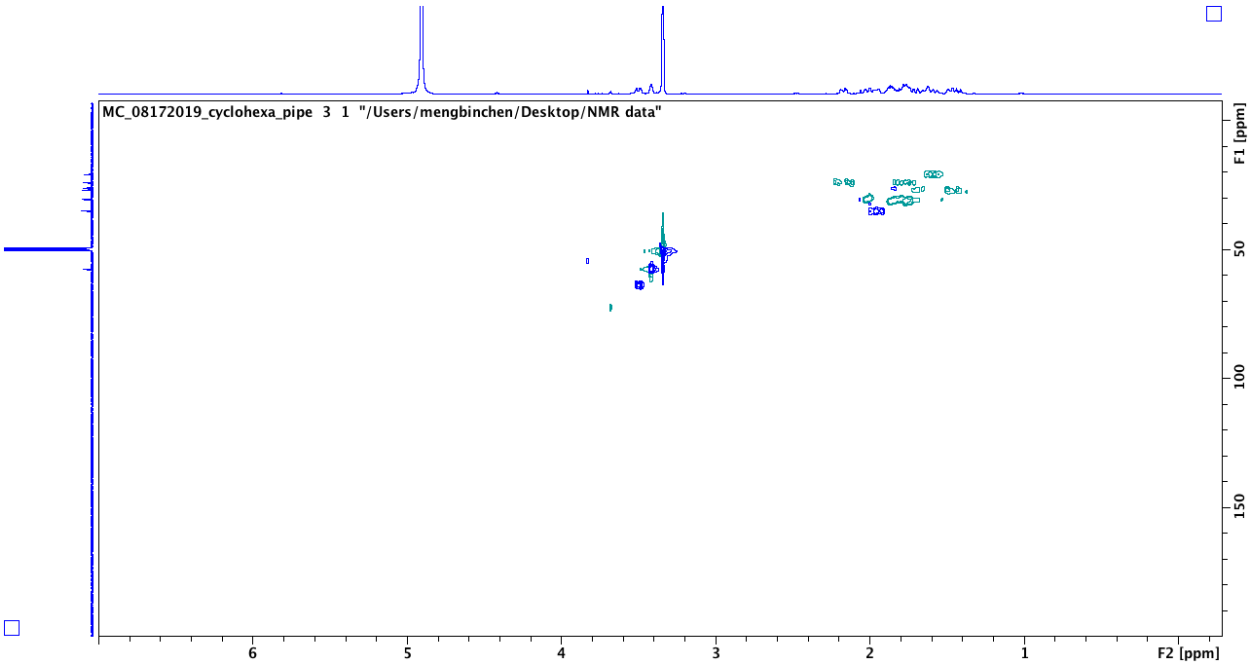

Fig S80. HSQC spectrum of compound **27$_{cis}$** in CD_3OD.

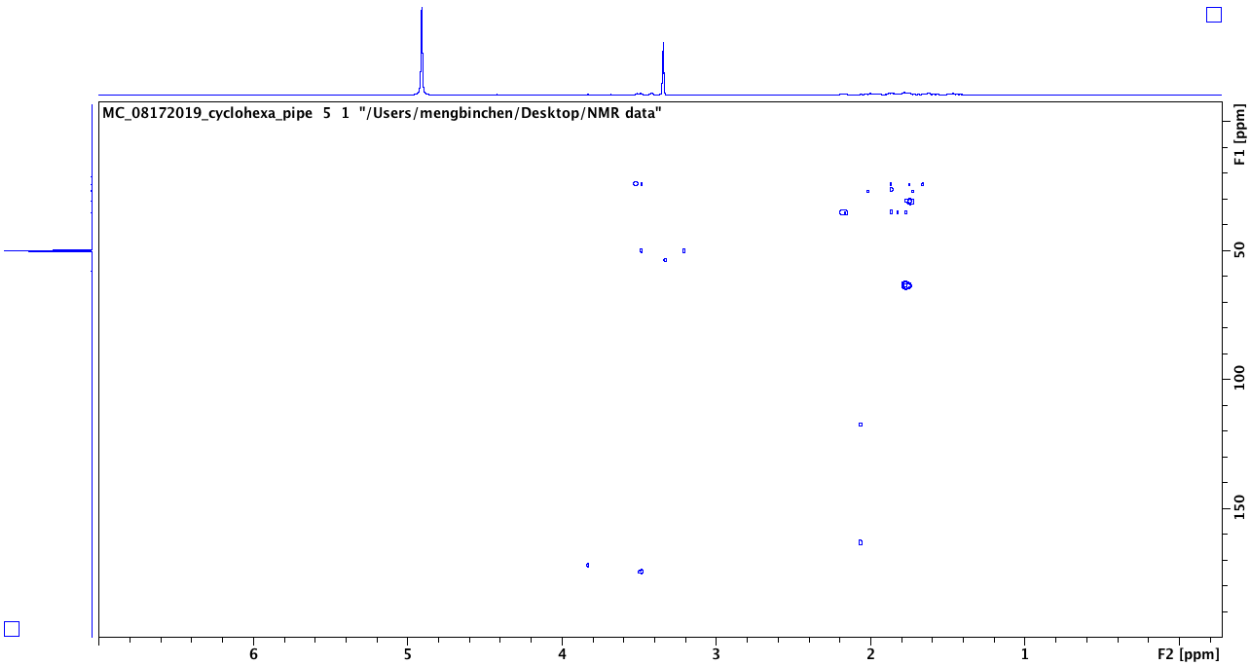

Fig S81. HMBC spectrum of compound **27$_{cis}$** in CD_3OD.

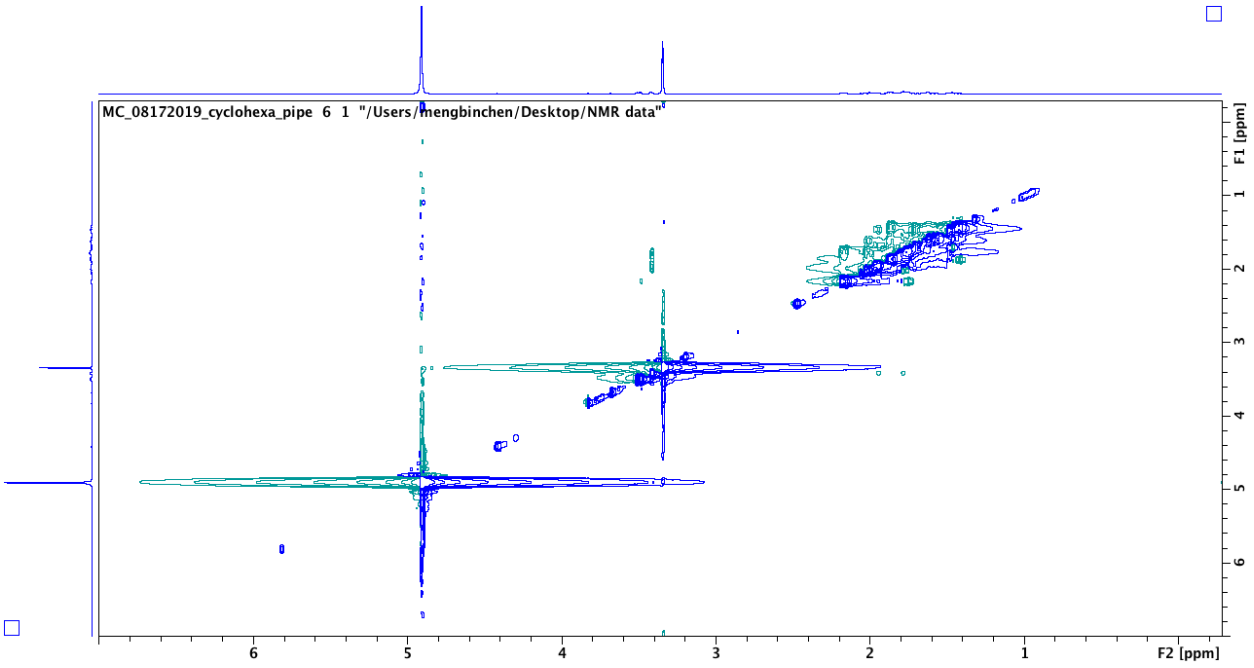

Fig S82. NOESY spectrum of compound **27$_{cis}$** in CD_3OD.

Reference:
1. Sato, M.; Dander, J. E.; Sato, C.; Hung, Y.-S.; Gao, S.-S.; Tang, M.-C.; Hang, L.; Winter, J. M.; Garg, N. K.; Watanabe, K.; Tang, Y., Collaborative Biosynthesis of Maleimide- and Succinimide-Containing Natural Products by Fungal Polyketide Megasynthases. *J. Am. Chem. Soc.* **2017,** *139*, 5317-5320.
2. Zhang, Z.; Jamieson, C. S.; Zhao, Y.-L.; Li, D.; Ohashi, M.; Houk, K. N.; Tang, Y., Enzyme-Catalyzed Inverse-Electron Demand Diels–Alder Reaction in the Biosynthesis of Antifungal Ilicicolin H. *J. Am. Chem. Soc.* **2019,** *141*, 5659-5663.
3. Bhushan, R.; Brückner, H., Marfey's reagent for chiral amino acid analysis: A review. *Amino Acids* **2004,** *27*, 231-247.
4. Tsuda, M.; Kasai, Y.; Komatsu, K.; Sone, T.; Tanaka, M.; Mikami, Y.; Kobayashi, J. i., Citrinadin A, a Novel Pentacyclic Alkaloid from Marine-Derived Fungus Penicillium citrinum. *Org. Lett.* **2004,** *6*, 3087-3089.
5. Bian, Z.; Marvin, C. C.; Martin, S. F., Enantioselective Total Synthesis of (−)-Citrinadin A and Revision of Its Stereochemical Structure. *J. Am. Chem. Soc.* **2013,** *135*, 10886-10889.
6. Kong, K.; Enquist, J. A.; McCallum, M. E.; Smith, G. M.; Matsumaru, T.; Menhaji-Klotz, E.; Wood, J. L., An Enantioselective Total Synthesis and Stereochemical Revision of (+)-Citrinadin B. *J. Am. Chem. Soc.* **2013,** *135*, 10890-10893.